Jordan Journal of Mechanical and Industrial Engineering (JJMIE)

JJMIE is a high-quality scientific journal devoted to fields of Mechanical and Industrial Engineering. It is published by The Hashemite University in corporation with the Jordanian Scientific Research Support Fund.

SUBMISSION ADDRESS:

Prof. **Nabil Anagreh** , Editor-in-Chief
Jordan Journal of Mechanical & Industrial Engineering,
Hashemite University,
PO Box 330127, Zarqa, 13133 , Jordan
E-mail: jjmie@hu.edu.jo

Hashemite Kingdom of Jordan

Hashemite University

Jordan Journal of Mechanical and Industrial Engineering

JJMIE

An International Peer-Reviewed Scientific Journal

Financed by Scientific Research Support Fund

http://jjmie.hu.edu.jo/

ISSN 1995-6665

Jordan Journal of Mechanical and Industrial Engineering (JJMIE)

JJMIE is a high-quality scientific journal devoted to fields of Mechanical and Industrial Engineering. It is published by The Jordanian Ministry of Higher Education and Scientific Research in corporation with the Hashemite University.

Introduction: The Editorial Board is very committed to build the Journal as one of the leading international journals in mechanical and industrial engineering sciences in the next few years. With the support of the Ministry of Higher Education and Scientific Research and Jordanian Universities, it is expected that a heavy resource to be channeled into the Journal to establish its international reputation. The Journal's reputation will be enhanced from arrangements with several organizers of international conferences in publishing selected best papers of the conference proceedings.

Aims and Scope: *Jordan Journal of Mechanical and Industrial Engineering* (JJMIE) is a refereed international journal to be of interest and use to all those concerned with research in various fields of, or closely related to, mechanical and industrial engineering disciplines. *Jordan Journal of Mechanical and Industrial Engineering* aims to provide a highly readable and valuable addition to the literature which will serve as an indispensable reference tool for years to come. The coverage of the journal includes all new theoretical and experimental findings in the fields of mechanical and industrial engineering or any closely related fields (Materials, Manufacturing, Management, Design, Thermal and Fluid, Energy, Control, Mechatronics, and Biomedical). The journal also encourages the submission of critical review articles covering advances in recent research of such fields as well as technical notes.

Guide for Authors

Manuscript Submission:
High-quality submissions to this new journal are welcome now and manuscripts may be either submitted online or email.

Online: For online and email submission upload one copy of the full paper including graphics and all figures at the online submission site, accessed via http://jjmie.hu.edu.jo. The manuscript must be written in MS Word 2010 Format. All correspondence, including notification of the Editor's decision and requests for revision, takes place by e-mail and via the Author's homepage, removing the need for a hard-copy paper trail.

Submission address and contact:
Prof. Nabil Anagreh
Editor-in-Chief
Jordan Journal of Mechanical & Industrial Engineering,
Hashemite University,
PO Box 330127, Zarqa, 13115, Jordan
E-mail: jjmie@hu.edu.jo

Types of contributions*:* Original research papers and Technical reports

Corresponding author: Clearly indicate who is responsible for correspondence at all stages of refereeing and publication, including post-publication. Ensure that telephone and fax numbers (with country and area code) are provided in addition to the e-mail address and the complete postal address. Full postal addresses must be given for all co-authors.

Original material: Submission of an article implies that the work described has not been published previously (except in the form of an abstract or as part of a published lecture or academic thesis), that it is not under consideration for publication elsewhere, that its publication is approved by all authors and that, if accepted, it will not be published elsewhere in the same form, in English or in any other language, without the written consent of the Publisher. Authors found to be deliberately contravening the submission guidelines on originality and exclusivity shall not be considered for future publication in this journal.

Withdrawing: If the author chooses to withdraw his article after it has been assessed, he shall reimburse JJMIE with the cost of reviewing the paper.

Manuscript Preparation:

General: Editors reserve the right to adjust style to certain standards of uniformity. Original manuscripts are discarded after publication unless the Publisher is asked to return original material after use. Please use MS Word 2010 for the text of your manuscript.

Structure: Follow this order when typing manuscripts: Title, Authors, Authors title, Affiliations, Abstract, Keywords, Introduction, Main text, Conclusions, Acknowledgements, Appendix, References, Figure Captions, Figures and then Tables. Please supply figures imported into the text AND also separately as original graphics files. Collate acknowledgements in a separate section at the end of the article and do not include them on the title page, as a footnote to the title or otherwise.

Text Layout: Use 1.5 line spacing and wide (3 cm) margins. Ensure that each new paragraph is clearly indicated. Present tables and figure legends on separate pages at the end of the manuscript. If possible, consult a recent issue of the journal to become familiar with layout and conventions. All footnotes (except for table and corresponding author footnotes) should be identified with superscript Arabic numbers. To conserve space, authors are requested to mark the less important parts of the paper (such as records of experimental results) for printing in smaller type. For long papers (more than 4000 words) sections which could be deleted without destroying either the sense or the continuity of the paper should be indicated as a guide for the editor. Nomenclature should conform to that most frequently used in the scientific field concerned. Number all pages consecutively; use 12 or 10 pt font size and standard fonts.

Corresponding author: Clearly indicate who is responsible for correspondence at all stages of refereeing and publication, including post-publication. The corresponding author should be identified with an asterisk and footnote. Ensure that telephone and fax numbers (with country and area code) are provided in addition to the e-mail address and the complete postal address. Full postal addresses must be given for all co-authors. Please consult a recent journal paper for style if possible.

Abstract: A self-contained abstract outlining in a single paragraph the aims, scope and conclusions of the paper must be supplied.

Keywords: Immediately after the abstract, provide a maximum of six keywords (avoid, for example, 'and', 'of'). Be sparing with abbreviations: only abbreviations firmly established in the field may be eligible.

Symbols: All Greek letters and unusual symbols should be identified by name in the margin, the first time they are used.

Units: Follow internationally accepted rules and conventions: use the international system of units (SI). If other quantities are mentioned, give their equivalent in SI.

Maths: Number consecutively any equations that have to be displayed separately from the text (if referred to explicitly in the text).

References: All publications cited in the text should be presented in a list of references following the text of the manuscript.

Text: Indicate references by number(s) in square brackets in line with the text. The actual authors can be referred to, but the reference number(s) must always be given.

List: Number the references (numbers in square brackets) in the list in the order in which they appear in the text.

Examples:
Reference to a journal publication:
[1] M.S. Mohsen, B.A. Akash, "Evaluation of domestic solar water heating system in Jordan using analytic hierarchy process". Energy Conversion & Management, Vol. 38 (1997) No. 9, 1815-1822.

Reference to a book:
[2] Strunk Jr W, White EB. The elements of style. 3rd ed. New York: Macmillan; 1979.

Reference to a conference proceeding:
[3] B. Akash, S. Odeh, S. Nijmeh, "Modeling of solar-assisted double-tube evaporator heat pump system under local climate conditions". 5th Jordanian International Mechanical Engineering Conference, Amman, Jordan, 2004.

Reference to a chapter in an edited book:
[4] Mettam GR, Adams LB. How to prepare an electronic version of your article. In: Jones BS, Smith RZ, editors. Introduction to the electronic age, New York: E-Publishing Inc; 1999, p. 281-304

Free Online Color : If, together with your accepted article, you submit usable color and black/white figures then the journal will ensure that these figures will appear in color on the journal website electronic version.

Tables: Tables should be numbered consecutively and given suitable captions and each table should begin on a new page. No vertical rules should be used. Tables should not unnecessarily duplicate results presented elsewhere in the manuscript (for example, in graphs). Footnotes to tables should be typed below the table and should be referred to by superscript lowercase letters.

Notification: Authors will be notified of the acceptance of their paper by the editor. The Publisher will also send a notification of receipt of the paper in production.

Copyright: All authors must sign the Transfer of Copyright agreement before the article can be published. This transfer agreement enables Jordan Journal of Mechanical and Industrial Engineering to protect the copyrighted material for the authors, but does not relinquish the authors' proprietary rights. The copyright transfer covers the exclusive rights to reproduce and distribute the article, including reprints, photographic reproductions, microfilm or any other reproductions of similar nature and translations.

Proof Reading: One set of page proofs in MS Word 2010 format will be sent by e-mail to the corresponding author, to be checked for typesetting/editing. The corrections should be returned within **48 hours**. No changes in, or additions to, the accepted (and subsequently edited) manuscript will be allowed at this stage. Proofreading is solely the author's responsibility. Any queries should be answered in full. Please correct factual errors only, or errors introduced by typesetting. Please note that once your paper has been proofed we publish the identical paper online as in print.

Author Benefits:

No page charges: Publication in this journal is free of charge.

Free offprints: One journal issues of which the article appears will be supplied free of charge to the corresponding author and additional offprint for each co-author. Corresponding authors will be given the choice to buy extra offprints before printing of the article.

JJMIE

Volume 8, Number 6, December 2014
ISSN 1995-6665

Jordan Journal of Mechanical and Industrial Engineering

JJMIE

Volume 8 Number 6, December 2014
ISSN 1995-6665
Pages 343 - 350

Jordan Journal of Mechanical and Industrial Engineering

Modeling of Creep Behavior for Graphene Filled Vinyl Ester Nano-Composites

Ahmad Almagableh[a *], P. Raju Mantena[b], Ahmed S. Awwad[c], Mahmoud[d] Rababah

[a] Mechanical Engineering Department, Assistant professor, The Hashemite University, Zarqa 13115, Zarqa, Jordan

[b] Mechanical Engineering Department, Full professor, The University of Mississippi, Oxford, MS 38677, USA

[c] Mechanical Engineering Department, Assistant professor, Al-Balqa Applied University, Amman 11134, Jordan

[d] Industrial Engineering Department, Assistant professor, The Hashemite University, Zarqa 13115, Zarqa, Jordan

Received 21 jun 2014 Accepted 3 Dec 2014

Abstract

The creep resistance of thermoset vinyl ester-based nanocomposites is studied by adding different weight percents of exfoliated graphite filler, characterized at different temperatures under constant loading. The creep response of these nanocomposites was analyzed using the TA Instruments Model Q800- DMA. Results showed that the nano-filler at some temperatures may hinder slippage and reorientation of polymer chain that, in turn, shows higher creep resistance for nanocomposites than the neat matrix. At a lower temperature, poor creep resistance was observed for neat matrix as compared to nano materials tested; however, at elevated temperatures (beyond the glass transition temperature), creep resistance in nanocomposites becomes close to that of neat vinyl ester.

To fully understand the complex creep deformation of polymeric based nanocomposites, a physical modeling is conducted to study the structure-property relationship as a function of filler content. Parametric studies for the suggested model, along with variations in the simulated model parameters, illustrate various deformation mechanisms. The predicted results from the models quite well agree with the obtained experimental results.

Keywords: *Polymers, Rheology, Nanoparticle.*

1. Introduction

Nanoparticles that may be dispersed on nanoscale would outcome in extremely great interaction between these particles and the matrix resin. For example, an interphase of 1 nm wide corresponds to about 30% of the total volume in case of nano-structure as compared to 0.3% of the total volume of polymer in case of micro filler composites [1].

Applications of polymeric-based nanocomposites involve marine composite structures: particularly lightweight glass/carbon polymeric based composites. Sandwich composites with balsa and foam cores are presently being featured in number of navy applications such as in surface ship deck structures, radar mast and boat hulls. Several new and emerging cores have been explored in sandwich construction to provide enhanced mechanical properties.

Many studies on creep performance of various materials were carried out and showed improvements in creep performance associated with filling nanoparticles into various polymer. Creep recovery is particularly noteworthy in engineering applications. Therefore, understanding the creep mechanism of polymer-based nanocomposites requires combined experimental characterization and efficient modeling that help in establishing failure design criteria.

The effect of the clay type, clay content and temperature on creep behavior of polycaprolactone/clay nanocomposites (prepared by melt intercalation) was modeled [2]. The Kelvin-Voight models (4 parameters) along with the power-law were used to establish a correlation between the creep behavior and the nanocomposite morphology. Both, the experimental curves and the models, demonstrated that the incorporation of the clay produces a significant improvement on the creep resistance with respect to the neat matrix.

Several studies have reported both positive and negative influences of fillers on the creep resistance of polymers. For example, improvements in creep performance for multiwall carbon nanotubes/epoxy

* Corresponding author. e-mail: amalmag1@gmail.com.

nanocomposite was not as high as anticipated through the use of mixture rule, indicated insufficient dispersion. However, variations in stiffness and creep strain-rate sensitivity obtained using nanoindentation showed quantifiable differences between the MWCNTs nanocomposite and epoxy specimens [3]. On the other hand, a significant improvement in tensile properties of polypropylene composites has been reported in terms of stiffening, strengthening and toughening with a low filled content of about 0.5% [4].

Based on above, modeling and simulating work, becomes a key issue in the future design of nano-based composites for engineering applications. An attempt based on the parameter analysis of the Burgers model had been accomplished [5] to explain the relationship between nano-structure and role of nano-particle toward creep performance of the bulk matrix. Results showed that the nanoparticles at some temperatures may hinder slippage and reorientation of polymer chain.

In the present study, the processed brominated 510A-40 vinyl ester is proposed to be used in the composite sheets of sandwich structures with fire-resistant foam layered in

between to decrease flammability combined with enhanced flexural rigidity [6].

A previous investigation on this class of vinyl ester resin systems [7] discussed the effects of nano-filler addition to this resin against dynamic-loading applications. In this article, an attempt is made to model creep performance and the structural long-term durability from molecular structure prospective and establish future design criteria for these nanocomposites.

2. Experimental

2.1. Materials and Creep Measurements

Nanocomposites were prepared by dissolving around 3 kg of vinyl ester resin with various concentrations of graphite platelets in a one gallon container for 4 hours. The above resin-solution was blended for two minutes using FlackTek speed mixer running at 3000 rpm speed. The well-mixed vinyl ester resin solution with graphite nano platelets was discharged into a 0.33 m x 0.33 m x 0.01m mold, let to rest for 30 minutes at ambient temperature, and then was post cured at 80°C for 3 hours.

Creep tests were conducted in flexural mode under different temperatures using the TA Instruments Model Q800 [8]/ dynamic mechanical analysis (DMA). The specimens for the creep and stress relaxation tests were 35 x 10 x 1.6 mm size. The creep-strain was measured as a function of the time. Prior to the creep tests, the stress level was derived from the proportional limit in stress-strain diagrams of the tensile tests and was fixed at 3 MPa. Low applied load ensures the creep measurements remained in linear viscoelastic deformation regime.

The testing temperature was in the range of 30–150^{o}C, incremented in 5^{o}C steps, and the isothermal tests were run on each specimen over 30 minutes duration in the DMA. The sample was initially settled at room temperature (30^{o}C) for about 4 minutes.

2.2. Stress-Relaxation Measurements of Nanocomposites

In the stress relaxation mode, the sample was held at a constant strain and the stress level measured as a function of time over the same temperature range. The method segments, executed during the relaxation test, were the same as that used in creep. The sample is initially equilibrated at RT for about 4 minutes, then displaced 0.1 mm for 30 minutes. The temperature is then incremented as in creep test and the process repeated until the final temperature of 150^{o}C.

3. Theory

DMA tests were performed in accordance with ASTM D4065-01: "Standard Practice for Plastics: Dynamic Mechanical Properties: Determination and Report Procedures" [9]. TA Instruments Mode Q800 DMA is a controlled stress with a Combined Motor and Transducer (CMT) machine in which the motor applies a force and displacement sensors measure strain. Force and amplitude are the raw signals recorded by the machine. The stiffness calculation for single-cantilever clamp type used in the TA Instruments Model Q800 DMA along with the appropriate correction factor is described below. The maximum level of strain occurs at the sample surface, while the centre experiences no strain at all, providing stress and strain are within the linear viscoelastic region.

4. Results and Discussion

4.1. Dynamic Properties

DMA spectra in the form of creep-strain as a function of temperature are plotted and demonstrated in Figures 1-3 for all nano-specimens, respectively. Creep deformation in the initial (pure elastic) segment is observed to be relatively small, associated with twisting and stretching of intermolecular bonds [10]. In the results shown, there was no evidence of creep rupture, which would require a longer time/temperature and maybe a larger load. As expected, these materials are viscoelastic in character, and, therefore, the shape of creep and relaxation curves is totally dependent on temperature. Creep strain increased with temperature, and, at the same time, similar behavior was exhibited by the nanocomposites. It is worth mentioning here that with the temperature rise from 100^{o}C to 125^{o}C the creep strain increases by 300% approximately at t = 1800 s for pure polymer (Figure not shown). Thus, the value of the creep-strain in response toward the temperature change is very sensitive. Moreover, results shown in Figure 3 can also indicate that creep strains of nanocomposites were lower than that of the neat matrix at all test temperatures and this implies that the creep behavior is improved by the addition of nanotubes. For example, the strain values at 82^{o}C were reduced by 17%, and 23% compared to brominated vinyl ester when the contents of xGnP were 1.25 wt.%, and 2.5 wt.%, respectively. In addition, it is also observed that the creep strain rate decreased with the incorporation of xGnP.

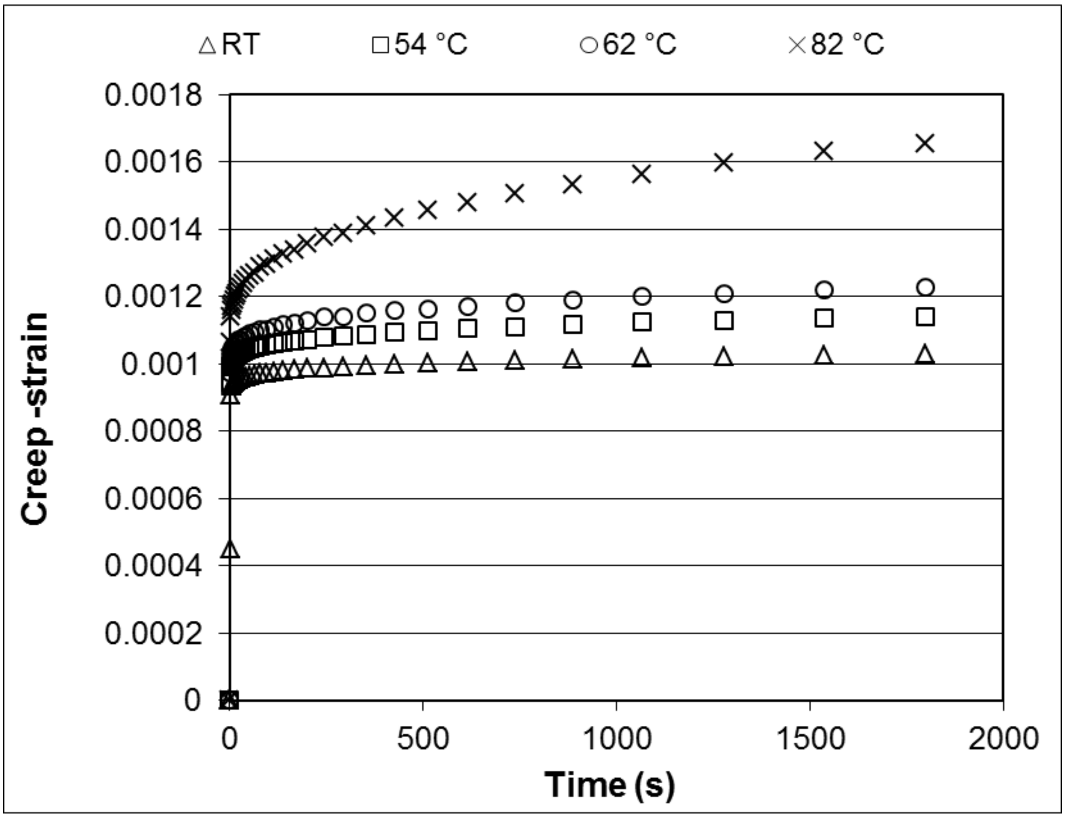

Figure 1. Creep-strain versus time for brominated vinyl ester.

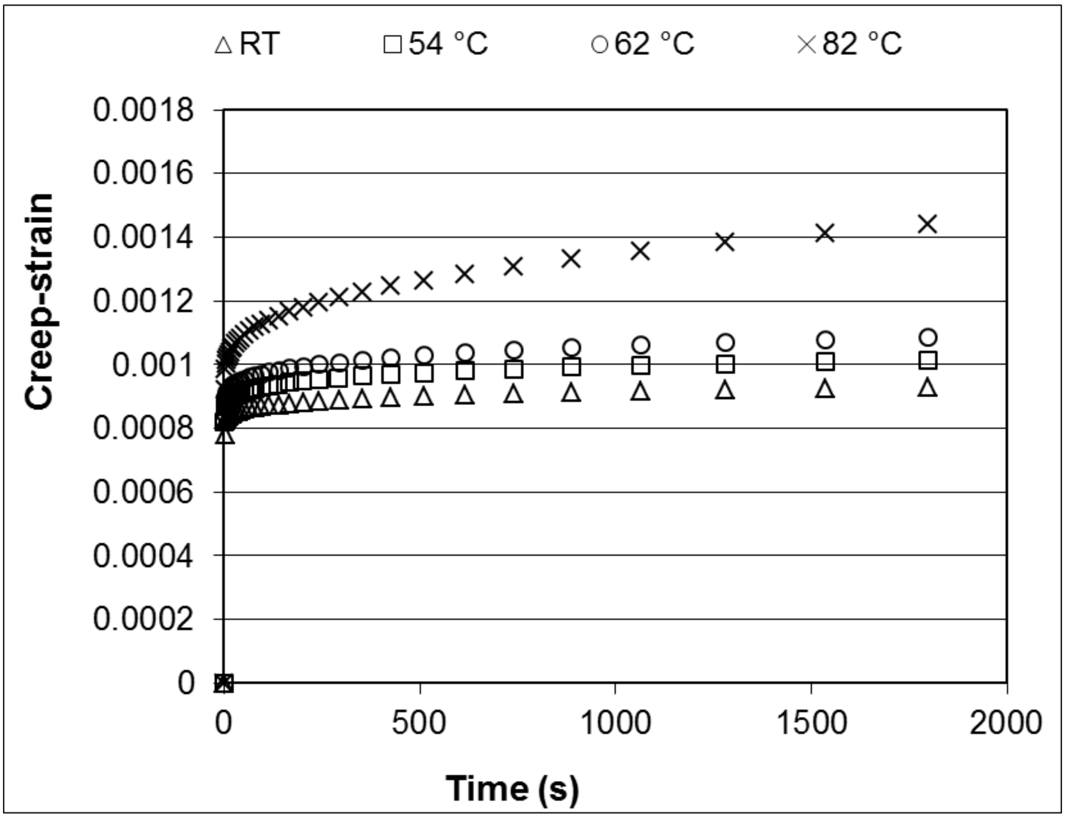

Figure 2. Creep-strain versus time for 1.25 wt% graphite platelet vinyl ester

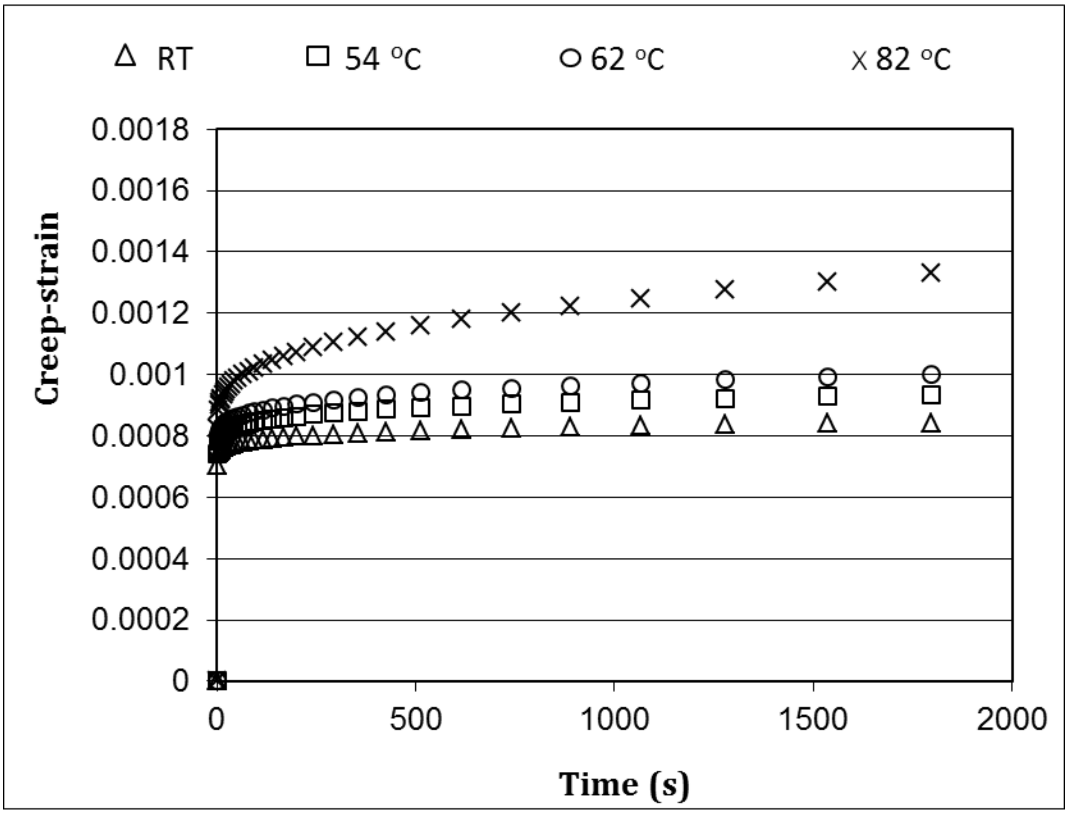

Figure 3. Creep-strain versus time for 2.5 wt%. graphite platelet vinyl ester.

4.2. Physical Model Formulation

Figure 4 shows the Standard Linear Solid Model that consists of a Maxwell element (linear spring and dashpot in series) and a linear spring in parallel. This model has been selected because it can explain two main deformations of plastics [8]; the spring represents deformations due to twisting and extension of intermolecular bonds, where as the dashpot refers to viscous deformation.

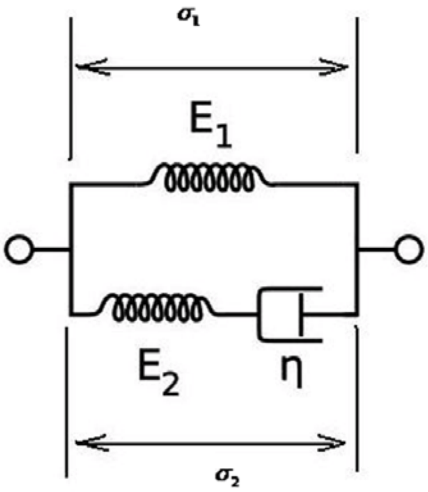

Figure 4. Schematic of the Standard Linear Solid model.

In the proposed viscoelastic model, the total stress at time t can be analyzed into time-rate dependent stress component in the spring E_2 and dashpot η (Maxwell element), and constant stress part (σ_1) in the spring element E_1 .

Thus, the total stress as per the Standard Linear Solid model is given as:

$$\sigma_o = E_1\varepsilon + \frac{\eta}{E_2}(E_1 + E_2)\ \varepsilon' \tag{1}$$

Based on the above suggested model, the creep-strain response is:

$$\varepsilon(t) = \frac{\sigma_o}{E_1}\left[1 - \frac{E_2}{E_1 + E_2}\ \ Exp(-t\ \ E_1 E_2 / \eta\ \ (E_1 + E_2)\right] \tag{2}$$

Where ε and σ_o are creep-strain and the applied stress in the creep experiment, respectively.

To simulate the model elastic parameters, data from the stress-relaxation experiments at a given temperature were accompanied. The relaxation modulus, according to the model, obtained from stress-relaxation data at quite large time, is basically representing E_1. E_1 alternatively can describe the elastic deformation in the crystalline structure, associated with no amorphous deformation or viscosity effect. In general, a polymer with large value of stiffness, E_1, may indicate highly crystalline structure. Accordingly, the neat resin exhibits higher values of E_1 with addition of nano-filler under all temperatures.

The total modulus (E_1+E_2), provided in the constitutive model, determines the immediate elastic creep strain (at time equal zero), which could be instantaneously recovered on the removal of creep load. In general, the composites showed greater values of (E_1+E_2) with the addition of filler compared to neat matrix at all temperatures. Among the nanocomposites, 2.25 wt. % appears to be the one with peak total elasticity, second is 1.25 wt.%, and finally is the neat matrix which depicted that the addition of nanoparticles was helpful in reinforcing the elasticity of the crystalline polymer as shown in Table 1. Moreover, it is worth mentioning that the change in variation of (E_1+E_2) value from one level of nano-filler loading to another illustrated the diverse reinforcing role of nanoparticle. For example, the total modulus increased by 3% in response to addition of 1.25 wt.% xGnP to the resin network, and this figure was magnified to become 22 % when the level of nano-filler was upgraded from 1.25 to 2.25 wt.%.

On the other hand, the elasticity dictated from total stiffness (E_1+E_2) of each specimen showed a decreasing affinity with temperature; it was easy to recognize that the substance materials became softer at higher temperatures and the stiffness was therefore reduced with diminished instantaneous modulus. For example, close to the glass transition temperature, the chain-segments of polymer began to travel and thus the elastic stiffness of substance material was decreased as compared to the one measured at room temperature.

ross linking density in general restricts the chain-movement from complete segmental motion at high temperatures where deformation is mainly viscous, it is typically given as the mean molecular weight between cross-links, is an important feature governing the mechanical properties of vinyl ester resin. Moreover, cross-linking can be altered by controlling the molecular weight of vinyl ester oligomers, and concentration of nano-filler in the matrix as well.

Cross linking density can be quantitatively evaluated as per Equation (3) which implies that cross-linking density, V, is dependent on Plateau or relaxation modulus in rubbery region, $G0^n$, temperature T, and the universal gas constant R.

$$V = G_o^n / RT \tag{3}$$

On comparing the modulus in the rubbery regions for vinyl ester with 2.5 wt.% and neat matrix as shown in Figure 5 (a, b), no major variation in plateau modulus was observed as opposed to the addition of nano-fillers. The influence of nano-filler addition in cross linking mechanism as per the above equation is not encouraging. As a result, the mechanism of hindering intermolecular slippage appears to be poor within rubbery region, and, therefore, the creep resistance in nanocomposites at elevated temperatures remains unaffected with regard to neat vinyl ester.

E_2 was subsequently developed in the model by subtracting E_1 from (E_1+E_2), at a specific temperature. The time-dependent E_2 might be associated with the stiffness and viscous deformation due to intermolecular slippage, damage from crystallized polymer or straightening out of the folded amorphous chains which is recoverable but not instantaneously. The retardant spring modulus E_2 and the dashpot viscosity η of each material showed conflicting dependency on temperature, E_2 increases with increasing temperature. The viscosity element η was much more dependent on temperature rather than concentration of nano-filler, unlike E_1 and E_2. Among the tested specimens, the viscosity η, showed comparatively slight changes between the neat matrix and the nano-specimens at specific temperature, which accounts that the dashpot viscosity was not much altered by the addition of nano-particles. Rather, viscous deformation as per the model (Maxwell unit) is mainly governed by temperature effect, and the relationship can be correlated as follow:

$$\eta = \text{constant} \ (T / T_r)^{\text{m}} \tag{4}$$

Where T_r is the reference temperature which is considered here as room temperature, m is a constant.

Table 1: The simulated parameters of the standard linear solid model

Material	Temp (^oC)	E_1 (MPa)	E_1+E_2 (MPa)	E_2 (MPa)	η (MPa.h)
Pure *VE*	30	2929	3160	231	7.6
	42	2750	3038	288	18.7
	62	2347	2801	454	65.2
	82	1683	2510	827	171.4
VE+1.25 wt.%	30	3002	3250	248	7.6
	42	3067	3405	338	18.7
	62	2627	3157	530	65.2
	82	1951	2858	907	171.4
VE+2.5 wt.%	30	3576	3971	395	7.6
	42	3404	3852	448	18.7
	62	2937	3596	659	65.2
	82	2175	3272	1098	171.4

Creep-strain data, at representative temperatures obtained from the creep tests, are plotted in Figure 6 through 8 along with the strain predicted including the modified effect of viscosity in Equation 4. As can be seen from these Figures, the model can predict the strain-time behavior of pure vinyl ester reasonably well except at high temperature (beyond 80^{o}C) where the onset of rubbery region started with complete motion of molecular segments occurred for pure vinyl ester and its nanocomposites at temperature around 110^{o}C. Agreement between model predictions and creep data for all nanocomposites is quite well.

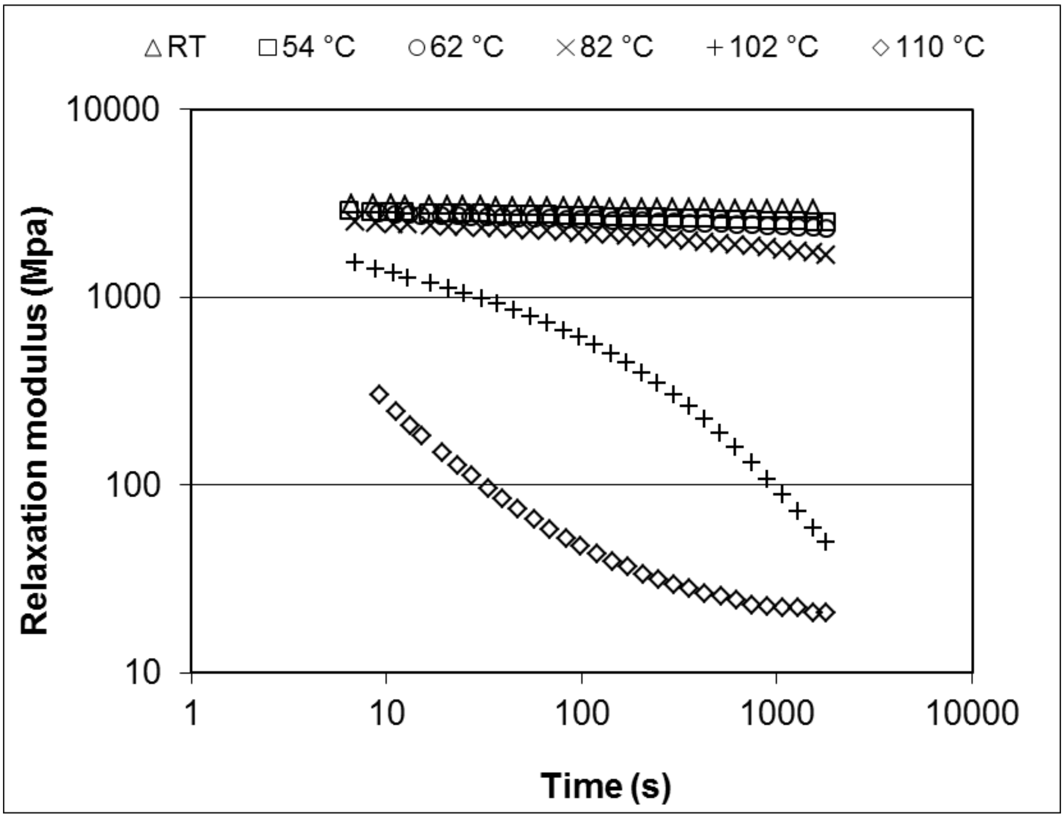

(a) Brominated vinyl ester and

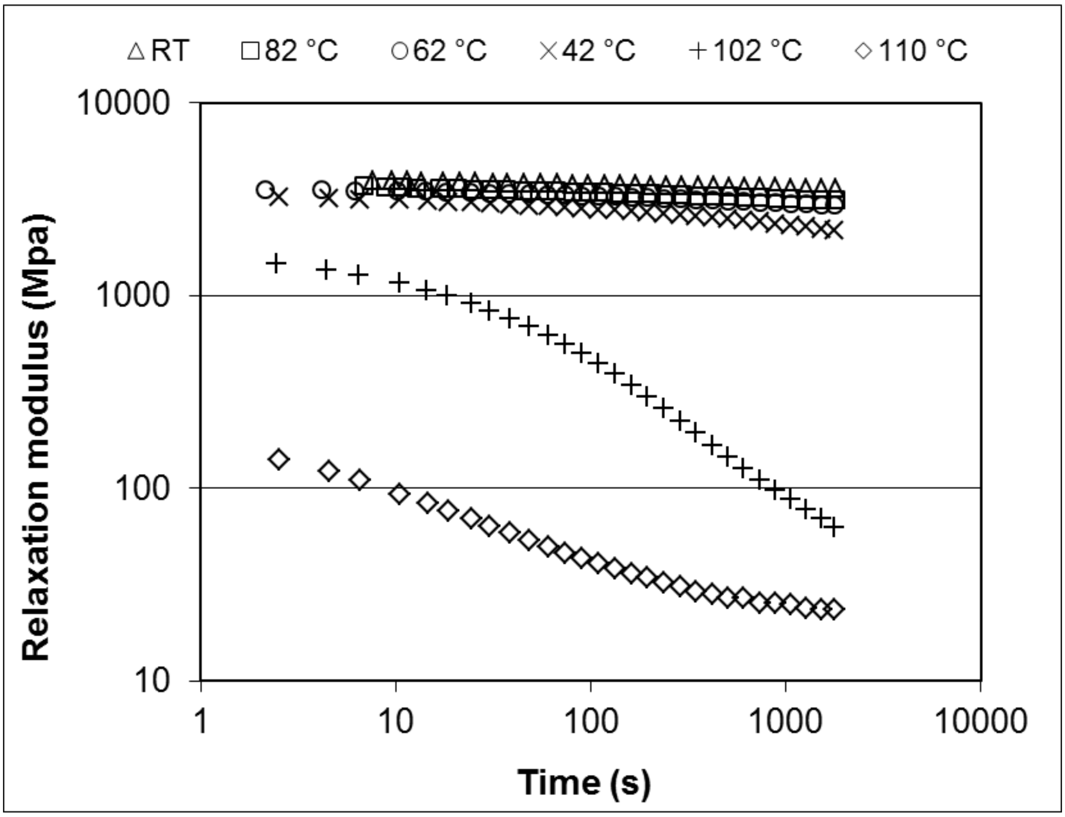

(b) Brominated vinyl ester with 2.5 wt.% graphite.

Figure 5. Relaxation modulus versus temperature.

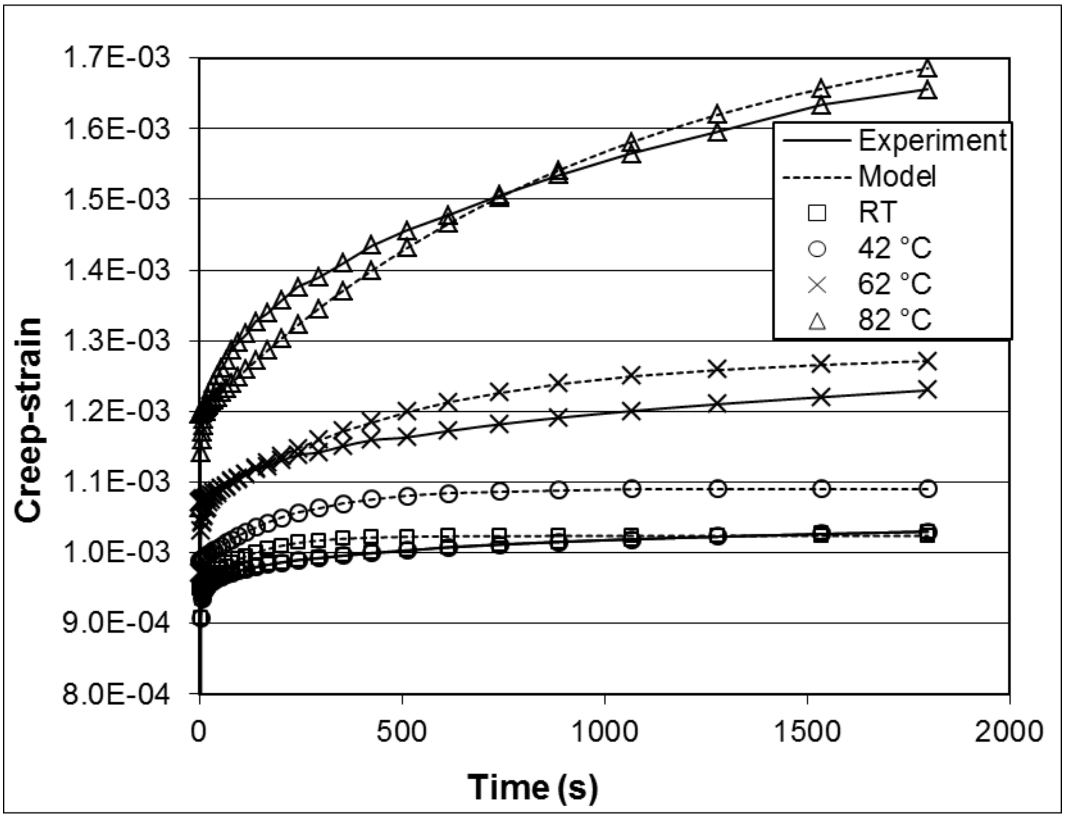

Figure 6. Predicted and experimental results of creep-strain versus time for brominated vinyl ester at selected temperatures based on the viscoelastic model.

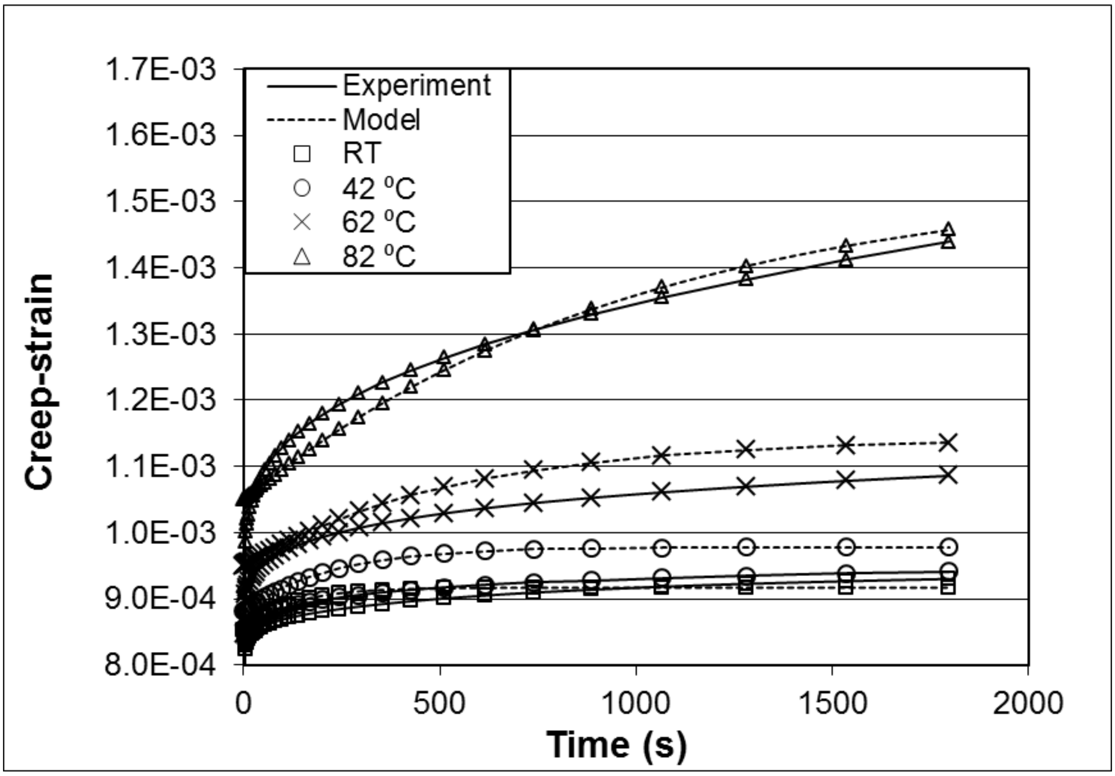

Figure 7. Predicted and experimental results of creep-strain versus time for 1.25 wt%. graphite platelet vinyl ester at selected temperatures based on the viscoelastic model.

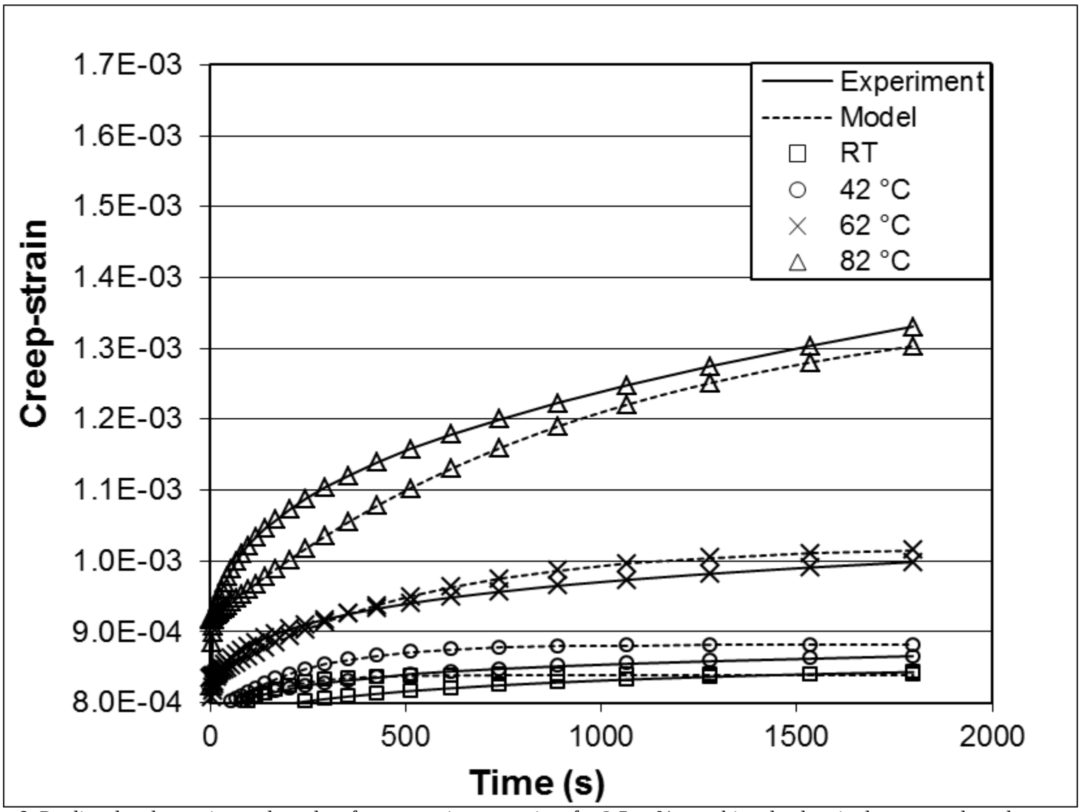

Figure 8. Predicted and experimental results of creep-strain versus time for 2.5 wt%. graphite platelet vinyl ester at selected temperatures based on the viscoelastic model.

5. Conclusions

The creep behavior of brominated vinyl ester and its nanocomposites were characterized in creep and relaxation tests using DMA Q800 over various isothermal temperatures. The standard linear solid model was established and developed to understand the relationship of nano-filler/structure property for these nano-materials. The variation in the simulated parameters in the proposed model describes the mechanism of nano-filler toward creep deformation in different regimes. The key findings of the present study are listed below:

- Poor creep resistance was observed for vinyl ester as compared to nanocomposite at low temperatures, while at elevated temperatures, creep resistance in nano-specimens was close in magnitude to that of pure polymer.
- The elastic modulus for the crystalline structure, simulated as (E_1+E_2) in the model, was observed to increase with nano-filler addition under all temperatures.
- The role of nano-particles toward cross-linking and hindering molecular slippage was found to be insensitive to filler addition at temperatures greater than glass transition temperatures.
- The viscous deformation was totally governed by the predicted model elements: E_2 and η, and was strongly dependent on temperature rather than on concentration of nano-filler.
- Analysis of microstructures for different types of nanocomposites and their impact on microscopic creep property can be suggested as a future work.

References

[1] Y. Kojima, K. Fukimori , et al., “Gas pemeabilities in rubber-clay hybrid”, J of Material Science, Vol.12 (1993) 889-900.

[2] L.N. Ludueña, A. Vazquez, V.A. Alvarez, “Creep behavior of pcl/clay nanocomposites”, Congreso SAM, CONAMET, 2007

[3] M. Tehrani, M. Safdari, M.S. Al-Haik, “Nanocharacterization of creep behavior of multiwall carbon nanotubes/epoxy nanocomposite”, International Journal of Plasticity, Vol. 27 (2011) 887–901

[4] P.C. LeBaron, Z. Wang , T.J. Pinnavaia, “Polymer-layered silicate nanocomposites: an overview”, J Applied Clay Science, Vol.15 (1999) 11-29.

[5] Y. Jing , Z. Zhong, K. Alois, F. Klaus, “On the characterization of tensile creeps resistance of polyamide 66 nanocomposites: Modeling and prediction of long-term performance”, J Polymer, Vol. 47 (2006) 6745-6758.

[6] U. Sorathia, J. Ness, M. Blum, “Fire safety of composites in the US navy”, J. Composites Part A: Applied Science and Manufacturing, Vol. 30 (1999) 707-713.

[7] Almagableh, P. R. Mantena, A. Alostaz, W. Liu, L. Drzal, “Effects of bromination on the viscoelastic response of vinyl ester nanocomposites”, J express Polymer Letter, Vol. 3 (2009) 724-731.

[8] TA Instruments, Dynamic Mechanical Analyzer. Q Series^{TM}, Getting started guide. Revision report, New Castle, Delaware, 2004.

[9] ASTM Standard, Standard practice for plastics, dynamic mechanical properties determination and report of procedure, International ASTM D 4065-01, 2000.

[10] Plaseied, A. Fatemi, “Deformation response and constitutive modeling of vinyl ester polymer including strain rate and temperature effects”, J Material Science, Vol. 43 (2008) 1191-1199.

JJMIE

Volume 8 Number 6, December 2014
ISSN 1995-6665
Pages 351 - 358

Jordan Journal of Mechanical and Industrial Engineering

Sliding Wear Response of an Aluminium Metal Matrix Composite: Effect of Solid Lubricant Particle Size

Gajendra Dixit [a*], Mohammad Mohsin Khan [b]

[a] *Professor, Maulana Azad National Institute of Technology Bhopal-462051, India*

[b] *Research Scholar, Maulana Azad National Institute of Technology Bhopal-462051, India*

Received 21 jun 2014 *Accepted 3 Dec 2014*

Abstract

The present work investigates the partial lubricated sliding wear behavior of 10 wt% SiC reinforced aluminum composites produced by Vortex method with the help of a pin on disc wear testing machine. The wear tests were conducted at the sliding velocities of 2.1 and 8.4 m/sec and at an applied load of 10 to 200 N in different lubricated environment [oil, oil+ 5wt %graphite (7-10 µm), and oil+ 5wt % graphite (100 µm)]. The influence of changing graphite particle size in the oil lubricant towards controlling the wear behavior of the samples has been studied. The (Aluminium-based) matrix alloy was also characterized under identical conditions to examine the influence of the dispersoid (SiC) phase on the wear behavior. The parameters studied are wear rate, frictional heating and friction coefficient. Results showed a large improvement in wear resistance of the Aluminium-based alloy after reinforcement with SiC particles. The composite experienced a higher frictional heating and friction coefficient than the matrix alloy in all the cases. The wear rate and frictional heating increased with load and speed while friction coefficient was affected in an opposite manner. Test duration influenced the frictional heating and friction coefficient of the samples in a mixed manner.

Keywords: *Aluminium Alloy; Composite; Lubricated Sliding Wear Behavior; Solid Lubricant*.

1. Introduction

In many engineering applications, aluminium alloys are desirable because of their low density and high strength-to-weight ratio. In several such applications, improved wear resistance of the alloys becomes imperative. Al–Si alloys form an interesting series of the alloy system in this context. Their composites containing hard particles are gaining importance. These materials have properties like high specific strength, high specific stiffness, improved high temperature performance as well as good wear and seizure resistance. The properties of composite materials can be tailored by suitably selecting the matrix alloy and the dispersoid phase. Owing to their versatile properties, composite materials hold a potential for applications in automotive, aerospace, sporting goods and in general engineering.

Available literature posits that the wear behavior of materials depends on a number of operational and material related conditions in a complex manner and even they have synergistic effects on the overall response of materials [1-14]. Chemistry, microstructure and shape, size, content and mode of distribution of the microconstituent, in terms of hardness, strength, cracking tendency, lubricating characteristics, load bearing capability as well as thermal stability are some of the important factors to affect wear behavior [1-14]. The sliding wear behavior is controlled by a number of experimental parameters such as speed, load, conditions, distance, etc. [1-28].

The conditions may be dry, lubricated, high temperature, oxidizing, reducing etc. Lubricants may be liquid, semi-solid, or solid. Nowadays, solid lubricants are added in order to further improve the performance of the liquid lubricants. A variety of solid lubricants are in existence. They are generally lamellar solids with (open) hexagonal structure with c/a ratio larger than that of an ideal close packed hexagonal [29, 30]. This enables them to easily smear along the contacting surfaces producing lubricating effect and thereby to improve wear performance. For the effective working of solid lubricants, the presence of a liquid lubricant is essential and the quantity of solid lubricant to be added to the liquid lubricant that would lead to the best wear performance. This depends on a number of factors like the ones related to material as well as test parameters and need to be determined /optimized for effective utilization of a liquid/solid lubricant. Recent studies have led to a limited understanding of some of the aspects but the role of lubricant's particle size has not practically been studied on the wear behavior of Aluminium based alloys. Moreover, there is a paucity of information pertaining to the influence

* Corresponding author. e-mail: dixitgajendra1@gmail.com.

of hard particle reinforcement on the partial lubricating wear behavior of the (Aluminium-based) matrix alloy(s).

In light of the above, an attempt has been made in this study to analyze the sliding wear behavior of an Aluminium alloy and its composite reinforced with 10 wt% SiC particles under the influence of varying applied loads and speeds in partial lubricated conditions [oil, oil+ 5wt %graphite (7-10 µm), and oil + 5wt % graphite (100 µm)]. The influence of changing particle size of graphite in the oil lubricant towards controlling the wear behavior of the samples has been studied.

Table 1. Chemical Composition of the Test Materials

Element	Elements, wt%							
	Si	Mn	Mg	Cu	Fe	Ni	Al	SiC
ADC-12	10.29	0.12	0.47	1.98	0.75	0.80	Balance	-
ADC-12 + SiC Composite	10.29	0.12	0.47	1.98	0.75	0.80	Balance	10

2. Experimental

2.1. Material Preparation

The experimental alloys and composite were prepared by the liquid metallurgy route in the form of 16 mm diameter,170 mm long cylindrical castings. The composite was synthesized by dispersing 50-100 µm silicon carbide particles at the vortex of the alloy melt. Table 1 shows the chemical compositions of the sample materials.

2.2. Microstructural Examination

Microstructural studies were carried out on 10 mm diameter, 15 mm thick samples. The samples were polished metallographically and etched suitably. Killer reagent was used for etching the samples of the aluminium (matrix) alloy and composite. A microstructural characterization of the samples was carried out using scanning electron microscopy.

2.3. Measurement of Hardness and Density

Hardness measurements were carried out on metallographically polished samples using a Vickers hardness tester. The applied load in this case was 30 kg. The water displacement technique was adopted for density measurement. A Mettler microbalance was used for weighing the samples in water and air.

2.4. Sliding Wear Tests

Sliding wear tests were carried out using SAE 20W-40 oil, SAE 20W- 40 oil plus (5 Wt %) graphite particles (size 7-10 μm), and SAE 20W- 40 oil plus (5 Wt %) graphite particles (size 100 μm) as lubricant using a Magnum Engineers (India) make pin-on-disc machine shown in Figure 1. Cylindrical test pins (8 mm diameter and 30 mm length) were held against a rotating heat-treated En31 steel disc conforming to AISIE 52100 (1.0 % C, 1.4 % Cr, 0.40 % Mn, 0.2 % Si, 0.05 % S, 0.05 % P and balance Fe). Hardness of the disc was HRC 62. The steel disc was polished mechanically up to a roughness (Ra) level of 1-2 μm prior to each test.

Wear tests were conducted over a range of applied loads and sliding speeds. The track diameter of 100 mm enabled the rotational speeds of 400 and 1600 rpm (selected in the present investigation) to attain linear sliding velocities of 2.09 and 8.38 m/s, respectively. The wear testing procedure involved inserting the disk into lubricant /lubricant mixture and allowing it to rotate at a speed of 3.35 m/s for 5 s. The lubricated disk was rotated in order to generate a low and uniform thickness by spinning off the excess lubricant. Thereby, maintaining conditions close to mixed lubrication generally encountered by components in situations dealing with sparse lubrication as well as during starting and stopping operations in the case of fully lubricated sliding. Further sample was fixed in the specimen holder, allowing the disk to rotate at the predetermined sliding speed up to the fixed distance of 2500 m or until specimen seizure, whichever occurred earlier. Specimen seizure was noticed in terms of large material adhesion on to the disc, higher rate of temperature rise of the test pin, and abnormal vibration and noise from the pin-on-disc assembly.

Frictional heating was monitored using a chromel-alumel thermocouple inserted in a 1.5 mm diameter hole on the test pin 1.5 mm away from the sliding surface. Output of the thermocouple is fed into a PC-based data logging system which continuously records the frictional heating of sample during each test. The loads were vertically applied on to the pin sample against the disc. Output from strain gauge is also fed into a PC-based data logging system which continuously records the tangential load on the pin sample during each test.

Coefficient of friction was calculated by dividing the tangential load with the applied normal load. The specimens were thoroughly cleaned in acetone for 10 min using ultrasonic cleaner (34 ± 3 kHZ), dried and weighed prior to and after each test. A Mettler instrument make microbalance was used for weighing the specimens. Weight loss was then converted into volume loss per unit sliding distance to compute wear rate.

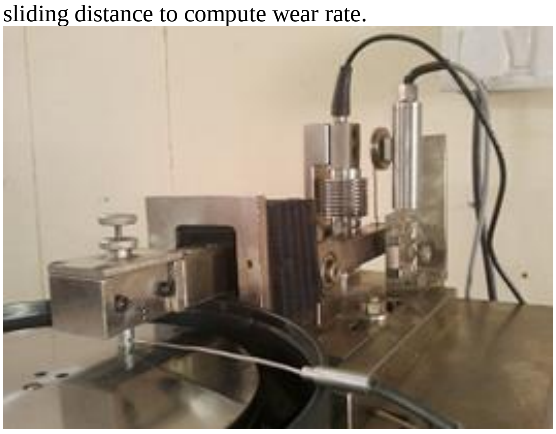

Figure 1. Schematic representation of the wear test configuration.

3. Results

3.1. Microstructure

Microstructure of Aluminum alloy (ADC12 alloy) solidified in a cast iron mold shows aluminum dendrites with dendretic arm spacing in the range of 25 microns. The eutectic silicon solidifies in the inter-dendretic region and around the dendrites. The micrograph (Figure 2) depicts plate shaped eutectic silicon and the other intermetallic phases. The plate shaped eutectic silicon is usually 20-30 micron in length and 2-5 micron in width. The composite showed features similar to the matrix alloy except the presence of the dispersoid SiC particles (Figure 3).

3.2. Hardness and Density

Table 2 represents various properties of the specimens. The composite attained somewhat a higher hardness than the corresponding matrix alloy. So far as the density of the specimen is concerned, it was highest for the composite followed by matrix alloy.

Table 2. Hardness and Density of Specimen

S No.	Type	Vickers Hardness (HV)	Density g/cm^3
1	ADC-12 Matrix Alloy	92.3	2.64
2	ADC-12 Matrix Alloy + Composite	98.7	2.78

3.3. Wear Behavior

3.3.1. Wear Rate

Wear Rate of the samples has been plotted as a function of applied load in Oil + 5% Graphite (7-10 µm), Oil + 5% Graphite (100 µm) & Oil Lubricated environment at sliding velocity of 2.1 and 8.4 m/sec in Figure 4 to Figure 6, respectively. Wear rate increases with the load and sliding velocity for all the sample material and in all environments. Incorporation of SiC significantly reduces the wear rate of the alloy irrespective of the test conditions (Figure 4 – Figure 6). The presence of solid lubricant reduces the wear rate for all the test material. However Oil + 5% Graphite (7-10 µm) is proven to be more effective than the Oil + 5% Graphite (100 µm) {Figure 7-Figure 8}.

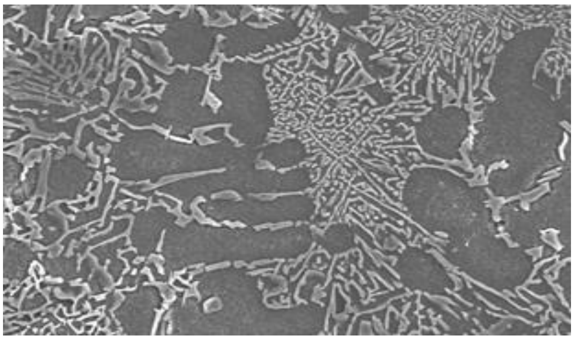

Figure 2. Microstructure of ADC-12 Alloy

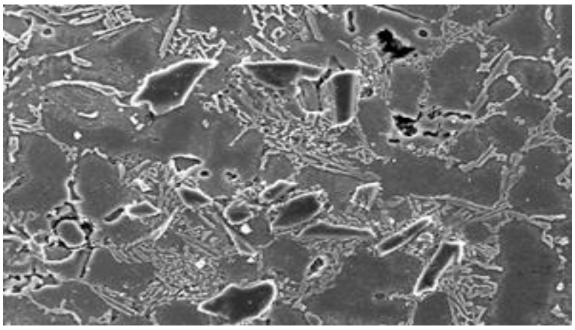

Figure 3. Microstructure of ADC-12 Alloy+ 10% SiC Composite

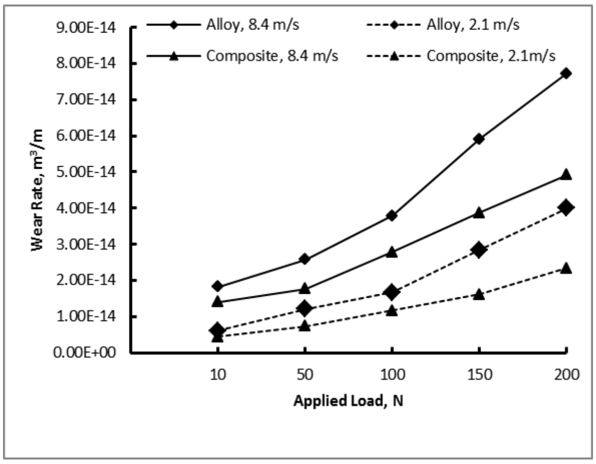

Figure 4. Wear Rate of Alloy and Composite plotted as function of a Applied load in Oil + (7-10µm Graphite) Lubricated Environment

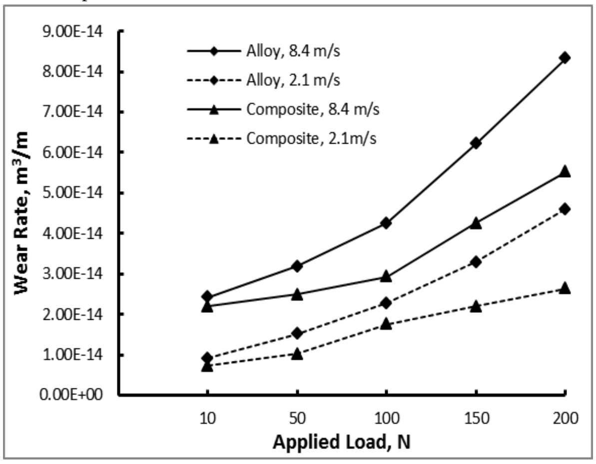

Figure 5. Wear Rate of Alloy and Composite plotted as a function of Applied Load in Oil + (100µm Graphite) Lubricated Environment

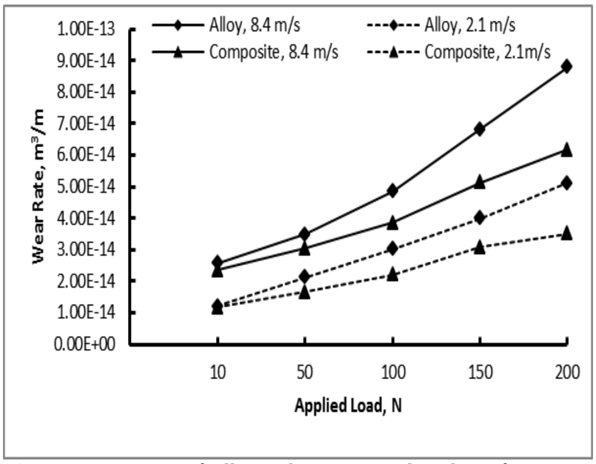

Figure 6 .Wear Rate of Alloy and Composite plotted as a function of Applied Load in Oil Lubricated Environment

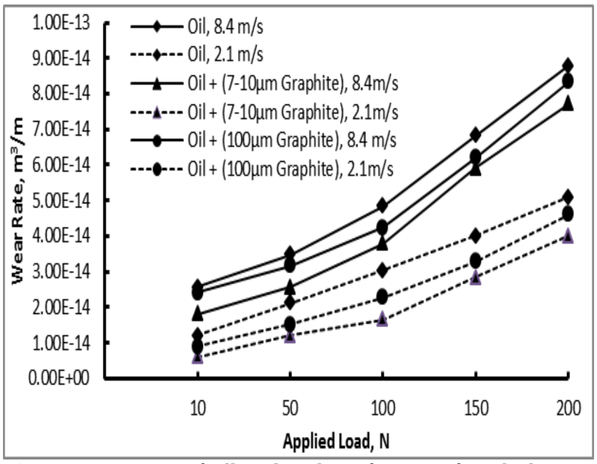

Figure 7. Wear Rate of Alloy plotted as a function of Applied load in various Environment

3.3.2. Frictional Heating

Temperature near the contacting surface for Alloy and composite at Sliding Velocity of 2.1 & 8.4 m/sec plotted as a function of applied load in various lubricated test environments in Figure 9 to Figure 13, respectively. The temperature increases with increase in load and velocity however the increment is more for the composite than the base alloy (Figure 9-Figure 11). The pattern of temperature is similar in all the environments despite of the fact that the addition of the solid lubricant peculiarly affects the pattern of temperature variation. For all the testing materials, the maximum temperature rise is observed at 8.4 m/sec sliding velocity is in Oil + 5% graphite (100 µm) lubricated environment followed by Oil and Oil + 5% graphite (7-10 µm) lubricated environment.

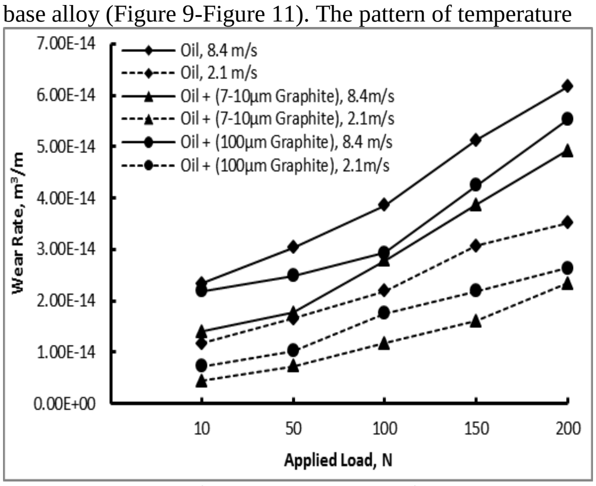

Figure 8 .Wear Rate of Composite plotted as a function Applied load in various Environment

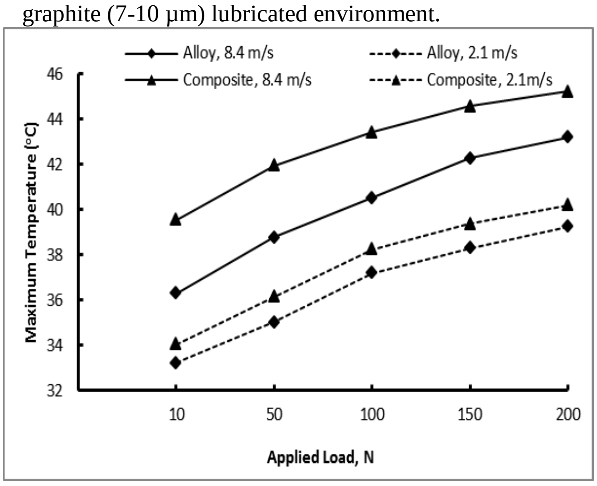

Figure 9. Maximum Temperature in Oil Lubricated Environment

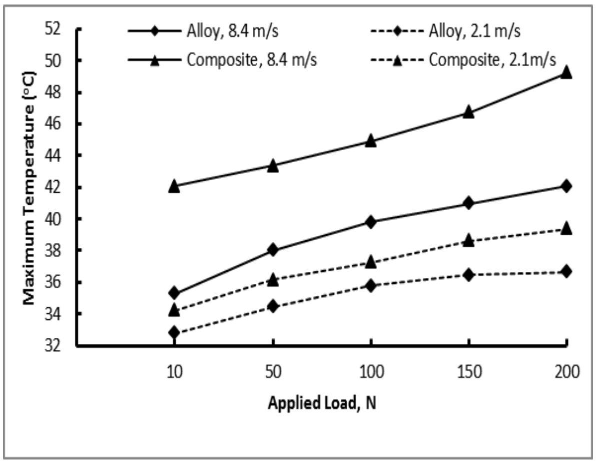

Figure 10. Maximum Temperature in Oil + (7-10µm Graphite) Lubricated Environment

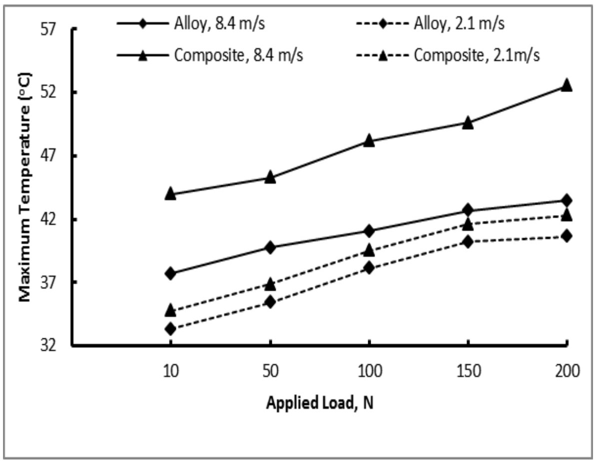

Figure 11. Maximum Temperature in Oil + (100µm Graphite) Lubricated Environment

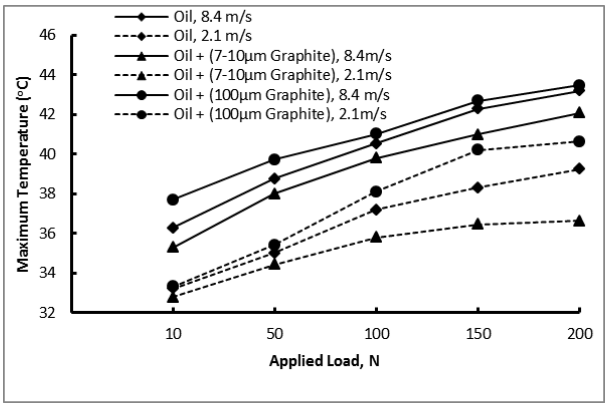

Figure 12. Maximum Temperature of Alloy in Various Environments

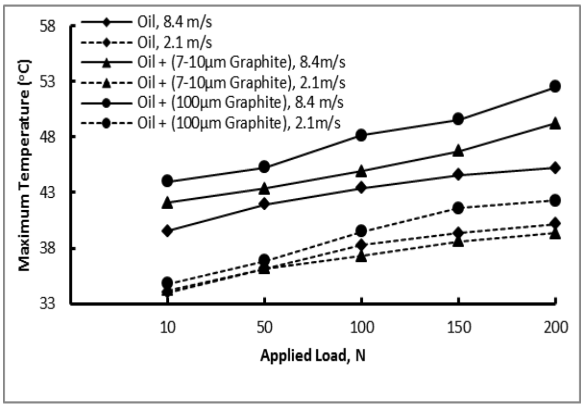

Figure 13. Maximum Temperature of Composite in Various Environments

3.3.3. Friction Coefficient

Figure 14 to Figure 16 represent the friction coefficient for Aluminium-Alloy and Aluminium -SiC composite as a function of Applied Load in various lubricated condition at a sliding velocity of 2.1 and 8.4 m/sec. friction coefficient decreases with the increase in applied load while it varies directly with the sliding speed irrespective of the test material. Incorporation of SiC particle increases the friction coefficient in Oil and Oil + 5wt% graphite (100 μm) lubricated environment however in Oil + 5wt% graphite (7-10 μm) environment it varies in some other manner.

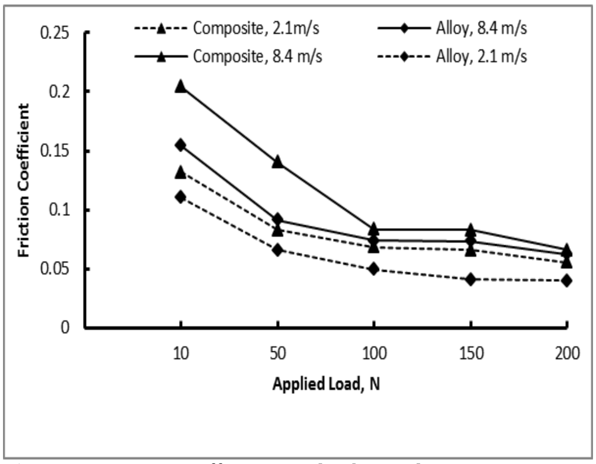

Figure 14. Friction Coefficient in Oil Lubricated Environment

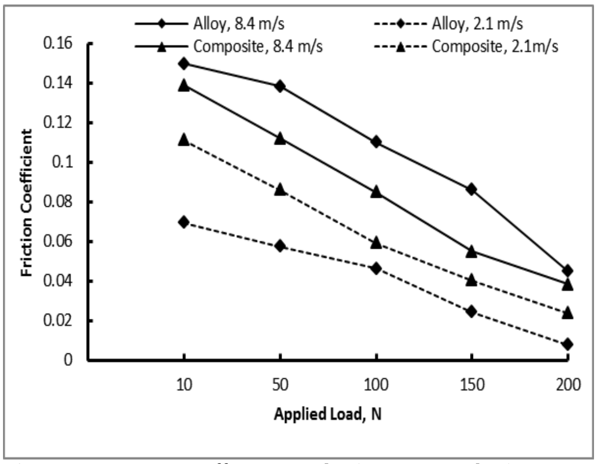

Figure 15 . Friction Coefficient in Oil + (7-10μm Graphite) Lubricated Environment

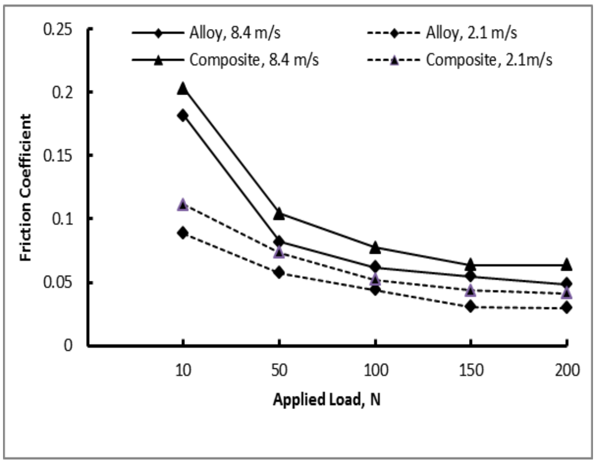

Figure 16. Friction Coefficient in Oil + (100μm Graphite) Lubricated Environment

4. Discussion

4.1. Microstructure

From microstructural characteristics point of view, the aluminium based alloy depicts plate shaped eutectic silicon and the other intermetallic phases (Figure 2). Reinforcing the alloy system with thermally stable micro-constituents through alloying with high melting elements and/or incorporation of hard ceramic particles improves its strength (Figure 3). Wear resistance under severe conditions also improves because of improved thermal stability while ambient temperature properties deteriorate over the matrix alloy due to enhanced cracking tendency introduced by the thermally stable micro-constituents **[**1-10**]**.

4.2. Wear Behavior

4.2.1. Wear Rate

Coming to the sliding wear tests, factors affecting the wear response of materials are applied load, sliding velocity, sliding distance and test environment. Applied load directly influences the wear rate, i.e., the higher the load is the greater the wear rate becomes. Other variables, such as distance and velocity, do not have well defined effects on the wear response of materials [1-10, 31-41]. As far as the environmental (lubricated, oil / oil + graphite) effects are concerned, a lot of complexity exists [1-10, 31-41].

Normally, the use of a lubricant improves the sliding wear characteristics of material because of the formation of a lubricating film consisting of a variety of reaction products [42-44]. The introduction of a solid lubricant into the liquid / semi solid lubricant brings about a further improvement in wear behavior by increasing the stability of the film. It looks logical for an optimum quantity of the (solid/liquid) lubricating constituents to exist in the (lubricant) mixture leading to the best wear performance of materials. The optimum of course may vary with material characteristics as well as operating conditions and, above all, the nature of the lubricating constituents. This is in view of the fact that the lubricant mixture should not lose adherence with the contacting surface and, at the same time, it should have enough lubricating characteristics. The question of losing adherence arises when the mixture become too dry, i.e., when the quantity of the solid lubricating phase in the mixture becomes too much to cause tearing-off the thick and dry lubricating film. Subcritical quantity of the solid lubricating phase reduces the probability of forming a stable lubricating film on the contacting surfaces. Accordingly, either side of the content of the solid lubricant constituent phase in the lubricant mixture may deteriorate the wear response of materials.

Having discussed the role of various material and operating variables on wear behavior, we will be able to better understand the observed wear response of the samples in this investigation.

The addition of graphite to oil lubricants increased the possibility of the formation of a more stable lubricating film causing further in the wear rate. However, this could be realized that for the (7-10 µm) size of graphite particle in the oil, minimum wear rate was obtained.

4.2.2. Frictional Heating

Increasing rate of frictional heating with test duration could be attributed to the increasing effective area of contact thereby reducing the severity of wear condition. A higher rate of temperature rises in some cases towards the end of the tests owing to the sticking /adhering tendency of the specimen material to the disc surface. A more severe wear condition, due to increasing applied load, led to a higher increase in the rate of temperature. The matrix alloy exhibited the generation of least frictional heat due to its excellent lubricating tendency. The abrasion caused by the fragmented dispersoid SiC particles caused larger frictional heating than the matrix alloy [9, 10]. The presence of the lubricant leading to the formation of a more stable lubricating film substantially reduced the temperature increase over dry wear. The addition of graphite further decreased the frictional heating through the formation of a still more stable lubricating film. The matrix alloy was most favorably affected in this case in view of the major constituent being solid lubricating in nature.

4.2.3. Friction Coefficient

The probability of more effective formation of a lubricant film caused the friction coefficient to decrease with an increase in the load. The abrasion caused through the entrapped dispersoid phase after fragmentation during wear led to higher friction coefficient of the composite than matrix alloy. More effective formation of lubricating film in the presence of liquid /liquid + solid lubricant led to a reduced friction coefficient. The lack of cracking tendency in the matrix alloy led to its reduced friction coefficient considerably under identical test conditions. Least friction coefficient in the event of adding graphite particle in the lubricating oil could be attributed to the formation of most stable lubricating film.

An appraisal of the observations made in this study clearly suggests varying effects of parameters like cracking tendency, lubricating characteristics, thermal stability, etc. of material constituents and experimental parameters like load and conditions. The overall effect of the parameters on the wear behavior of the samples seems to be complex in nature.

5. Conclusion

Based on the observations made in this study, the following conclusions could be drawn:

- The Matrix Alloy depicts plate shaped eutectic silicon and the other intermetallic phases while the composite revealed the presence of the dispersed SiC particles in addition to the features of the matrix alloy.
- The density was the least for aluminium-based (matrix) but the composite exhibited the maximum hardness.
- Wear Rate increased with load and speed. Testing the samples in oil plus graphite lubricated conditions led to less wear rate than that in oil alone. Addition of 5 wt% graphite (7-10 µm) to the oil lubricant led to minimum wear rate. The composite exhibited lowest wear rate while it was the maximum for the matrix alloy.
- Frictional heating increased with load and test duration; the frictional heating increased at a higher rate initially

followed by a lower rate of increase at longer test durations. Testing the samples in oil plus graphite lubricants led to a marginal change in frictional heating.

- The friction coefficient decreased with test duration. Testing the samples in oil lubricated conditions decreased the friction coefficient of the samples especially at low loads. Test duration had a mixed influence on friction coefficient. The addition of graphite to the lubricating oil further reduced the coefficient of friction. No definite influence of the graphite content (to the oil) on friction coefficient of the materials was noted.

References

[1] B. K. Prasad, A. H. Yegneswaram, A. K. Patwardhan, “Characterization of the wear response of a modified zinc-based alloy vis-à-vis a conventional zinc-based alloy and a bearing bronze at a high sliding speed”. Metallurgical & Material Transaction A, Vol. 27A (1996) 3513-3523.

[2] B.K. Prasad, “Mechanical Properties & Sliding Wear Characteristics of Zinc Based Alloys: Effects of Partially Substituting Copper by Silicon”. Zeitschrift fur Metallkunde, Vol. 88 (1997) 929-933.

[3] B. K. Prasad, “Tensile Properties of Some Zinc Based Alloys Comprising 27.5% Al: Microstructure & Test conditions”. Materials Science & Engineering A, Vol. 245A (1998) 257-266.

[4] B. K. Prasad, A.K. Patwardhan and A.H. Yegneswaram, “Microstructural Modifications through Compositional alterations and their Influence on the Mechanical and Sliding Wear Properties of Zinc-Based Alloys”. Scripta Materiallia, Vol.37 (1997) 323-328.

[5] B.K. Prasad, A.K. Patwardhan and A.H. Yegneswaram, “Microstructure- Property characterization of some zinc based alloys: Effect of heat treatment parameters”. Zeitschrift fur Metallkunde Vol. 87 (1996) 967-972.

[6] B.K. Prasad, “Response of Some Cast Zinc 37.5% Al Based Alloys Comprising Nickel/Silicon under Different Tensile Loading Conditions”. Journal of Materials Engineering and Performance, Vol. 7 (1998) 632-636.

[7] B.K. Prasad, “Effect of Microstructure on the Sliding Wear Performance of a Zn-Al-Ni Alloy”. Wear, Vol. 240 (2000) 100-112.

[8] H.X. Zhu and S.K. Liu, “Mechanical Properties of Squeeze Cast Zinc Alloy Matrix Composites Containing α-Alumina Fibers” Composites, Vol. 24 (1993) 437-442.

[9] B.K. Prasad, S.Das, O.P. Modi, A.K. Jha, R. Dasgupta, A.H. Yegneswaram, “Wear Response of a Zinc-Based Alloy in the Presence of SiC Particle Reinforcement: A Comparative Study with a Copper Base Alloy”. Journal of Materials Engineering and Performance, Vol. 8 (1999) 693-700.

[10] B.K. Prasad, A.K. Jha, S. Das, O.P. Modi, R. Dasgupta and A.H. Yegneswaram, “Sliding wear response of a Zinc Aluminium alloy as affected by SiC particle dispersion and test condition”. Journal of Materials Science Letters, Vol. 18, (1999) 1731-1734.

[11] B.K. Prasad, A.K. Jha, O.P. Modi, S. Das and Yegneswaram, “Abrasive Wear Characteristics of a Zn - 37.2 Al - 2.5 Cu - 0.2 Mg Alloy Dispersed with Silicon Carbide Particles”. Materials Transactions of Japan Institute of Metals, Vol. 36 (1995) 1048-1057.

[12] B.K. Prasad, S. Das, A.K. Jha, O.P. Modi, R. Dasgupta and A.H. Yegneswaram, “Factors Controlling the Abrasive Wear Response of a Zinc-Based Alloy Silicon Carbide Particle Composite” Composites A, Vol. 28A (1997), 301-308.

[13] B.K. Prasad, “Abrasive Wear Characteristics of a Zinc-Based Alloy and Zinc-Alloy/SiC Composite”. Wear, Vol. 252 (2002) 250-263.

[14] B. K. Prasad, “Effects of Alumina Dispersion on the Erosive-Corrosive Wear Response of a Zinc-Based Alloy under Changing Slurry Conditions and Distance” Wear, Vol. 238 (2000) 150-158.

[15] B.K. Prasad, A.K. Patwardhan and A.H. Yegneswaram, “Wear characteristics of a Zinc based alloy compared with a conventional bearing bronze under mixed lubrication condition: Effects of material & test parameters” Canadian Metallurgical Quarterly, Vol. 40 (2001)193-210.

[16] B.K. Prasad, “Effects of Heat Treatment on the Partially Lubricated Sliding Wear Behaviour of a Zinc-Based Alloy” Materials Transactions of Japan Institute of Metals, Vol. 40 (1999) 578-585.

[17] S. W. Kima, U. J. Leea, S. W. Hana, D. K. Kima and K. Ogib, “Heat treatment and wear characteristics of Al/SiCp composites fabricated by duplex process”. Composites: Part B, Vol. 34 (2003) 737–745.

[18] R.K. Uyyuru, M.K. Surappa and S. Brusethaug, “Effect of reinforcement volume fraction and size distribution on the tribological behavior of Al-composite/brake pad tribo-couple”. Wear, Vol. 260 (2006) 1248–1255.

[19] S. Zhang and F.Wang, “Comparison of friction and wear performances of brake material dry sliding against two aluminum matrix composites reinforced with different SiC particles”. Journal of Materials Processing Technology, Vol.182 (2007)122–127.

[20] R.N. Rao, S. Das, D.P. Mondal and G. Dixit, “Dry sliding wear behaviour of cast high strength aluminium alloy (Al–Zn–Mg) and hard particle composites”. Wear, Vol. 267 (2009)1688–1695.

[21] R.N. Rao, S.Das, D.P.Mondal and G.Dixit, “Effect of heat treatment on the sliding wear behaviour of aluminium alloy (Al–Zn–Mg) hard particle composite”. Tribology International, Vol. 43 (2010) 330–339.

[22] S. Suresha and B.K. Sridhara, “Effect of addition of graphite particulates on the wear behaviour in aluminium-silicon carbide-graphite composites”. Materials and Design, Vol. 31, (2010)1804-1812.

[23] R.N. Rao and S. Das, “Effect of matrix alloy and influence of SiC particle on the sliding wear characteristics of aluminium alloy composites”. Materials and Design, Vol. 31 (2010) 1200–1207.

[24] G. Naveen Kumar, R. Narayanasamy, S. Natarajan, S.P. Kumaresh Babu,K. Sivaprasad and S. Sivasankaran, “Dry sliding wear behaviour of AA 6351-ZrB2 in situ composite at room temperature”. Materials and Design, Vol.31 (2010) 1526–1532.

[25] R.N. Rao and S. Das, “Effect of SiC content and sliding speed on the wear behaviour of aluminium matrix composites”. Materials and Design, Vol. 32, (2011)1066–1071.

[26] G.B. Veeresh Kumar, C.S.P. Rao and N. Several, “Studies on mechanical and dry sliding wear of Al6061–SiC composites”. Composites: Part B, Vol.43 (2012)1185–1191.

[27] M. Uthayakumar, S. Aravindan and K. Rajkumar, “Wear performance of Al–SiC–B4C hybrid composites under dry sliding conditions”. Materials and Design, Vol. 47 (2013) 456–464.

[28] Devaraju, A. Kumar, A. Kumaraswamy, B. Kotiveerachari, “Influence of reinforcements (SiC and Al2O3) and rotational speed on wear and mechanical properties of aluminum alloy 6061-T6 based surface hybrid composites produced via friction stir processing”. Materials and Design, Vol. 51 (2013) 331–341.

[29] E.R.Braithwaite and G.W. Rowe, "Principles and application of lubrication with solids". Scientific Lubrication, (1963) 92-110.
[30] Y. Ttsuya, R. Takagi, "Lubricating properties of lead films on copper". Wear, Vol. 7 (1964) 131-143
[31] Rac, "Influence of load and speed on wear characteristics of grey cast iron in dry sliding — selection for minimum wear". Tribology International, Vol 18 (1985) 29-33
[32] E. Takeuchi, "The mechanisms of wear of cast iron in dry sliding" Wear, Vol. 11 (1968) 201–212.
[33] R.S. Montgomery, "The mild wear mechanism of nodular iron". Wear, Vol. 13 (1969) 337–343.
[34] F. Wilson, T.S. Eyre, "Effect of matrix structure and hardness on the wear characteristics of an S.G. cast iron". Wear, Vol. 14 (1969) 107–117.
[35] M. Kawamoto, K. Okabayashi, "Study of dry sliding wear of cast iron as a function of surface temperature". Wear, Vol. 58 (1980) 59-95.
[36] Y. Zhang, Y. Chen, R. He, B. Shen, "Investigation of tribological properties of brake shoe materials — phosphorous cast irons with different graphite morphologies". Wear, Vol. 166 (1993) 179-186.
[37] E.P. Fordyce, C. Allen, "The dry sliding wear behaviour of an austempered spheroidal cast iron". Wear, Vol. 135 (1990) 265-278.
[38] J. Sugishita, S. Fujiyoshi, "The effect of cast iron graphites on friction and wear performance I: Graphite film formation on grey cast iron surfaces". Wear, Vol. 66 (1981) 209-221.
[39] P. W. Leach, D. W. Borland, "The unlubricated wear of flake graphite cast iron". Wear, Vol. 85 (1983) 257-266.
[40] Y.S. Lerner and G.R. Kingsbury, "Wear Resistance Properties of Austempered Ductile Iron". Journal of Materials Engineering and Performance, Vol. 7(1) (1998) 48-52.
[41] S.M.A. Boutorabi, J.M. Young, V. Kondic, M. Salehi, "The tribological behaviour of austempered spheroidal graphite aluminium cast iron". Wear, Vol. 165 (1993) 19-24.
[42] D.A. Rigney, L.H. Chen, M.G.S. Naylor, A.R. Rosenfield, "Wear processes in sliding systems". Wear, Vol.100 (1984) 195-219.
[43] F. P. Bowden and D. Tabor, "The Lubrication by Thin Metallic Films and the Action of Bearing Metals". Journal of Applied Physics, Vol. 14 (1943) 141-151.
[44] G.D. Gamulya, I.L. Lebedeva, Yu.V. Vvedensky, T.P. Yukhno, "Secondary structure formation and wear mechanisms for solid lubricant coatings under friction in vacuum". Wear, Vol. 171 (1994) 143-148.

JJMIE

Volume 8 Number 6, December 2014
ISSN 1995-6665
Pages 359 - 367

Jordan Journal of Mechanical and Industrial Engineering

On Phase Equilibria of Sn-Sr and Mn-Sn-Sr Systems

Mohammad Aljarrah[a *], Atef Alkhazali[a], Suleiman Obeidat[a], Ahmad Almagableh[b], and Mahmoud Rababah[b]

[a] *The Hashemite University, Industrial Engineering Department, Zarqa 13115, Jordan*

[b] *Mechanical Engineering Department, Faculty of Engineering, The Hashemite University, Zarqa 13115, Jordan*

Received 16 Jul 2014 *Accepted 21 Oct 2014*

Abstract

Sn-Sr system is critically evaluated and the most reliable experimental data are incorporated in thermodynamic modeling. Thermodynamic properties of the binary liquid solution are estimated using the modified quasichemical model (MQM). The optimized Sn-Sr phase diagram and the corresponding thermodynamic properties are found to be in fair agreement with the experimental data in the previous related literature. For all the compounds in Sn-Sr system, a comparison between the calculated enthalpy of formation and that calculated by Miedema and first-principles has been reported. Combining Sn-Sr with the self-established thermodynamic database of Mn-Sr and Mn-Sn was used to calculate liquidus projection of Mn-Sn-Sr ternary system.

Keywords: *Modified Quasichemical Model, Magnesium Alloys, Thermodynamic Modeling*.

1. Introduction

Magnesium alloys have a great potential for structural applications because of their significant weight savings, superior damping capacity and good castability [1]. Therefore, the automotive industry leads the way in the growing interest in Mg alloys in order to decrease fuel consumption and reduce emissions [1-3]. Recently, research activities have been carried out to improve the elevated temperature properties of the magnesium alloys through precipitation hardening and/or solid solution hardening [4-8]. The most common magnesium alloys for automotive industry contain aluminum as a major alloying element (AZ91 and AM60). Aluminum improves the mechanical properties at room temperature; however the loss of the mechanical strength at service temperature (above 120°C) of Mg alloys is reported due to the discontinuous precipitation of γ-$Mg_{17}Al_{12}$ [9-15]. Alloying Mg with Ca, Zn, Sr, Mn and Sn are found to improve the elevated temperature properties of Al containing Mg alloys by delaying or inhibiting the formation of γ and/or precipitating of thermally stable compounds such as Al_2Ca or Al_4Sr intermetallic phase [9-19]. Strontium is an important element in multi-component magnesium and aluminum alloys. Alloying magnesium with strontium refines the microstructure and improves the mechanical properties. Moreover, Sr enhances the corrosion resistance of Mg and Al-based alloys [20-23]. On the other hand, tin addition to magnesium based alloys has a potential to improve creep and corrosion resistance of these alloys. Tin is also a reasonably cheap element as compared to RE elements and has a low melting point and is known to improve castability [24-26]. Mn addition to Mg-Sr alloys enhances creep resistance by precipitation of α-Mn at the interdendritic regions and Mn dissolves in the Mg matrix and $Mg_{17}Sr_2$ phase [27, 28].

An understanding of thermodynamic characteristics and equilibrium phase diagram for magnesium and its alloys will allow a better control in developing and designing a new Mg-alloy with desired properties. The present study deals with thermodynamic modeling of the Mn–Sn-Sr system which is one of the important systems in Mg-Mn multi-component systems. Sn-Sr binary system will be critically evaluated and optimized using the available phase equilibrium and thermodynamic data. The latest published journal article on thermodynamic modeling of the Sn-Sr system used Bragg-Williams model [29]. In their work [29], the enthalpies of formation for the stoichiometric compounds at 0 K were computed by first-principles calculations. In the present study, this system will be optimized using the modified quasi-chemical model (MQM). The MQM is considered more physically sound than other models such as the associate solution model [30]. Sn-Sr and Mn-Sr binary systems have been optimized using most up-to-date experimental data. Each of the phases in any binary system has been critically assessed based on the thermodynamic properties.

[*] Corresponding author. e-mail: maljarrah@hu.edu.jo.

In this research article, the experimental phase diagram and thermodynamic properties of Sn-Sr binary system will be critically evaluated and the most reliable data will be used in optimization. Sn-Sr phase diagram will be optimized and combined with the self-established thermodynamic database of the Mn-Sn and Mn-Sr systems. The optimized parameters of the constituent binary sub-systems will be used to draw liquidus projections of the Mn-Sn-Sr ternary phase diagram.

2. Experimental data

2.1. Sn-Sr phase diagram

Ray [31] tracks the thermal history of twelve tin-strontium alloys within the composition range of 0-29.65 at.% Sr using thermal analysis and optical microscopy. In Ray's study, alloys were prepared by electrolysis of a mixture of sodium and strontium chlorides over molten tin in an iron crucible. During electrolysis, strontium reacted with iron crucible and the fused salts were rapidly volatilized. Therefore, Ray's [31] thermal data were in error and will not be used in the current optimization. Phase equilibria of thirteen tin-strontium alloys were investigated by Marshall and Chang [32] using DTA, XRD and optical microscopy from pure tin up to 65 at.% Sn. They reported that Sn_3Sr forms peritectically at 598±1^{0}C which is in contrast with the work of Ray who showed that Sn_3Sr melted congruently at 607^{0}C and forming a eutectic at 26.5 at% Sr and 580^{0}C. Marshall and Chang also reported that Sn_4Sr is in equilibrium with Sn instead of Sn_5Sr as reported by Ray [31] and Sn_4Sr decomposes peritectically at 334±4^{0}C. They [32] found that Sn_4Sr and Sn form an eutectic at 230±2^{0}C and 1 at.% Sr. Widra and Schafer [33] studied Sn-Sr phase diagram in the composition range of 35-100 at.% Sr using DTA and XRD. Five intermetallic compounds, which are Sr_2Sn, Sr_5Sn_3, SrSn, $SrSn_3$ and $SrSn_5$, were reported in their phase diagram, of which only the first four phases were melted congruently. The assessment proposed by Massalski *et al.* [34] is the summary of the work of Marshall and Chang [32], and Widra and Schafer [33]. In the composition range of 11.6 to 43 at.% Sr, Hoffmann *et al*. [35,36] tracked phase transformation temperatures during cooling and heating for seven Sn-Sr alloys using DTA. Phase stability of Sr_3Sn_5 intermetallic compound were shown from the works of Hoffmann *et al*. [35,36] and Zürcher *et al*. [37]. The phase equilibria over the whole composition range in the Sn-Sr system were investigated by Palenzona and Pani [38] using XRD, DTA and optical composition. According to their work, five intermetallic compounds were confirmed namely; Sr_2Sn, SrSn, Sr_5Sn_3, $SrSn_3$ and $SrSn_4$, where, Sr_2Sn and SrSn melt congruently. In their work, three eutectic reactions were detected in the Sr-Sn system and $SrSn_4$ was confirmed instead of $SrSn_5$ as reported by Ray [31] and Widra and Schafer [33]. Experimental phase diagram data of Palenzona and Pani [38] and Hoffmann and Fassler [37] were in agreement. Those experimental data were the most recent and in good agreement; therefore, they will be used in the current optimization. Crystal structures of the compounds in the Sn-Sr system were reported by [35-37, 39-45].

Limited thermodynamic data for the Sn–Sr system could be found in previous literature. Strontium is highly reactive and, hence, it is very difficult to handle the alloys during high temperature experiments. However, enthalpy of mixing of the Sn-Sr liquid was measured by Esin *et al*. [46] using high temperature calorimeter at 1773 K within the composition range from 0 – 50 at.% Sr. Enthalpy of mixing from Esin *et al*. [46] will be used in the current optimization. Morozova *et al*. [47] estimated the enthalpy of formation of $SrSn_2$ compound to be -82.7±1 kJ/mole.atom at 25^{0}C. Zhao *et al*. [29] calculated the enthalpy of formation for all compounds in the Sn-Sr system using first-principles method and Miedema model and these data will be used only for comparison. Activity of Sr in Sn-Sr system was measured by Klebanov *et al.* [48] at 900 K.

2.2. Mn-Sr System

Based on the experimental data of Obinata *et al.* [49], Peng *et al*. [50] modeled all phases in the Mn-Sr binary system as completely disordered solutions. In order to construct a self-consistent thermodynamic database of the Mn-Sn-Sr ternary system, the optimized parameters of Mn-Sr binary system by Aljarrah *et al*. [56] will be adopted in the current calculations.

2.3. Mn-Sn-Sr Ternary System

There is no experimental data for Mn-Sn-Sr system could be found in the literature.

3. Thermodynamic Modeling

3.1. Pure Elements

The Gibbs free energy of a pure element with a certain structure φ is described as a function of temperature as:

$$^{\circ}G_A^{\varphi}(T) = a + bT + cT\ln T + dT^2 + eT^3 + fT^{-1} + gT^7 + hT^{-9}$$

The parameters *a* through *h* are taken from the SGTE compilation by Dinsdale [51].

3.2. Stoichiometric Compounds

The intermetallic compounds in the Sn-Sr phase diagram are considered stoichiometric and the Gibbs free energy of these compounds is described by the following equation:

$$G^{phase,\ \varphi} = x_i\,^{\circ}G_i^{\varphi} + x_j\,^{\circ}G_j^{\varphi} + \Delta G_f$$

Where $^{\circ}G_i^{\varphi}$ and $^{\circ}G_j^{\varphi}$ denote Gibbs free energy of element *i* and *j* in their standard state and $\Delta G_f = a + bT$ is the Gibbs energy of formation of the stoichiometric compound. Where a and b are the model parameters to be optimized based on experimental data of phase equilibria and thermodynamic properties.

3.3. Liquid Phase

In the present work, the liquid phase is modeled using the MQM where the pair approximation is utilized to describe the short range ordering in the liquid. A detailed description of the MQM for binary and multi-components solutions is available elsewhere [52-54]. Only a brief description will be presented here. The molar Gibbs energy of the liquid phase, derived from the modified quasichemical theory [52], is described by the following equation:

$$G^{liq} = n_i\,{}^{\circ}G_i^{liq} + n_j\,{}^{\circ}G_j^{liq} - T\Delta\Delta^{config} + \frac{n_{ij}}{2}\Delta^{exs}G^{liq}$$

Where n_i and n_j are the number of moles of the component i and j, n_{ij} is the number of (i-j) pairs, ΔS^{config} is the configurational entropy of mixing given for randomly distributing the (i-i), (j-j), and (i-j) pairs.

$$\Delta S^{config} = -R[n_i \ln(x_i) + n_j \ln(x_j)] - R[n_{ii} \ln(\frac{x_{ii}}{y^2_i}) + n_{jj} \ln(\frac{x_{jj}}{y^2_j}) + n_{ij} \ln(\frac{x_{ij}}{2y_i y_j})]$$

Where x_i and x_j are the overall mole fractions of the components i and j, respectively.

4. Results and Discussions

4.1. Sn-Sr Phase Diagram

Figure 1 shows the calculated Sn-Sr phase diagram in relation with the experimental data from the previous literature. A good agreement with the liquidus line between the calculated values in this work and the experimental values of Palenzona and Pani [38], Marshall and Chang [32], and Hoffman [35] is found in Figure 1. The calculated invariant points of Sn-Sr phase diagram in comparison with the experimental data are listed in Table 1. The activity of Sr in Sn-Sr liquid reported by Klebanov *et al*. [48] was used in the optimization of the Sn-Sr system. Comparison between the calculated activity of Sr from Klebanov *et al.* [48] is shown in Figure 2. The calculated activity shows a good agreement with the experimental data. The optimized model parameters of the stable phases in the Sn-Sr binary system are summerized in Table 2.

The data of enthalpy of mixing by Esin *et al*. [46] was used in the optimization and matched the calculated enthalpy of mixing curve seen in Figure 3. As can be seen from this figure, the calculated enthalpy of mixing of liquid Sn-Sr is in fair agreement with the experimental data. The lowest point of the curve is located where thermally high stable compounds are formed. This indicates stronger atomic interactions in the liquid at the composition of the intermetallic compounds.

Figure 4 shows a comparison between the calculated enthalpy of formation for all phases in Sn-Sr system and that reported by Zhao *et al*. [29]. The current enthalpies of formation for intermetallic compounds are in fair agreement with that obtained by Miedema model.

4.2. Mn-Sn-Sr Ternary System

The Gibbs energy of the liquid phase was calculated using the symmetric Kohler-like approximation [55] with no ternary interaction parameters for the liquid phase. The invariant reactions for the Mn-Sn-Sr system are listed in Table 3. The liquidus projection of the Mn-Sn-Sr ternary system is shown in Figure 5. The miscibility gap covers most of the composition triangle, as shown in Figure 5. Since there is no ternary experimental data available for the entire Mn-Sn-Sr system, it is possible that the size of the miscibility gap is over or underestimated by the extrapolation.

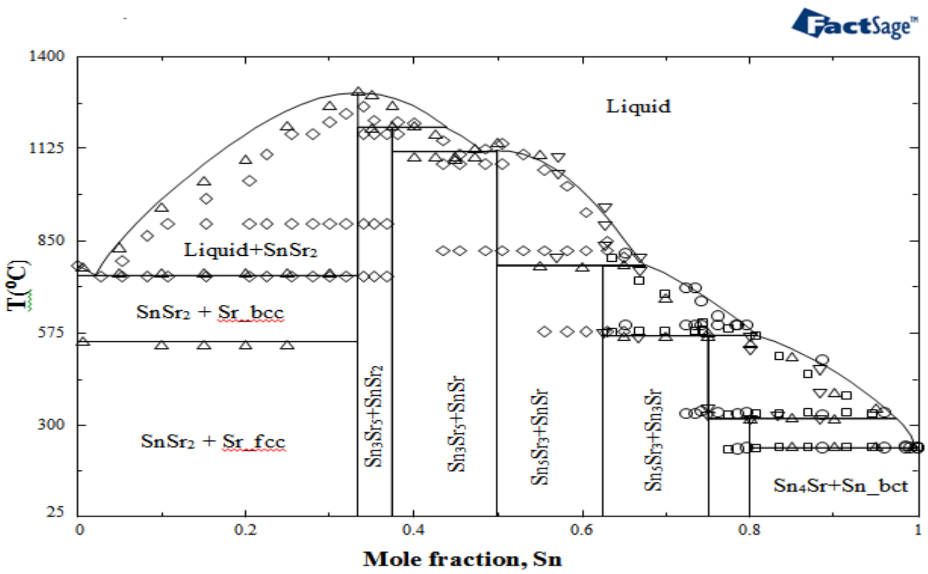

Figure 1. Re-optimized Sn-Sr phase diagram in comparison with experimental data from literature: Palenzona and Pani △ , Marshall and Chang ○ , Ray □ , Widra and Schafer ◇ and Hoffman ▽

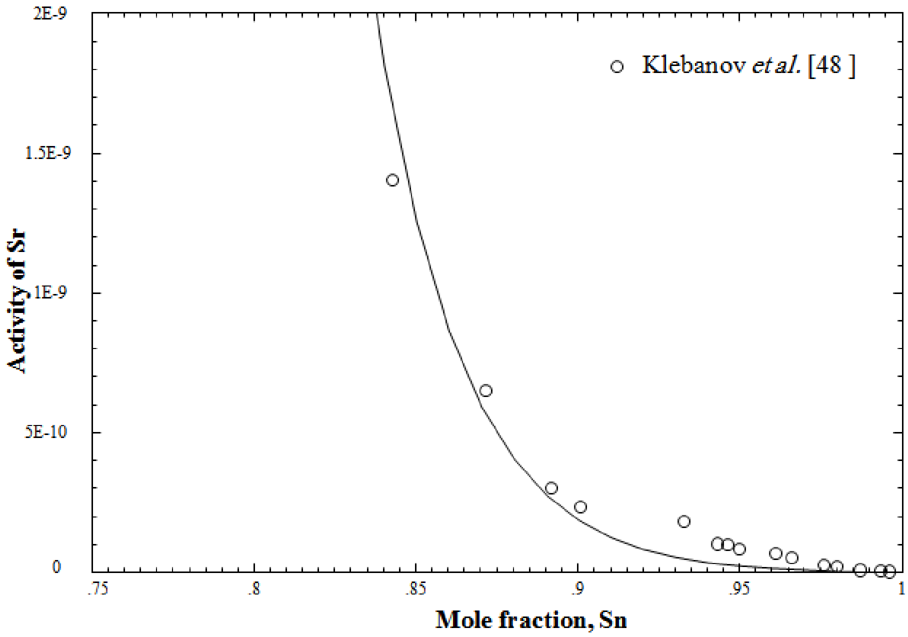

Figure 2. Plot of calculated activity of Sr against mole fraction Sn for the Sn-Sr liquid at 900 K in comparison with experimental data of Klebanov et al. [48]

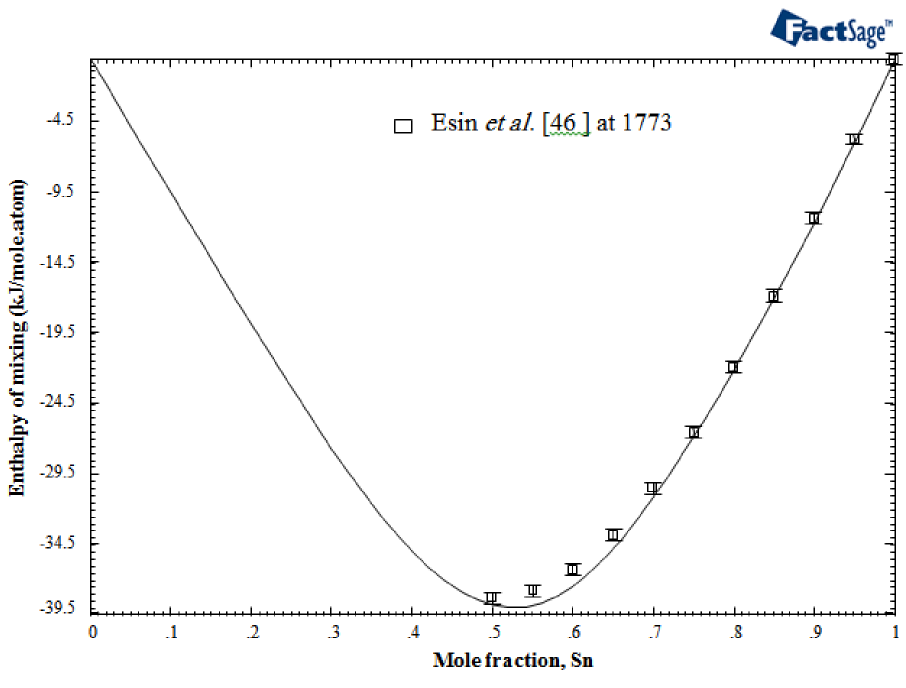

Figure 3. Calculated enthalpy of mixing against mole fraction Sn for the Sn-Sr liquid at 1773 K in comparison with the experimental data of Esin et al. [46]

Table 1: Comparsion between calculated and experimental values of the invariant reactions in the Sn-Sr system.

Reaction type	Reaction	Composition (at.%Sn)	T(^{0}C)	Reference
		2.22	741	This work
Eutectic	Liquid ↔ Sr_BCC + Sr_2Sn	2.7	745	[33]
		2.5	752 ± 5	[38]
		33.3	1288	This work
Congruent	L1↔ Sr_2Sn		1295± 5	[38]
			1255	[33]
		37.5	1185	This work
Pereticitic	Liquid + Sr_2Sn↔ Sr_5Sn_3	39.9	1190 ± 5	[38]
		36.7	1170	[33]
		50	1141	This work
Congruent	L1↔ SrSn	50	1140	[33]
		50	1140 ± 5	[38]
		62.5	776	This work
		65	775 ± 5	[38]
Pereticitic	Liquid + SrSn↔ Sr_3Sn_5		780	[36]
			810	[37]
		75	557	This work
		79.7	598±1	[32]
Pereticitic	Liquid + Sr_3Sn_5↔ $SrSn_3$		563	[36]
			560± 5	[38]
		73.5	580	[31]
		80	320	This work
		95.1	338	Ray
Pereticitic	Liquid + $SrSn_3$↔ $SrSn_4$	96	334±4	[32]
		95.8	315±5	[38]
			316	[36]
Eutectic	Liquid ↔ Sn_BCC + $SrSn_4$	99.8	231	This work
		99.7	232	[31]
		99	230±2	[32]
		99	230±5	[38]
			212	[32]
Eutectic	Liquid ↔ SrSn + Sr_5Sn_3	48.7	1144	This work
		45.6	1100±5	[38]
		46.1	1080	[33]

Table 2: Optimized parameters of all phases in Sn-Sr and Mn-Sr systems.

Phase		Thermodynamic parameters
Liquid	Sn-Sr Liquid	$Z^{Sn}_{SnSr} = 5;\ Z^{Sr}_{SnSr} = 5$
		$\Delta g^{0}_{SnSr} = -2127.2 - 1.55T;\ \Delta g^{10}_{SrSn} = -478 - 2.39T$
		$\Delta g^{01}_{SrSn} = -1.43T$
Sn-Sr intermetallic phases	SrSn	$^{\circ}G^{SrSn}_{298.15K} = -93500 + 8.13\mathrm{T}$
	Sr_2Sn	$^{\circ}G^{Sr2Sn}_{298.15K} = -80666.7 + 17.4\mathrm{T}$
	$SrSn_3$	$^{\circ}G^{SrSn3}_{298.15K} = -59500 + 0.78\mathrm{T}$
	Sr_5Sn_3	$^{\circ}G^{Sr5Sn3}_{298.15K} = -90875 + 8\mathrm{T}$
	$SrSn_4$	$^{\circ}G^{SrSn5}_{298.15K} = -47880 + 0.61\mathrm{T}$
	Sr_3Sn_5	$^{\circ}G^{Sr3Sn5}_{298.15K} = -83375 + 1.05\mathrm{T}$

Table 3. The calculated enthalpies of formation for all the stable compounds in the Sn–Sr system in comparison with literature.

Compound	Miedema Model	First-principle method	MQM
$SnSr_2$	−68.02	−63.40	-66.00
Sn_3Sr_5	−75.47	−64.47	-75.75
SnSr	−90.55	−68.88	-90.00
Sn_5Sr_3	−88.83	−57.93	-83.38
Sn_3Sr	−67.84	−41.74	-59.5
Sn_4Sr	−55.32	−33.96	-47.88

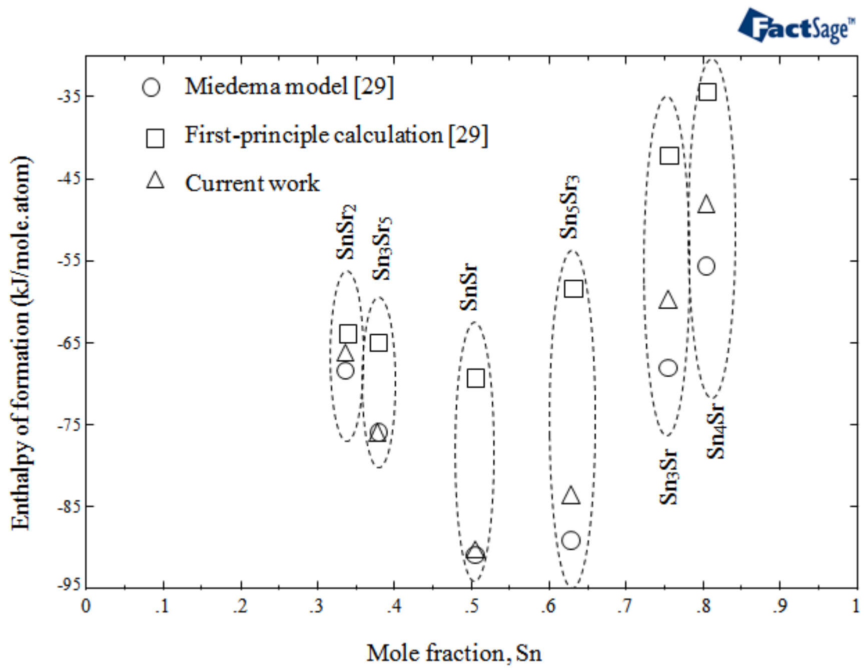

Figure 4. The calculated enthalpy of formation of all intermetallic compounds in comparison with work of Zhao *et al*. [29].

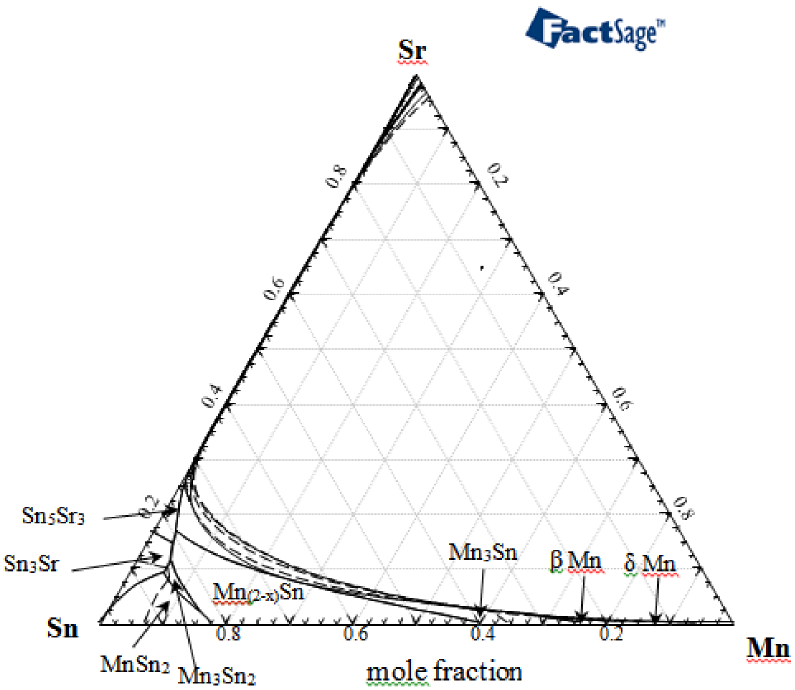

Figure 5. Liquidus projection of Mn-Sn-Sr ternary phase diagram

5. Conclusions

The experimental phase diagram data and thermodynamic properties of the Sn-Sr binary system was evaluated and optimized to obtain self-consistent model parameters for the Gibbs energy of all phases. The calculated liquidus line of Sn-Sr phase diagram was compared with the experimental data and found to be in a good agreement. The calculated thermodynamic properties such as activity and enthalpy of mixing of the Sn-Sr system were in accord with the experimental data in the literature. By combining self-consistent set of optimized parameters of the phases of the constituent binary sub-systems, liquidus projection of the ternary Mn-Sn-Sr phase diagram was obtained.

6. Acknowledgment

Financial support from the Deanship of Scientific Research and Graduate Studies, The Hashemite University, Jordan, is gratefully acknowledged. Authors would like to thank Prof. M. Medraj, Mechanical and Industrial Engineering Department, Concordia University, Canada, for useful discussions and suggestions.

References

[1] E. F. Emely "*Principles of Magnesium Technology"*, Pergamon Press Ltd., New York,1966.
[2] H. Mao, *et al.*, "Microstructural Characteristics of Die Cast AZ91D and AM60 Magnesium Alloys," *SAE Technical Paper*, 1999.
[3] R. Gradinger and P. Stolfig, "Magnesium wrought alloys for automotive applications," in *Proceedings of the Minerals, Metals & Materials Society (TMS)*, (2003), pp. 231-236.
[4] E. Aghion, *et al.*, "Dead sea magnesium alloys newly developed for high temperature applications," in *Proceedings of the Minerals, Metals & Materials Society (TMS)*, (2003), pp. 177-182.
[5] M. O. Pekguleryuz, *et al.*, "Creep resistant Mg-Al-Sr alloys," *J. Adv. Mater.*, Vol. 35 (2003), pp. 32-38.
[6] E. Ma and J. Xu, "The glass window of opportunities," *Nat. Mater.*, Vol. 8 (2009), pp. 855-857.
[7] Humble P., "Toward a cheap creep resistant magnesium alloy", *Material forum*, 21 (1997), pp. 45-56.
[8] Greenfield P., "Magnesium", Mills and Boo Limited, London, pp. 7-19, 1972.
[9] A.A. Luo, "Recent magnesium alloy development for elevated temperature applications", International Materials Reviews, Vol 49 (2004) No. 1, 13-30.
[10]M. Pekguleryuz, M. Celikin, "Creep Mechanisms in Magnesium Alloys", Int. Mater. Rev., Vol. 55 (2010) No. 4, pp. 197-217.
[11] A. Suzuki, N.D. Saddock, J.W. Jones, T.M. Pollock, "Solidification paths and eutectic intermetallic phases in Mg–Al–Ca ternary alloys" Acta Mater., Vol. 53 (2005), pp. 2823–2834.
[12] M. Celikin, F. Zarandi, M. Pekguleryuz, "Compressive Creep and Texture Evolution in Cast-Pure Magnesium at Stresses above the Yield Strength," Can. Met. Quart. Vol.48 (2009), No. 4, pp. 419-432
[13] N. Ishimatsu, Y. Terada, T. Sato, K. Ohori, "Internal Stress during Creep in a Die-Cast AM50 Magnesium Alloy at 473 K", Materials Transactions, Vol. 47 (2006), No. 10, pp.2493-2496
[14]I.P. Moreno, T.K. Nandy, J.W. Jones, J.E. Allison, T.M. Pollock, "Microstructural stability and creep of rare-earth containing magnesium alloys", Scripta Materialia, Vol. 48 (2003), 1029–1034

[15] J. Zhang, K. Liu,D. Fang, X. Qiu, D. Tang, J. Meng, "Microstructure, tensile properties, and creep behavior of high pressure die-cast Mg-4Al-4RE-0.4Mn (RE=La, Ce) alloys", J. Mater Sci, Vol. 44 (2009) No. 8, 2046−2054

[16] M. Aljarrah "Thermodynamic modeling and experimental investigation of the Mg-Al-Ca-Sr system" Ph.D. thesis 2008, Concordia University, Montreal, QC, Canada.

[17] A. Janz, Thermodynamics and constitution of quaternary Mg-Al-Ca-Sr and the extension to the quinary Mg-Al-Ca-Sr-Mn system, Ph.D. Thesis, Clausthal University of Technology, TU Clausthal, Germany, 2008.

[18] M. Aljarrah, M.A. Parvez, J. Li, E. Essadiqi, M. Medraj, "Microstructural characterization of Mg–Al–Sr alloys", Science and Technology of Advanced Materials, Vol. 8 (2007) No. 4, 237-248.

[19] M. Aljarrah, M. Medraj, X. Wang, E. Essadiqi, A. Muntasar, G. Denes, "Experimental investigation of the MgAlCa system", Journal of alloys and compounds, Vol. 436 (2007) No. 1, 131-141

[20] M.B. Yang, F.S. Pan, R.J. Cheng, J. Shen, "Comparison about effects of Sb, Sn and Sr on as-cast microstructure and mechanical properties of AZ61-0.7Si magnesium alloy", [J]. Mater Sci Eng A, Vol. 489 (2008), No. 1/2, 413−418.

[21] S.K. Guan, S.J. Zhu, L.G. Wang, Q. Yang, W.B. Cao, "Microstructures and mechanical properties of double hot-extruded AZ80+*x*Sr wrought alloys", [J]. Transactions of Nonferrous Metals Society of China, Vol 17 (2007), No. 6, 1143−1151.

[22] M.B. Yang, J. Shen, L. Bai, F.S. Pan, "Effects of Sr on the microstructure, tensile and creep properties of AZ61-0.7Si magnesium alloy", [J]. Inter J Minerals, Metallurgy and Materials, Vol. 16 (2009), No. 1, 89−95.

[23] M.B. Yang, F.S. Pan, R.J. Cheng, A.T. Tang, "Effect of Mg-10Sr master alloy on grain refinement of AZ31 magnesium alloy", [J]. Mater Sci Eng A, Vol. 491 (2008) No. 1/2, 440−445.

[24] Dead Sea Magnesium Ltd., *High Strength and Creep Resistant Magnesium Alloys*, European Patent, EP 1 308 531 A1, 2003.

[25] A. Hitachi Ltd., *High Strength Mg Based Alloy and its Uses*, EP1 108799 A2, European Patent, 2001.

[26] L. Bowles, C. Blawert, N. Hort and K. U. Kainer, "Microstructural investigations of the Mg-Sn and Mg-Sn-Al alloys systems", Magnesium Technology (2004), TMS 2004, pp. 307-310.

[27] M. Celikin and M. Pekguleryuz, "The role of α-Mn precipitation on the creep mechanism of Mg-Sr-Mn", Material Science & Engineering A, Vol. 556 (2012), 911-920.

[28] M. Masoumi and M. Pekguleryuz, "Effect of Sr on the texture of rolled Mg-Mn-based alloys", Material letters, Vol. 71 (2012), 104-107.

[29] J. Zhaoa, Y. Du, L. Zhang, A. Wang, L. Zhou, D. Zhao, J. Liang, "Thermodynamic assessment of the Sn–Sr system supported by first-principles calculations", Thermochimica Acta 529 (2012) , 74– 79.

[30] A.D. Pelton, S.A. Degterov, G. Eriksson, C. Robelin, Y. Dessureault, The modified quasichemical model I-Binary solutions, Metall. Mater. Trans. B 31B (2000) 651–659.

[31] K.W. Ray, Properties of strontium–tin alloys, Ind. Eng. Chem. 22 (1930) 519–522.

[32] D. Marshall, Y.A. Chang, Constitution of the tin-strontium system up to 35 at.% Sr, J. Less-Common Met. 78 (1981) 139–145.

[33] A. Widera, H. Schafer, Das Zustandsdiagramm Sr–Sn und die Verbindung Sr_3SnO (The phase diagram of Sr–Sn system and the compound Sr_3SnO), J. Less-Common Met. 77 (1981) 29–36 (in German).

[34] T.B. Massalski (editor-in-chief), Binary Alloy Phase Diagrams, second ed., Vol.3, Materials Information Soc., Materials Park, OH, 1990.

[35] S. Hoffmann, Darstellung, Struktur und Eigenschaften von Stanniden sowie Tetrelid-Silicaten und Silicaten, Ph.D. Thesis, Humboldt-Universität, Berlin, 2002 (in German).

[36] S. Hoffman and T.F. Fassler, $SrSn_4$: a superconducting stannide with localized and delocalized bond character, Inorg. Chem., 42(2003), pp. 8748-8754.

[37] F. Zürcher, R. Nesper, S. Hoffmann, T.F. Fässler, Novel arachno-type X56- zintl anions in Sr_3Sn_5, Ba_3Sn_5, and Ba_3Pb_5 and charge influence on zintl clusters, Z. Anorg. Allg. Chem. 627 (2001) 2211–2219.

[38] A. Palenzona, M. Pani, The phase diagram of the Sr–Sn system, J. Alloys Compd. 384 (2004) 227–230.

[39] M.T. Klem, J.T. Vaughey, J.G. Harp, J.D. Corbett, A3Tt5 phases Sr_3Sn_5, Ba_3Pb_5, and La_3Sn_5. Structure and bonding in a series of isotypic metallic compounds with increased electron count and their comparison with the nominal zintl phase La_3In_5, Inorg. Chem. 40 (2001) 7020–7026.

[40] T.F. Fassler, S. Hoffmann, $SrSn_3$—eine superleitende Legierung mit freien Elektronenpaaren ($SrSn_3$—a superconducting alloy with non-bonding electron pairs), Z. Anorg. Allg. Chem. 626 (2000) 106–112 (in German).

[41] A. Widera, H. Schafer, Das Zustandsdiagramm Sr–Sn und die Verbindung Sr_3SnO (The phase diagram of Sr–Sn system and the compound Sr_3SnO), J. Less-Common Met. 77 (1981) 29–36 (in German).

[42] G. Bruzzone, E. Franceschi, On the occurrence of M_2X intermetallic compounds (M = Ca, Sr, Ba; X = Si, Ge, Sn, Pb), J. Less-Common Met. 57 (1978) 201–208.

[43] W. Dorrscheidt, A. Widera, H. Schäfer, Darstellung und Kristallstruktur von Sr_5Sn_3 und Ba_5Sn_3 (Preparation and crystal structure of Sr_5Sn_3 and Ba_5Sn_3), Z. Naturforsch., Teil B: Anorg. Chem., Org. Chem. 32B (1977) 1097–1099 (in German).

[44] W. Rieger, E. Parthé, Alkaline earth silicides germanides and stannides with CrB structure type, Acta Crystallogr. 22 (1967) 919–922.

[45] F. Merloa, M.L. Fornasini, CrB-type equiatomic compounds of europium, ytterbium and alkaline-earth metals with Si, Ge, Sn, Pb, J. Less-Common Met. 13 (1967) 603–610.

[46] Yu.O. Esin, V.V. Litovskii, S.E. Demin, M.S. Petrushevskii, Partial and integral enthalpies of formation of liquid alloys of strontium and barium with tin, Zh. Fiz. Khim. 59 (1985) 766–767 (in Russian).

[48] M.P. Morozova, M. Li, M.V. Golomolzina, Enthalpy of formation of the compounds of strontium with the elements of the main subgroup of group IV, Vestnik Leningradskogo Universiteta, Ser. Fiz. Khim. 14 (1959) 83–86 (in Russian).

[49] E.B. Klebanov, O.O. Tvaradze, A.G. Moroachevskii, Activity of strontium in molten alloys with tin, Izv. Vyssh. Uchebn. Zaved., Tsvetn. Metall. (1985) 106–107 (in Russian).

[50] I. Obinata, Y. Takeuchi, K. Kurihara, and M. Watanabe, "Alloys of Manganese and Silicon with Alkali and Alkaline-Earth Metals", Metallurgy, Vol. 19 (1965), 21-35

[51] Y. Peng, D. Zhao, B. Hu, L. Zhou, Y. Du, T. Gang, S. Liu and K. Chang, Thermodynamic modeling of the Sr-M (M=Fe, Mn, Ni, Ti, V) Systems, J Phase Equilib Diffus Vol. (2011), No. 1, 42-47.

[52] A.T. Dinsdale, SGTE Data for Pure Elements, CALPHAD Vol. 15 (1991) No. 4, 317-425.

[53] A.D. Pelton, P. Chartrand," The modified quasichemical model: Part II. Multicomponent solutions, Metall Mater Trans A, Vol. 32 (2001) No. 6,1355-1360.

[54] A.D. Pelton, M. Blander, Computer assisted analysis of the thermodynamic properties and phase diagrams of slags, in:

Proc. 2nd Int. Symp. On Metall. Slags and Fluxes, TMS-AIME, Warrendlae, PA, USA, (1984), 281-294.
[55] F. Kohler, Estimation of the thermodynamic data for a ternary system from the corresponding binary systems, Monats. Chem. Vol. 91 (1960), 738–740
[56] M. Aljarrah, S. Obaidat, Rami H. Fouad, M. Rababah and A. Almagableh, A. Itradat, "Thermodynamic Calculations of the Mn-Sn,Mn-Sr and Mg-Mn-{Sn, Sr} systems". Accepted in IET, 2014

JJMIE

Volume 8 Number 6, December 2014
ISSN 1995-6665
Pages 369 - 375

Jordan Journal of Mechanical and Industrial Engineering

Design, Construction and Evaluation of Chrysanthemum Flower Stem Cleaner Machine

Seyed Habib Hashemi Fard Dehkordi[a *], Parvin Jafarhassani Hanjani[b], Golam Reza Chegini[c]

[a] *Mechanical Engineering of Agricultural Machinery Department,, Dezful Branch, Islamic Azad University (IAU), Dezful, Iran.*

[b] *Department of Shahr-e-Kord Education, Shahr-e-Kord, Iran.*

[c] *Mechanical Engineering of Agricultural Machinery Department, Tehran University, Tehran, Iran.*

Received 14 Jul 2014 *Accepted 11 Dec 2014*

Abstract

The purpose of the present study is to design, construct and evaluate a prototype flower stem cleaner machine. Designing the processing equipments of agricultural products requires information about their physical and mechanical properties. In order to construct the design, the effect of leaf picking velocity and the tensile direction and location were studied on maximum picking force and energy. Results showed that picking force and deformation data ranged from 18 to 61 N and from 4.1 to 8.7 mm, respectively. The mean values of tangent modulus for top and bottom groups were 7.22 MPa and 10.1 MPa, respectively. The effect of the picking velocity, the location and stretch direction on the picking force and the tangent modulus was significant ($P = 0.01$). After measuring the physical and mechanical properties of stems, the machine were designed and constructed. Machine design is based on the use of the rotational axis hit with leaves, which causes leaves to release from the stem. The prototype consists of two axes: rubber fingers that are oriented at angles of 90 degrees on axes, and an axis distance control mechanism and transmission system. After completing the design and construction, the prototype was evaluated to determine the optimum operating conditions. For this purpose, the effects of rotational speed in five levels (200, 350, 500, 650, 800 rpm), axis distance in five levels (-10, -5, 0, +5, +10 mm) and hardness of fingers in two levels (30, 60 shore A) are studied. In the best condition, the machine is able to remove 100% of the leaves. Optimal working conditions happened with 500 rpm for rotational speed, -5 mm for axis distance and 60 shore A for finger hardness. The prototype had the capacity of twenty flower stems cleaning at an average time of 10 s.

Keywords: *Cleaner Machine, Chrysanthemum Flower, Picking, Leaf*.

Nomenclaures

Di	Axes distance (mm)
H	Finger hardness (shore A)
s	Speed (rpm)
m_s	Mass (kg)
n	Rotational speed (rpm)
A	Stem area (mm^2)
C	Stem diameter (mm)
E	Modulus of elasticity (MPa)
F	Force (N)
MC	Moisture of content (%)

1. Introduction

The intersection of art, design and horticulture, represented by the ornamental plant industry, has led to the use of a very wide variety of plant organs, such as cutting flowers for ornamental purposes [1].

Cut chrysanthemum flowers have a longer vase life than most other cut flowers. The loss of quality is mainly due to their leaves wilting [2] because of impeded water transport [3]. The water uptake and the rehydration of chrysanthemum stems have been facilitated by postharvest manipulations, such as immersion into detergent solution and cold water; the addition of antibacterial agents in the holding solution has been recommended [4]. Removing the stem leaves immediately after cutting can lead to retarding flower wilt, and, the subsequence may result in a longer vase life.

* Corresponding author. e-mail: maljarrah@hu.edu.jo.

A review of the literature revealed a lack in information on mechanical post harvesting system for removing leaves from cut chrysanthemum flowers, but many old research studies have been conducted on removing leaves and torn from rose flower. Chung invented a rose stem stripper that is accomplished by two metal arms. A rose stem is inserted between the pair of jaws where each jaw has a V-shaped opening, allowing only the rose stem to pass, and, thereby removing thorns and foliage [5]. A flower stem cleaning device including a body through which a cleaning opening extends was invented by Richardson. The opening is defined by a flexible surface portion of the body to prevent damage to the plant stems. The stem to be cleaned is pulled through the opening manually to remove thorns and miscellaneous foliage from the stem [6].

Apparatus for bunching flowers including a rotating endless belt defining made by Monic included stem trimming apparatus, stem cleaning apparatus and tying means mounted adjacent the endless belt downstream of the leaf removing apparatus [7]. Maeyer and Huisman [8] used a rotary brush to defoliate hemp. The use of rotary brush to remove the leaf and seed head was partially successful in that less stem was removed but the brush was not sufficiently effective in removing leaf. A device was developed to harvest cereals by stripping based around a rotor with stripping elements of a 'keyhole' design made of a stiff polymer. Besides being very effective for removing the seed and grain from a range of crops, the stripping system has also proved to be very effective for defolianting crops, including mint, lucerne and nettles [9].

Without a database of basic and mechanical characteristics, engineers must design plant handling and processing equipments using empirical methods that increase the development time and costs. information about the physical and the mechanical properties is vital for the proper and effective design of mechanization and automation equipment when the plant material is to be directly handled or manipulated. Equipment, such as transplanters [10], singulation devices [11] and robotic work cells [12], has been developed without benefitting from accurate property data concerning the crop for which the apparatus was intended. To support the mechanization research on flower process, related information is needed on physical (average diameter, specific gravity, and moisture content) and mechanical (bending strength, compression strength, shear strength and leaf picking force) properties of chrysanthemum. Mcrandal and McNulty [13] evaluated the shear strength of grass stems with quasi-static shear test. They studied the effect of shear velocity, at 15, 28, and 41 mm/min, bevel angle, at 10, 30, and 45, and diameter of stem. They found that shear velocity and bevel angle did not have a significant effect on shear strength, but their interaction was significant at the 5% level. Prasad and Gupta [14] determined the shearing force and energy for cutting maize stem. They concluded that the ultimate shear strength and the shear energy in the direct shear test were observed to decrease with the shear velocity. Average ultimate shear strength decreased from 36.36 bar to 21.07 when the shear velocity was increased from 200 to 1000 mm/min. Maximum shear energy was related to 300 mm/min, and with increasing the shear velocity it was decreased. Halyk and Hurlbut [15] observed that the shear strength of alfalfa stem internodes varied from 4.08 to 183.5 bar. Singh and Burkhardt [16] investigated spikelt detachment strength in tension parallel to the grain under a quasi-static load. Khazaei *et al.* [17] studied the effect of bevel angle, oblique angle, shear velocity and blade type on shear strength, and shearing energy of pyrethrum flower stem, tensile strength and energy per unit area for picking up the flowers were evaluated. Chattopadhyay *et al.* [18] determined shear properties of sorghum stalks with quasi-static shear test, They found that the maximum shear strength increased from 3.74 to 8.18 MPa at the forage stage and from 4.68 to 9.02MPa at the seed stage when the bevel angle was increased from 30 to 70 degree at a 10 mm/min rate of loading. Specific shearing energy was determined for sunflower stalk by Ince *et al.* [19]. Their results showed that the shearing stress and the specific shearing energy increased as the moisture content increased, also both the shearing stress and the specific shearing energy were found to be higher in the lower region of the stalk due to structural heterogeneity [19].

The objective of this research is to design, construct and evaluate a prototype machine for removing leaves of cut chrysanthemum flowers.

2. Material and Method

2.1. Design and Operation

The method that was developed causes cut chrysanthemum flower stem to be cleaned from foliage as a result of hit the rotating fingers with leaves. The prototype consists of two rotational axes and rubber fingers that are oriented at angles of 90 degrees on axes. Bouquet is entered between two rotational axes as the flower stems are perpendicular to the axes. The axes rotate in opposite directions to each other and fingers strike foliage's and clean the flower stems. The required outcomes and the principles of this method are as follows: (1) the machine must be cleaned to cut flowers in bouquet without damaging the flower stems; (2) the operating mechanism must be based on impacting the rotating fingers with stationary bouquet; (3) the construction must be compact and portable; (4) the mechanism must be simple, strong and sturdy; (5) the mechanism must be capable of being operated by one person; the prototype comprised two rotational axes, rubber fingers, a distance control, a rotary speed control and a power transmission system (Figure 1).

Finger shaped as a frustum of height 50 mm with main diameter 10 mm and small diameter of 8 mm made from molded rubber, each rotational axe is made of steel bar Ø30mm which drilled and threaded 13 holes with 20 mm distance on each side for finger mounting, an 0.37 kW electromotor with 2980 rpm and four 6006-2z ball bearing has been selected for rotating axes.

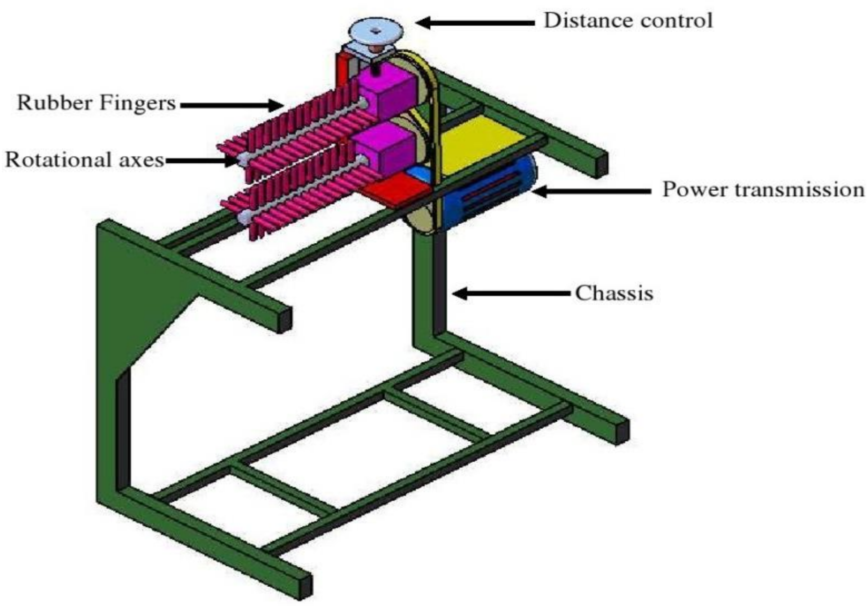

Figure1. Schematic of flower stem cleaner machine

The operating procedure is as follows. First, the cleaning machine is switched on and the axes were rotated. The Bouquet which is held with operator in perpendicular direction to axes is entered between two axes slowly. Rubber fingers are impacted through foliage and removed until bouquet was completely cleaned.

2.2. Test Procedure

2.2.1. Determining Physical Properties of Cut Chrysanthemum Flower

The stems of chrysanthemum flower were harvested from Ashian-e-Sabz greenhouse in Tehran, Iran, from healthy mother stock plants by a sharp knife at a height of 10 cm above the soil surface in the morning of each testing date. Harvested stems were covered and transported in an insulated container to a cooling chamber (1°C) to the Tarbiat-modares university biomechanics research laboratory for testing. Testing was completed as rapidly as possible in order to reduce the effects of drying. Two tests were conducted. Test I involved measuring the stem diameter and moister content. Test II measured bending strength and leaf picking force in relation to variation in load speed. In the first test, the diameter of the stem was measured by a vernier calliper and the specimen was dried in an electric oven (ISOTEMP, USA) to determine its moisture content according to the ASAE Standard [20]. The second test measured specimens from the growth tip end and the root internode end of the stem. A universal testing machine (UTM, HOUNSFIELD H50K-S) with a 500 N load cell was used for measuring the bending and picking force. A three-point loading apparatus with a span of 15 mm was used to support the stem specimens below the UTM probe (Figure 2a) for measuring the bending strength. Support and indenting rods were 3 mm in diameter. Specimens were placed in the three-point loading apparatus under the UTM probe and the force was applied to the centre of the stem at a loading speed of 25 mm/min (ASAE Standard, 1998) until it fractured. For the beam experiment, an apparent modulus of elasticity was computed using equations from Mohsenin (1980, p. 200)

$$E_d = \frac{f.l^3.10^6}{48\pi.d.c^4/64} \tag{1}$$

A device similar to the one shown in Figure 2b is constructed for picking force measuring. The device held the leaf and connected it to the UTM crosshead. The end of the stem was also clamped by the lower UTM jaw. Effect of picking velocity at 10, 100, and 500 mm/min, tensile direction, up and down direction and two sample groups were studied on maximum picking force and energy. Each test was replicated 10 times. Analysis of variance and the Duncan Multiple Rang Test were applied to determined the influence of factors upon the picking force and determine proper axes rotation speed for prototype machine.

2.2.2. Performance Test of Prototype Cleaning Machine

Before starting the test, the number of leaves from each flower stem was counted, then the axes rotational speed was calibrated with tachometer (Prova). To obtain optimum operating condition of cleaning, machine initial tests were conducted in accordance with the Table 1. Independent affecting factors on machine performance are rotational speed, axes distance and finger hardness (Figure 3). Performance parameters of the cleaning machine, which include the percent of removed leaves, the time required to stem cleaning and cleaned flower vase life were recorded and analyzed. Analysis of variance and the Duncan Multiple Rang Test were applied to determine the influence of factors upon the picking performance parameters. For vase life determination and flower stem bases were immersed to a depth of 4 cm in glass vials containing 400 ml of the double-distilled water include 2% ethanol, 2% methanol, 5ppm BA and 5ppm paclobutrizol. Experiments were carried out at 21 ±1°C and 60% RH under continuous fluorescent light (49 mol m^{-2} s^{-1}). Wilting of flower was used as the criterion for termination of vase life.

Figure 2a. Apparatus for the strength in bending experiment

Figure 2b. Device to held and connect the leaf to UTM for picking force measuring

Figure 3. Prototype of the flower stem cleaner machine**.**

Table 1. Initial test levels of cleaning machine

Parameter	**Level I**	**Level II**	**Level III**	**Level IV**	**Level V**
Rotational speed (rpm)	200	350	500	650	800
Axes distance (mm)	-10	-5	0	+5	+10
Finger hardness (shore A)	30	60	-	-	-
Replication	3	3	3	3	3

3. Results and Discussion

3.1. Physical Properties of Cut Chrysanthemum Flower

Samples taken from the bottom of the cutting were significantly larger in diameter than those taken from the top of the cutting. Samples taken from the bottom tended to be lower in the moisture content than those from the top (Table 2). The results of variance analysis showed that the sample group had a significant effect on all the measured physical properties ($P = 0.01$). Observations indicate differences in the woody versus succulent nature of tissue depending upon the physiological age of the stem section (Table 2).

Compiled data from the strength in the parallel plate compression tests can be seen in Table 2. The summarized data are segregated by group. As with the strength in bending tests, differences between groups were primarily in magnitude of force and deformation. Note that the bio-yield "hump" is the dominant and characterizing feature of each force-deformation curve for the compression tests (Figure 4). The nature of the failure of the stem cross-sections versus the resistive loading of the compacted tissue indicates that the data past the bio-yield region is of little value for machine design purposes. Samples from the bottom of the cutting had significantly higher bio-yield forces and deformations than did those from the top. Force and deformation data for calculating the tangent modulus were taken from the point of inflection on the force-deformation curve (Figure 4).

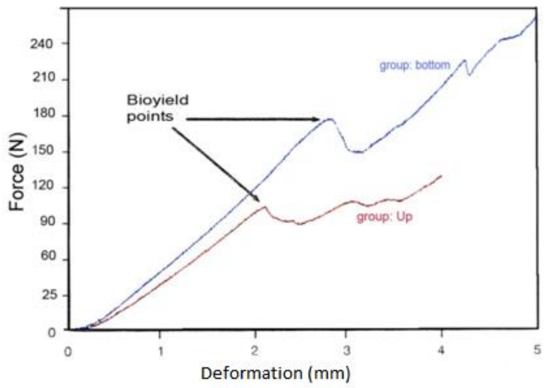

Figure 4. Typical force-deformation curve for strength in compression experiment.

Table 2. Summary of results of the strength in Compression

Property	Mean	Minimum	Maximum	Std
Group top				
Diameter (mm)	4.44[a]	3.38	5.37	0.65
MC (%)	78.17[a]	74.52	80.81	2.43
Bio yield force (N)	23[a]	18	29	4.17
Bio yield deformation (mm)	5.1[a]	4.1	6.5	0.65
Tangent modulus (MPa)	7.22[a]	5.8	8.1	0.66
Group bottom				
Diameter (mm)	5.45[a]	4.19	6.85	0.92
MC (%)	75.99[a]	72.43	80.15	2.46
Bio yield force (N)	45.25[a]	30	61	9.14
Bio yield deformation (mm)	6.8[a]	5.4	8.7	1.25
Tangent modulus (MPa)	10.1[a]	8.5	12.3	1.14

a significant at 1% and ns not significant.

Picking force increased with the increase in the stem diameter. Based on variance analysis (Table 3), the picking force was affected significantly with the picking velocity ($P = 0.01$).

Results of the Duncan Multiple Range Test show that, with increasing the picking velocity from 10 to 500 mm/min, the mean values of the picking force increased from 4.475 to 7.312 N. There was no significant difference between mean values of the picking force at 10 and 100 mm/min levels. Result of the variance analysis for location of samples showed that the difference between the picking force was not significant. Mean values of the picking force varied from 5.335 to 6.471 N for top and bottom location.

The picking direction had a significant difference at 0.01 levels on force values. Results of Duncan's Multiple Range Test show that the mean values for up and down direction were 10.52 N and 1.89 N, respectively. Hag *et al.* (1971) found that the effect of loading rate on tensile strength of cotton stem was further influenced by the density of the stem. For high density specimens (0.400 g/cm^3), the tensile strength increased directly as the rate of loading, but for lower density specimens (0.3759 g/cm^3) the tensile strength decreased with an increase in loading rate from 7.6 to 25.4 mm/min and then increased with further increases of loading rate. Results of Kazaie *et al*. (2002) research showed that the picking velocity has a significant effect on the picking force and energy of pyrethrum flower stem.

Table 3. Analysis of variance of effect of velocity, Location on picking force

Source of variation	Degree of Freedom	Picking force (N)
Treatment	11	163.72[a]
Location (*L*)	1	6.244[ns]
Tensile direction (*D*)	1	1353.13[a]
Velocity (*V*)	2	68.12[a]
*L***D*	2	1.34[ns]
*L***V*	2	4.05[ns]
*D***V*	2	45.41[a]
*L***D***V*	2	3.09[ns]
Error	48	321.68

3.2. Performance of Prototype Cleaning Machine

Table 4 shows the results of the statistical analysis carried out to examine the effect of axes distance, rotational speed and finger hardness on the percentage of the removed leaves for chrysanthemum flower. ANOVA indicated that two independent variables axes distance, rotational speed significantly influenced the percentage of the removed leaves (Table 4). The interaction effects of the independent variable were also significant, exept for the interaction between axes distance and finger hardness. Additionally, a difference in the rate of increase in the percentage of the removed leaves was obtained in the interction between the factors. The data showed that it is possible to remove nearly 100% of the chrysanthemum flower leaves with a minimal damage to flower stalk.

Table 4. Analysis of variance of considered parameters on removed leaves.

Source of variation	Degree of Freedom	Sum Squares	*F* Value	*P* Value
Treatment	49	14676	18.95	0.0001
Distance (*Di*)	4	481.9	7.58	0.0001
Speed (*S*)	4	11166	175.6	0.0001
Hardness (*H*)	1	1.21	0.07	0.7841
*Di***S*	16	1421.1	5.59	0.0001
*Di***H*	4	142.4	2.24	0.049
*S***H*	4	353.5	5.59	0.0004
*Di***S***H*	16	1201.1	4.72	0.0001
Error	98	1558.1		

The results of the interaction effects of axes distance and rotational speed on the percentage of the removed leaves are reported in Figures 5 and 6 for finger hardness of 30 and 60 shor A, respectively. With an increase in rotational speed from 200 to 800 rpm, the value of the percentage of the removed leaves for both Fingers 30 and 60 shor A increased. Additionally, with decreasing the axes distance from +10 to -10 mm, the value of the percentage of the removed leaves for finger hardness 30 shor A increased, but for finger hardness 60 shor A, most value of the percentage of the removed leaves related to axes distance -5 mm. For this finger, with an increase in rotational speed from 200 to 650 rpm, the value of the percentage of the removed leaves increased from 91.88 to 100% for axes distance of -5mm. Wheras for finger hardness of 60 shor A and axes distance of -5mm, increasing the rotational speed from 200 to 500 rpm caused increases in the value of the percentage of the removed leaves from 94.3 to 100%.

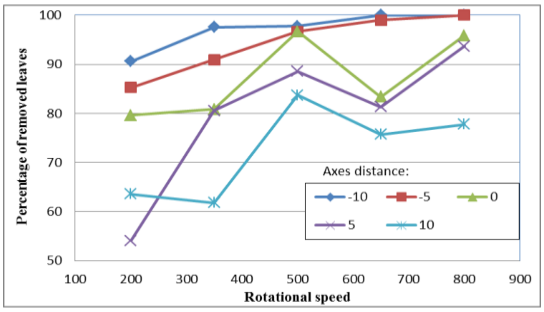

Figure 5. Effect of rotational speed on percentage of removed leaves for hardness 30 shor A.

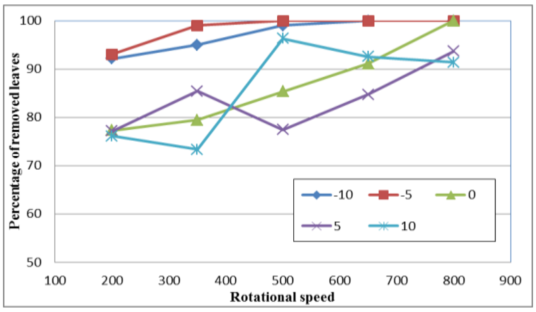

Figure 6. Effect of rotational speed on percentage of removed leaves for hardness 60 shor A.

Optimal working conditions happened with 500 rpm for rotational speed, -5 mm for axis distance and 60 shore A for finger hardness. Bruce *et al.* (2001), with the same method, succeded to remove more than 92% of leaves and flower heads using a rotor fitted with stiff polymer teeth. Also they found that a high rotation speed can increase damage of stems; therefore, from 545, 645 and 770 rpm, they introduced 645 rpm as an optimal speed [22].

4. Conclusion

Testing of a prototype for flower stem cleaning machine resulted in the determination of the optimal operating conditions in terms of rotational speed, axis distance and finger hardness. Subsequent performance tests of the prototype using the selected machine settings indicated that the machine could clean a bouquet with twenty flowers stem at an average time of 10 s. Good levels of cleaning efficiency and consumer acceptance were achieved.

References

[1] Reid M.S, Jiang C. Postharvest biology and ttechnology of cut flowers and potted plants. 1st ed. Wiley-blackwell. 2012.

[2] Halery, H. Mayak, "Senescence and postharvest Physiology of cut flowers. Part I". hortic, Vol.1 (1979) No. 10, 204- 236.

[3] W.G. Van Dooran, "Vascular occlusion in cut flowers. General principles and recent advances". Acta Hortic, (1999) No. 482: 59-63.

[4] M. Petridou, C. voyiatzi, "methanol, ethanol and other compounds retard leaf senescence and improve the vase life and quality of cut chrysanthemum flowers". Postharvest biology and technology, Vol.23 (2001), 79-83.

[5] Doobong, "Rose stem stripper". United States patent. patent number: 5561904. 1996.

[6] R.L. Richardson. "Floral stem cleaner and method of cleaning floral stems". United States patent. Patent number: 5044115. 1991.

[7] K. Monic, H.frankstein. "Apparatuse for sorting and bunching flowers and other agricultural produce". United States patent. Patent number: 4704846. 1987.

[8] E. A. A. Maeyer, W. Huisman. "Techniques for harvesting and storage of fiber hemp". 2nd international conference of biomass for energy, environment, agriculture and industry, Vienna. 1994.

[9] W. E. Klinner, M.A. Neale, R. E. Arnold, "A new stripping header for combine harvesters". Agricultural engineering Journal, (1987) No. 42, 9-14.

[10] L. J. Kutz, G. E. Miles, P. A. Hammer and G. W. Krutz, "Robotic transplanting of bedding plants". Transactions of the ASAE, Vol. 30 (1987) No. 3, 586-590.

[11] W. Maw, C. W. Suggs and P. Harris, "Progress in the mechanical singulation and sorting of seedlings", Transactions of the ASAE , (1980) No. 80, 1048-1055.

[12] W. Simonton, "Automatic geranium stock processing in a robotic workcell", Transactions of the ASAE, (1990). No. 33(6), 2074-2080.

[13] M. McRandal, P. B. McNulty, "Mechanical and physical properties of grasses". Transactions of the ASAE, (1980). No. 23(2), 816–821.

[14] J. prasada, C. P. Gupta, "Mechanical properties of maize stem as related to harvesting", Journal of agriculture Engineer Research. (1975). No. 20, 79-87.

[15] R. M. Halyk, L. W. Hurlbut, "Tensile and shear strength characteristics of alfalfa stems", Transactions of the ASAE. Vol. 11(1968). No.1, 256-257.

[16] K. N. Singh, T. H. Burkhardt, "Rice plant properties in relation to loading". Transactions of the ASAE. Vol. 27 (1974) No. 6, 1169-1172.

[17] J. Khazaei, H. Raban, A. Ebadi, F. Golbabaei, "Determining the shear strength and picking force of pyrethrum flower". 2nd Agricultural International Conference, Manson Ville, Que, Canada, 2002.

[18] P. S. Chattopadhyay, K. P. Pandey. "Mechanical Properties of Sorghum Stalk in relation to Quasi-static Deformation", Journal of Agricultural Engineering Research. Vol. 73 (1998), 199-206.

[19] Ince, S. Ugurluay, E. Guzel, M. T. Ozcan. "Bending and Shearing Characteristics of Sunflower Stalk Residue". Biosystems Engineering, Vol. 92 (2005) No. 2, 175–181.

[20] ASAE. Standards, 32nd Ed. St. Joseph, MI: ASAE; 1994.

[21] Mohsenin. N. N, Physical Properties of Plant and Animal Materials. Gordon and Breach Sci. Publication, New York; 1980.

[22] [22] D. M. Bruce, R. N. Hobson , R. P. white, "stripping of leaves and flower heads to improve the harvesting of fiber hemp". Journal of agriculture engineering research. (2001). No. 78, 43-50.

JJMIE

Volume 8 Number 6, December 2014
ISSN 1995-6665
Pages 377 - 384

Jordan Journal of Mechanical and Industrial Engineering

Fixture Designers Guidance: A Review of Recent Advanced Approaches

Heidar Hashemi* , Awaluddin Mohamed Shaharoun, Izman S.

Department of Manufacturing & Industrial Engineering, Faculty of Mechanical Engineering, Universiti Teknologi Malaysia

Received 20 Feb 2014 *Accepted 31 Oct 2014*

Abstract

Fixture design is an important issue in the process of manufacturing. Fixture design is a critical design activity process which bridges Computer-Aided Design (CAD) and Computer-Aided Manufacturing (CAM). The present paper presents a literature review of the Computer-Aided Fixture Design (CAFD) approaches performed. The purpose of this research is to give a deep and quick understanding of fixture design, its criteria and approaches used in this field. The significant techniques used in this field along with their applications, criteria and assumptions are also considered. The shortcomings of the existing research studies are stated and some issues pertaining to handling the weaknesses of the current research are suggested to be hopefully taken into account in future research.

Keywords: *Literature Review; Computer Aided Fixture Design; Fixtures Taxonomy; Artificial Intelligence.*

1. Introduction

An important type of tooling utilized in assembling, manufacturing, inspecting and other operation processes is known as fixtures. Fixtures are to hold workpieces stable and constraint without any movement during the manufacturing process. They set and secure the orientation and position required by the workpieces based on the specifications of the design [1]. An accurate fixture design is critical for quality of product based on accuracy, precision, and final product of the designed parts. About 40% of the parts that are rejected are mainly rejected because of the dimensioning errors due to poor fixture designs [2]. Fixture design is under the combined influence of workpiece specifications, machining methods, material performances and etc. It demands rich experience of the designers, which leads to a significant increase in the design cycle time and costs. Diminishing the need of potential rework on parts can also lower the time and cost of the manufacturing process [3]. Costs related to fixturing represents 10-20% of the total costs of a system in manufacturing [4].

To reduce the lead-time and cost of product development in fixture design field, automation and computerization of fixture design are required. Thus, CAFD has been introduced and utilized as an integration of computer-aided designs and computer-aided manufacturing (CAD/CAM) [5]. However, fixture design is still an issue of concern in the present manufacturing field even though many new CAFD techniques have been introduced [2]. Various approaches have been attempted in fixture design, i.e., Case Based Reasoning (CBR), Rule-based expert system, Genetic Algorithm (GA), Multi-agent Approach, Machine Learning, Geometric Analysis, etc.[6, 7].

Although many attempts have been made in the fixture design domain, there still remains some requirements to report and evaluate the used techniques in this area sharply and simply. Therefore, the techniques need to be addressed based on their principles, applications, criteria of use, adapting in fixture design area, and so on. This can help researchers to quickly understand the fields of fixture design and the strengths and weaknesses of each technique(s) in each field. The quick understanding can save time of researchers in fixture design and facilitate boring review process.

This paper is organized as follows: section 2 is about CAFD by focusing on the types of fixtures, design requirements and steps of fixture design. The next step is about aspects of significant techniques that have been used in fixture design. The significance of this study is that it offers a deep, but simplified, understanding of the current and innovative methods of fixture design that are useful and required for fresh researchers in the manufacturing field as a guideline.

2. Computer Aided Fixture Design (CAFD)

CAFD is the use of computers to help in the design of fixtures [8]. CAFDs have grown remarkably since the 1980s, and a lot of work has been done to enhance the

* Corresponding author. e-mail: heidar.hashemi63@gmail.com.

process of fixture designs [9]. Computers have dramatically reduced the design process time. By using a computer, designers are able to design in a virtual atmosphere. This helps the designers identify potential problems and undertake different ideas without actually creating fixtures physically. These programs have the added benefit of keeping a designer from missing steps while designing; and by avoiding mistakes, time and costs can be kept low [8].

However, the contrasting features of the design's requirements can be rather challenging. For instance, having a heavy fixture can be beneficial to the stability but this would make the material costs to rise exponentially and affect the usability, as the added weight would discourage handling carried out manually. These factors complicate the fixture design further and call for the necessary research of CAFD further [10].

2.1. Taxonomy of Fixtures

Fixtures are utilized as a work-holding device to locate and clamp a part surface that supports the operations of manufacturing. A normal part manufacturing process requires the use of many fixture setups to hold the working part in place as different orientations need to be operated [11]. Many manufacturing processes use fixtures widely, such as welding, testing, inspection, assembly, and machining that include milling, turning, drilling, grinding, etc. Figures 1-4 demonstrate the actual cases of fixture design in the manufacturing field. Based on the fixture's flexibility, the fixtures would be categorized in modular fixtures, dedicated fixtures and general-purpose fixtures, such as conformable and reconfigurable fixtures [2, 12].

Figure 1. Machining fixture [13]

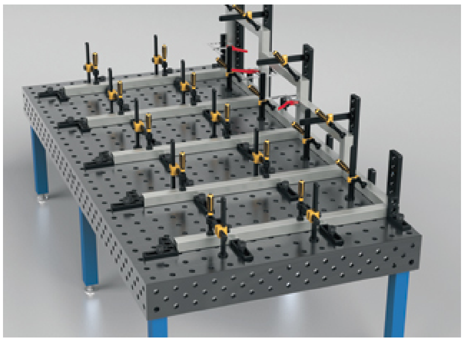

Figure 2. Assembly fixture [2]

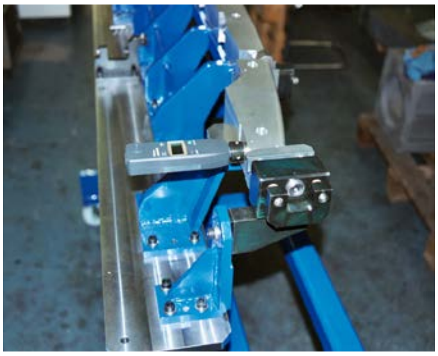

Figure 3. Inspection fixture [2]

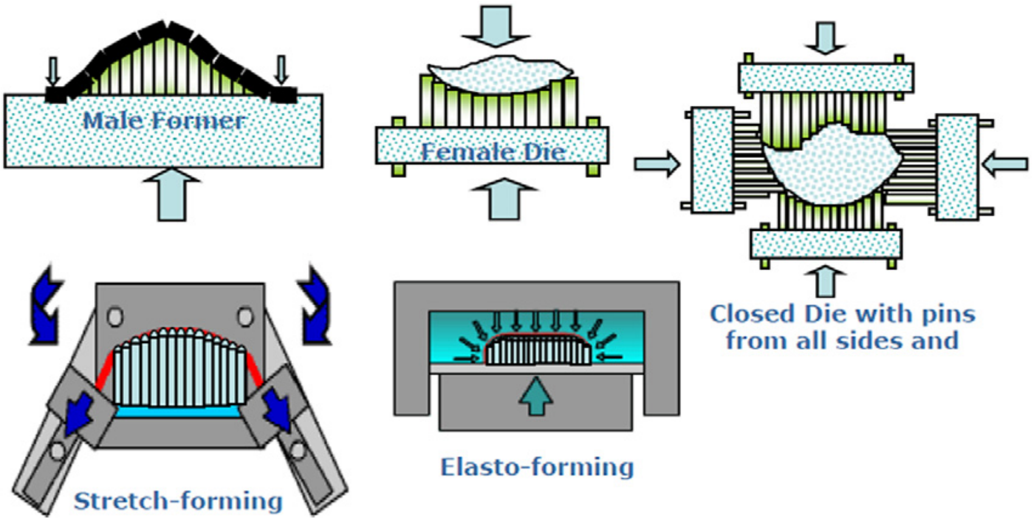

Figure 4. Typical pin-array fixture as one type of conformable fixtures [2]

Dedicated fixtures are fixtures that are produced for one specific workpiece and one setup. One of the benefits of the dedicated fixtures is that they have a high stiffness and are generally used for high batch sizes because they are created to perfectly locate and clamp a workpiece [14]. Most dedicated fixtures are, at first, originally at first designed for the purpose of one workpiece only. The dedicated fixtures have many beneficial properties, among which are high tolerances and rigidity; however, they are very expensive [8]. Dedicated fixtures are particularly essential in manufacturing for mass production and for precise, sophisticated, and advanced parts. In comparison to the modular fixtures, dedicated fixtures are carefully designed in accordance with the requirements of manufacturing and the design of the workpiece [15].

Flexible Manufacturing Systems (FMS) are dependent on fixtures that are not particularly fixed to just one workpiece. The fixtures should be reusable and changeable to suit the variations of the workpieces. The variations are inclusive but not limited to the same parts with various dimensions and oddly parts shaped. Therefore, general-purpose fixtures, such as reconfigurable, conformable and modular fixtures, are used as a solution in FMS [16].

Conformable and reconfigurable fixtures can be designed to receive portions of the different sizes and shapes [2]. Specifically, the technology on conformable pin-array fixture is used widely in a lot of fixture designs as certain components consist of internal variables which are adjustable to address the various workpieces and their features [17]. Figure 4 illustrates the typical application of the pin-array fixture. Several precision works in manufacturing utilize the materials-related phase change fixtures. In the aerospace industry, for example, metals with low melting-point are utilized to surround the turbine blades and create surfaces that are well-defined for the parts of locating and clamping the grinding processes [18].

Modular fixture technology is the most widely used type of reconfigurable fixtures. Modular fixturing systems have been looked at as a possible solution for FMS due to the high variability and standard set of parts they contained [8]. They include a base that has extensions that are highly movable, which helps the configuration changes to take place quickly. CAFD tools can be utilized to make the fixtures quickly and the advantage is that they can be reused in more than one configuration. They are made according to really tight tolerances to make sure that the number of errors is kept to a minimum in the finished product [19]. Most of the CAFD systems are developed based on the use of modular fixture design. This suggests that modular fixtures are the most suitable type of fixture design in terms of a CAFD process, which can be applied to produce a greater computerization impact in the researches [8, 20]. There are several limitations nevertheless [2]:

- These components only result in a limited number of combinations, which means that there is a possibility that no appropriate combination can be designed for some of the workpieces that contain complex or irregular geometries.
- At times, it is hard to maintain the modular fixtures with the structural properties. The modular fixtures' structural properties include features such as locating accuracy, stability, stiffness, operating speed, loading and unloading, etc. It is commonly known that utilizing modular fixtures may not gain the quality of an optimal fixture.
- It is not appropriate for mass production, such as automotive productions and the manufacturing of their components.

The principles of modular fixturing are used in many documented CAFD studies and applications to design fixture designs given the extensive usage in the present manufacturing and standardized productions [2]. Modular machining and modular assembly fixtures are widely used in the classification of modular fixtures. These kinds of fixtures' requirements are different but, comparatively, the approach to design them is quite standard [8].

Assembly fixture and welding fixture are mostly similar and they have obvious differences with machining fixture, as shown in the following [2, 6, 21]:

- The workpieces in the process of welding are normally an assembly of a few parts, while the workpieces that go through the machining process have just a single part;
- Normally, the requirements for accuracy in the processes of assembly and welding are less, compared to machining;
- The fixing and machining forces in the processes of assembly and welding are normally smaller, compared to machining; and
- The welding's thermal reactions should be considered thoroughly.

During the machining operation, the machining fixtures are utilized to locate and constrain the workpieces. The workpieces must be suitably located and clamped to make sure that they are machined based on particular dimensions and tolerances [22].

It is essential to minimize the deflection of the workpiece and fixture tooling caused by the forces of clamping and cutting to enable an accurate and quality production results in the machining process [23]. In general, there are two fundamental functions in a machining fixture [24, 25]: (1) to locate the right position of the component related to the cutting tools; and (2) to secure the components tightly to prevent it from moving in the machining process.

2.2. Steps of Fixture Design

Generally, fixtures contain four components, namely clamps, locators, base plates and supports. Fixture designs commonly assist in placing components onto a workpiece so that it remains immobile and stable in the process of machining or related operations [26].

There are normally four phases in the design process of the fixtures: fixture planning, setup planning, verification and unit design, as demonstrated in Figure 5 [27, 28]. The identification of machining setup by not moving the parts in each setup is known as setup planning. Fixture planning is defined as the physical fixture requirements, layout plan and prevention of collision. Verification is used to ensure that the developed fixture designs meet the requirements of fixturing. Unit design consists of the detailed and conceptual definition of the locating and clamp units of the fixture made with the base plate. In addition, the design must adhere to the other design issues, which may include the fixture weight, fixture cost, assembly time, etc. [14].

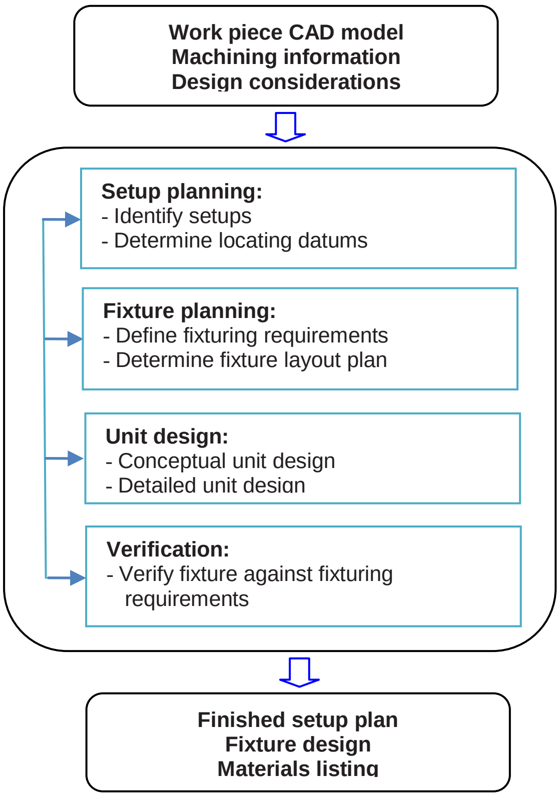

Figure 5. Steps of fixture design [27]

These steps can be generalized as: analyze the part, define the suitable locating and clamping points, identify the tooling and environmental requirements, and create a fixture to satisfy the criteria. These steps can be highly individual and can require an exhaustive trial of an error approach until experience is gained [8], which are described below.

In the fixture planning stage, the requirements of fixturing are normally created; these can be divided into six classifications as shown in table 1 [29]. Fixture planning and configuration is mainly an activity that is driven by experience to decide the location and clamping of the workpieces precisely based on the designs of the parts and the requirements of the process. The output of this step configures the fixture layout automatically, which guarantees the stability of the part [11].

The unit design phase is carried out to gain an accurate location and stiffness and to prevent the deformation of the fixture components [30]. For example, the tolerances of the locating units must be in such a way that the accuracy of the location is reached. However, the deformation, as a result of forces from the machining and clamping, must be prevented. It is critical that these requirements are followed as a guideline to design the units for locating and clamping [26].

Fixture design verification is the method of verifying the current fixture design by examining its achieved tolerance, geometric constraint's ability, fixturing accessibility, and the deformation and stability of the fixture workpiece system. The verification phase also provides the associated suggestions for improving the design [27-29]. Solutions for the verification of a fixture design are required due to the following reasons:

- The design process includes too many factors; it is quite hard to set an accurate model of the analysis in this process;
- The constraints of the design are individually viewed; some of the contrasting constraints may be created when they are regarded altogether; and
- Fixture design is closely linked to other activities such as CAM software, manufacturing systems and Computer-Aided Process Planning (CAPP) [2].

Thus, the CAFDs' strengths need to be part of the verification approaches that emphasize checking stability and the deformation of the workpieces while machining. A further advantage in this area is the layout planning techniques that aim to minimize the deformation of the workpiece made by the forces during machining [10]. Even though that several research efforts have been undertaken to support all the four phases to overcome the entire process of fixture design activity [31-33], the strength of the provided support differs across each phase and is normally not as good as the research efforts that focus on supporting particular phases only. Joneja and Chang's [32] ability, for example, to carry out the setup planning is not as impressive as that of Yao *et al.* [34], who exclusively concentrate on that particular task and consider the tolerance of the stack-ups.

3. Significant Techniques and the Applications in Fixture Design

Fixture design is a process that is complex and experience-based and requires trial-and-error to make the design. Therefore, during the past two decades various approaches have been attempted in fixture design to facilitate and computerize this task. Among these approaches are: Rule-Based Reasoning (RBR), CBR, GA, Neural Network (NN), Finite Element Method (FEM), Geometric Analysis, etc. [6, 35]. Table 2 catalogs the significant approaches used in CAFDs.

As the Artificial Intelligent (AI) technology has gained a greater level of acceptance in manufacturing, expert systems can offer a logical tool in automating the fixture design by utilizing the benefits of the management with the experience-based knowledge [36]. RBR is an experts system approach that utilizes induction rules to decide if a new problem should be further inspected or not [9]. Nnaji [37] and Nee & Kumar [38] typically used this technique. They carried a limited assessment of the likely displacement at each locating point caused by the machining forces and implemented an easy justification module that utilized heuristic rules to decide if a dedicated or modular fixture design should be created.

Fixture designs commonly and heavily depend on knowledge and experience. Simultaneously, fixture design resources and knowledge are required to be suitably retained for reuse in the future [1]. However, CBR [39, 40] includes indexing, representing, and organizing the current design cases as experience and knowledge so that they can be reused, recalled, and modified, for future design conditions. For these reasons, CBR approaches, as one of most effective methods, have been applied in this field [41].

The main assumption in CBR based fixture design methods is Kumar & Nee's assumption so that similar workpieces would require similar fixtures [18]. Thus, in this kind of system, the workpieces are grouped together into families of parts and an appropriate fixture design is attached to each workpiece. The fixture structures' similarity relies on the similarity of parts' structures and process methods where the fixtures are utilized [1, 6, 21, 42, 43]. Now automatically this seems to be a valid and sensible approach.

Applications of GAs to support the fixture planning, fixture layout plan and fixture configuration design are encoded in binary strings. GA has been examined, evaluated, and allowed to go through crossover, mutation, and reproduction. Until an optimal state is derived, the modification continues to develop improved solutions [44, 45]. GA has been interfaced with the FEM for optimization problems in the fixture layout in most cases [22, 46]. Finite element analysis (FEA) is being recognized as a typical platform for simulation and modeling of different manufacturing operations [47]. Normally, deformation testing is utilized by employing a finite element analysis where a workpiece is discretized to generate a node series that reflects the potential points of contact for locating and clamping [48]. FEM and GA are utilized in several fields of fixture design, such as in designing the optimal layouts for fixture configuration [49]. These layouts indicate the optimum points where the fixture should contact the workpiece being machined.

NNs are interconnected networks consisting of simple components. These networks can develop solutions for new problems that are entered into the network. NN techniques have been utilized to support fixture design systems that are case-based, as the similarity evaluator [50] and as the conceptual unit design. Research by Kumar *et al.* [51] utilized a combination of GA/NN techniques where the NN is trained with selections of past design problems and the possible solutions. The GA creates a possible solution that is assessed utilizing the neural network, which, in turn, works as a guide for the GA.

Geometry is an important aspect of designing individual units where the aim is to choose and to assemble the defined unit elements to offer a unit of appropriate acting heights [25, 52]. Researchers have mainly utilized geometric techniques to design a complete fixture unit [52, 53] in which the fundamental notion is to identify the essential dimensions of specific fixture units, typically being its height and to, later, link all the other dimensions of this component to the essential dimension through mathematical relationships that pre-exist. Typically, a geometry-based system is designed where the dimensions of the individual element are generated in association with the primary dimension of that element (normally the necessary height) through parametric dimension links. This is augmented with a relation knowledge base of how various elements are configured to create one unit [54].

Table 1. Requirements of fixture design adapted from [29]

General requirements	Examples of abstract sub-requirements
Tolerance	The locating tolerances should meet the design tolerances requirements of the parts
Physical	The fixture must be capable of physically accommodating the work-piece's weight and geometry.
	The fixture must allow access to the features of the work-piece that needs to be machined.
Affordability	The fixture's cost should not be more than the desired levels.
	The fixture's assembly/disassembly times should not be more than the desired levels.
	The fixture's operation time should not be more than the desired levels.
Constraint	The fixture should guarantee the stability of the work-piece by ensuring that the work-piece's moment and force equilibrium are kept.
	The fixture should make sure that the fixture/work-piece's stiffness is enough to avoid the occurrence of deformation, which could prevent the design tolerances from being reached.
Usability	The fixture's weight should not be more than the desired levels.
	The fixture should not result in damaging the surface at the work-piece/fixture's interface.
	The fixture should offer tool guidance to the features of the designated work-piece.
	The fixture should be error-proof, i.e., the fixture should be able to avoid wrong work-piece insertions into the fixture.
	The fixture should assist in chip shedding by providing a way to allow the machined chips to flow away from the fixture and the work-piece.
Collision prevention	The fixture should not result in collisions of the tool path-fixture.
	The fixture should result in work-piece fixture collisions, other than the designated clamping and locating positions.
	The fixture should not result in fixture-fixture collisions besides the designated points for fixture component connection.

Table 2. The significant techniques in CAFD

Method	Fundamental Procedure	Applications	To Improve the Performance	Working Process
RBR	Design based on basic heuristic rules	Setup planning, Fixture planning, unit design, verification Strength: Fixture planning	Mostly combined with: CBR	Evaluate and improve design by using some existing and derived basic rules in fixture design
CBR	Storing and using experiences to solve new problems	Fixture Planning, Unit design, Verification The strength: Fixture planning	Mostly used with: RBR	Finding appropriate fixture design for target work-piece in database
GA	Optimization process by generating possible solutions	Fixture layout configuration, fixture planning, verification The strength: verification	Mostly used with: FEM	Minimizing work-piece deformation by determining minimum forces at the locating and/or clamping points
FEM	Deformation analysis by meshing the work-piece and examine every single mesh	Fixture layout configuration, fixture planning, verification The strength: verification	Mostly used with: Optimization techniques	Deciding on acceptable candidate regions with minimized deformation of the work-piece
NN	A set of existing solved problem used to teach the network	Verification, unit design	Mostly combined with: GA	Supporting conceptual unit design and optimal location of units
Geometric Approaches	Pre-existing mathematical relationships based on parametric dimension relationships	Verification, fixture planning, unit design Strength: verification	Can be combined with: RBR	Determining critical dimensions of fixture units and fixture-work-piece contact points

4. Conclusion

Although many research studies have been conducted in the domain of fixture design, this task is still a blockage in the manufacturing process. A cause of that problem is that most of the CAFD techniques have been examined for simple workpieces, which do not reflect obstacles that are really faced in the industry; hence, the success of the developed methods cannot be confidently stated. Another cause is that there is a requirement to integrate the segmented CAFD techniques cohesively in a framework that includes a comprehensive knowledge of fixture requirements that can be used to drive the process of fixture design. An approach that can be helpful in this case is CBR, so that by combining CBR with other intelligent methods, effective and more comprehensive fixture design systems can be achieved.

Future research could focus on the significance of a more efficient integration of fixture systems to other systems in manufacturing. It is important to place the task of fixture design into the overall process of manufacturing to gain the best performance of each fixture design solution. Regarding the advances in nowadays technology, testing the performance of two approaches would be valuable and efficient in the case of fixture design; these approaches are: (1) placing a multi-sensor network inside the workpiece-fixture system (2) utilizing intelligent online control methods to adjust the fixturing forces and contacts.

References

[1] Y. Zhou, Y. Li, and W. Wang, "A feature-based fixture design methodology for the manufacturing of aircraft structural parts". Robotics and Computer-Integrated Manufacturing, Vol. 27 (2011) 986-993.

[2] H. Wang, Y. Rong, H. Li, and P. Shaun, "Computer aided fixture design: Recent research and trends". Computer-Aided Design, Vol. 42 (2010) 1085-1094.

[3] N. Wan, Z. Wang, and R. Mo, "An intelligent fixture design method based on smart modular fixture unit". The International Journal of Advanced Manufacturing Technology, Vol. 74 (2013) 1-21.

[4] Z. Bi and W. Zhang, "Flexible fixture design and automation: review, issues and future directions". International Journal of Production Research, Vol. 39 (2001) 2867-2894.

[5] K. Yu, T. Lam, and A. Lee, "Immobilization check for fixture design". Proceedings of the Institution of Mechanical Engineers, Part B: Journal of Engineering Manufacture, Vol. 217 (2003) 499-512.

[6] H. Wang and Y. Rong, "Case based reasoning method for computer aided welding fixture design". Computer-Aided Design, Vol. 40 (2008) 1121-1132.

[7] H. Hashemi, A. Mohamed Shaharoun, S. Izman, and D. Kurniawan, "Recent Developments on Computer Aided Fixture Design: Case Based Reasoning Approaches". Advances in Mechanical Engineering, Vol. 2014 (2014) 15.

[8] S. Price, "A Study of Case Based Reasoning Applied to Welding Computer Aided Fixture Design," Worcester Polytechnic Institute, 2009.

[9] G. Peng, G. Chen, C. Wu, H. Xin, and Y. Jiang, "Applying RBR and CBR to develop a VR based integrated system for machining fixture design". Expert Systems with Applications, Vol. 38 (2011) 26-38.

[10] I. Boyle, Y. Rong, and D. C. Brown, "A review and analysis of current computer-aided fixture design approaches". Robotics and Computer-Integrated Manufacturing, Vol. 27 (2011) 1-12.

[11] S. Nelaturi, A. Rangarajan, C. Fritz, and T. Kurtoglu, "Automated fixture configuration for rapid manufacturing planning". Computer-Aided Design, Vol.43 (2013).

[12] B. O. Nnaji, S. Alladin, and P. Lyu, "A framework for a rule-based expert fixturing system for face milling planar surfaces on a CAD system using flexible fixtures". Journal of Manufacturing Systems, Vol. 7 (1988) 193-207.

[13] M. Sabareeswaran, K. Padmanaban, and K. Sundararaman, "FEM–based vibration control in end milling using fixture layout". International Journal of Machining and Machinability of Materials, Vol. 15 (2014) 201-211.

[14] Y. Rong, S. H. Huang, and Z. Hou, Advanced computer-aided fixture design: Academic Press, 2005.

[15] A. S. kumar, J. Y. H. Fuh, and T. S. Kow, "An automated design and assembly of interference-free modular fixture setup". Computer-Aided Design, Vol. 32 (2000) 583-596.

[16] T. Kow, A. Kumar, and J. Fuh, "An integrated approach to collision-free computer-aided modular fixture design". The International Journal of Advanced Manufacturing Technology, Vol. 16 (2000) 233-242.

[17] C. Munro and D. Walczyk, "Reconfigurable pin-type tooling: a survey of prior art and reduction to practice". Journal of manufacturing science and engineering, Vol. 129 (2007) 551-565.

[18] A. Y. C. Nee, K. Whybrew, and A. S. kumar, Advanced fixture design for FMS: Springer-Verlag, 1995.

[19] J.-L. Hou and A. Trappey, "Computer-aided fixture design system for comprehensive modular fixtures". International journal of production research, Vol. 39 (2001) 3703-3725.

[20] Q. Li, "Virtual reality for fixture design and assembly," University of Nottingham, 2009.

[21] H. Hashemi, M. S. Awaludin, and S. Izman, "To Improve Machining Fixture Design: A Case Based Reasoning Paradigm". Journal of Basic and Applied Scientific Research, Vol. 3 (2013) 931-937.

[22] S. Selvakumar, K. Arulshri, K. Padmanaban, and K. Sasikumar, "Design and optimization of machining fixture layout using ANN and DOE". The International Journal of Advanced Manufacturing Technology, (2013) 1-14.

[23] W. Zhun, "Studying the Design and Verification of 5-axis NC program under the Manufacturing System". Jordan Journal of Mechanical & Industrial Engineering, Vol. 8 (2014) 34-39.

[24] J. Asante, "Effect of fixture compliance and cutting conditions on workpiece stability". The International Journal of Advanced Manufacturing Technology, Vol. 48 (2010) 33-43.

[25] Y. Rong and Y. Bai, "Automated generation of fixture configuration design". Journal of manufacturing science and engineering, Vol. 119 (1997) 208-219.

[26] I. Boyle, "CAFixD–A Case-Based Reasoning Method for Fixture Design," Worcester Polytechnic Institute, 2006.

[27] Y. Kang, Y. Rong, and J. C. Yang, "Computer-Aided Fixture Design Verification. Part 1. The Framework and Modelling". The International Journal of Advanced Manufacturing Technology, Vol. 21 (2003) 827-835.

[28] Y. Kang, Y. Rong, and J. C. Yang, "Computer-Aided Fixture Design Verification. Part 3. Stability Analysis". The International Journal of Advanced Manufacturing Technology, Vol. 21 (2003) 842-849.

[29] Y. Kang, Y. Rong, J. Yang, and W. Ma, "Computer-aided fixture design verification". Assembly Automation, Vol. 22 (2002) 350-359.

[30] A. Y. C. Nee, Z. J. Tao, and A. S. Kumar, An advanced treatise on fixture design and planning vol. 1: World Scientific Publishing Company, 2004.

[31] I. M. Boyle, K. Rong, and D. C. Brown, "CAFixD: A case-based reasoning fixture design method. Framework and indexing mechanisms". Transactions of the ASME-S-Computing and Information Science in Engineering, (2006) 40-48.

[32] A. Joneja and T.-C. Chang, "Setup and fixture planning in automated process planning systems". IIE transactions, Vol. 31 (1999) 653-665.

[33] A. Y. C. Nee, "A framework for an object/rule-based automated fixture design system". CIRP Annals-Manufacturing Technology, Vol. 40 (1991) 147-151.

[34] S. Yao, X. Han, Y. Yang, Y. K. Rong, S. Huang, D. Yen, et al., "Computer aided manufacturing planning for mass customization: part 2, automated setup planning". The International Journal of Advanced Manufacturing Technology, Vol. 32 (2007) 205-217.

[35] J. Cecil, "Computer-aided fixture design–a review and future trends". The International Journal of Advanced Manufacturing Technology, Vol. 18 (2001) 790-793.

[36] S. Hargrove and A. Kusiak, "Computer-aided fixture design: a review". The International Journal of Production Research, Vol. 32 (1994) 733-753.

[37] B. O. Nnaji and S. Alladin, "E-CAFFS: an expert computer-aided flexible fixturing system". Computers & industrial engineering, Vol. 18 (1990) 297-311.

[38] A. S. Kumar, A. Y. C. Nee, and S. Prombanpong, "Expert fixture-design system for an automated manufacturing environment". Computer-Aided Design, Vol. 24 (1992) 316-326.

[39] J. L. Kolodner, "An introduction to case-based reasoning". Artificial Intelligence Review, Vol. 6 (1992) 3-34.

[40] M. L. Maher and A. Gomez de Silva Garza, "Case-based reasoning in design". IEEE Expert, Vol. 12 (1997) 34-41.

[41] H. Hashemi, A. M. Shaharoun, and I. Sudin, "A case-based reasoning approach for design of machining fixture". The International Journal of Advanced Manufacturing Technology, Vol.74 (2014) 1-12.

[42] W. Li, P. Li, and Y. Rong, "Case-based agile fixture design". Journal of Materials Processing Technology, Vol. 128 (2002) 7-18.

[43] S. H. Sun and J. L. Chen, "A fixture design system using case-based reasoning". Engineering Applications of Artificial Intelligence, Vol. 9 (1996) 533-540.

[44] N. Wu and K. Chan, "A genetic algorithm based approach to optimal fixture configuration". Computers & Industrial Engineering, Vol. 31 (1996) 919-924.

[45] M. Hamedi, "Intelligent fixture design through a hybrid system of artificial neural network and genetic algorithm". Artificial Intelligence Review, Vol. 23 (2005) 295-311.

[46] H. Hashemi, A. Mohamed Shaharouna, I. Sudin, G. Bijan, N. Zafar, and S. Saeed, "Fixture Design Automation and Optimization Techniques: Review and Future Trends". International Journal of Engineering, Vol. 27 (2014) 1787-1794.

[47] S. Ratchev, K. Phuah, and S. Liu, "FEA-based methodology for the prediction of part–fixture behaviour and its applications". Journal of Materials Processing Technology, Vol. 191 (2007) 260-264.

[48] S. Kashyap and W. DeVries, "Finite element analysis and optimization in fixture design". Structural optimization, Vol. 18 (1999) 193-201.

[49] Y. Wang, X. Chen, Q. Liu, and N. Gindy, "Optimisation of machining fixture layout under multi-constraints". International Journal of Machine Tools and Manufacture, Vol. 46 (2006) 1291-1300.

[50] Z.-C. Lin and J.-C. Huang, "The application of neural networks in fixture planning by pattern classification". Journal of Intelligent Manufacturing, Vol. 8 (1997) 307-322.

[51] V. Subramaniam, A. Senthil kumar, and K. C. Seow, "Conceptual Design of Fixtures using Genetic Algorithms". The International Journal of Advanced Manufacturing Technology, Vol. 15 (1999) 79-84.

[52] Y. Wu, Y. Rong, W. Ma, and S. LeClair, "Automated modular fixture planning: geometric analysis". Robotics and Computer-Integrated Manufacturing, Vol. 14 (1998) 1-15.

[53] G. Peng, X. Hou, C. Wu, T. Jin, and X. Zhang, "Fast collision detection approach to facilitate interactive modular fixture assembly design in a virtual environment". The International Journal of Advanced Manufacturing Technology, Vol. 46 (2010) 315-328.

[54] Z. An, S. Huang, Y. Rong, and S. Jayaram, "Development of automated dedicated fixture configuration design systems with predefined fixture component types: Part 1, Basic design," International Journal of Advanced Manufacturing Technology, Vol. 15 (1999) 99-105.

JJMIE

Volume 8 Number 6, December 2014
ISSN 1995-6665
Pages 385 - 392

Jordan Journal of Mechanical and Industrial Engineering

Optimization Studies on Thrust Force and Torque during Drilling of Natural Fiber Reinforced Sandwich Composites

Rajamanickam Vinayagamoorthy[a*], Nagamalai Rajeswari[b], Balasubramanian Karuppiah[c]

[a]Research Scholar, Department of Mechanical Engineering, Dr. M.G.R Educational and Research Institute University, Maduravoyal, Chennai- 600095, Tamilnadu, India.

[b]Professor, Department of Mechanical Engineering, Veltech Multitech Dr. Rangarajan Dr. Sakunthala Engineering College, Avadi, Chennai-600062, Tamilnadu, India

[c]Principal, Vel Tech Engineering College, Avadi, Chennai-600062, Tamilnadu, India

Received 1 April 2014 Accepted 25 Oct 2014

Abstract

This research is carried out to investigate thrust force and torque during drilling on the developed bio-degradable sandwich composites. Two natural fibers, namely vetiveria zizaniodes (vetiver) and jute, and one synthetic fiber, namely E-glass, are used as reinforcements with vinyl ester resin to form three composite specimens. The fiber compositions in each specimen are varied while the resin composition is kept as a constant. The vetiver fibers are pre-treated with alkali and followed by furnace heating in order to improve its surface properties. The specimens are subjected to a set of 28 drilling operations during which the machining parameters, like speed, feed rate, tool point angle and work sample, are varied between four levels to form a four-factor mixed level D-optimal factorial design. During each drilling operation, the thrust force and torque are measured as responses by using a kistler make drill dynamometer with an accuracy level of 0.01N. The responses are analyzed by using response surface method, and non-linear regression equations are developed. Optimization on the experimental data resulted in selection of a high level of speed of 2000 rpm, low level feed of 0.1 mm/rev, tool angle between 600 to 900 and selection of sample level I as optimized values with a thrust force of 82.47 N and torque of 4.4 Nm. Confirmatory runs are conducted and the responses are again measured. The average error between the developed model and the confirmatory runs is found to be minimal and hence the optimization is highly satisfactory.

Keywords: *Vetiver, Jute, Glass, Thrust, Torque, Optimization*.

1. Introduction

In recent days, composites have been developing in the shape of a final component during their manufacturing stage in order to reduce the machining operations. They still need machining operations for producing holes and slots, finishing the holes, slots, edges and exterior surfaces. The damage of the hole is measured by using delamination factor. During the drilling of carbon fiber reinforced composites, it was observed that the delamination decreases with the increase in speed. Also, it was concluded that a low feed rate and a low point angle are found to be the optimum conditions for drilling [1]. During turning of carbon reinforced cylindrical rods, using cubic boron nitride and polycrystalline diamond tools, surface roughness increases with the increase in feed rate, but decreases as the cutting speed is increased [2, 3]. Drilling induced thrust force and torque on work sample. Drilling of unidirectional glass fiber reinforced plastics revealed that both thrust force and torque have a major influence on delamination on the material and the residual strength decreases with the increase in delamination [4]. Optimization studies on surface roughness during end milling of aluminium metal matrix composites concluded that the feed rate has a predominant influence on surface roughness [5, 6].

Machinability is also influenced by the selection of resin, fiber, additives and their proportions used in composites. An investigation drilling of glass fiber reinforced composite reported that the type of chip formed, thrust force and surface roughness depend upon the type of resin used. It was concluded that the thrust force and surface roughness are found to be larger for a composite made of polyester resin when compared to that of composites made of the polypropylene composite [7]. Extensive research has been done in machinability associated issues by using different synthetic fibers as

* Corresponding author. e-mail: vmmailbox@rediffmail.com..

reinforcements in composites. In the few recent years, many natural fibers like jute, vetiver, bamboo, sisal, licuri etc. have been introduced in composites. Studies on their mechanical properties showed that, by careful selection of fiber proportions in composites, they could serve as a possible alternative for synthetic fibers [8-11].

Studies on drilling of natural coir reinforced plastics reported that the feed rate has a major influence on thrust force and torque. It was concluded that a medium feed rate of 0.2 mm/rev, a high speed of 1503 rpm and a medium drill diameter of 8 mm are found to be optimum conditions for machinability [12]. Investigations during the drilling of Medium Density Fiberboards (MDF) reported that the delamination factor increases when the feed rate is increased and decreases when the cutting speed is increased [13]; such results are similar to the results obtained during the machining of synthetic fiber reinforced composites. In another study, commercially woven jute fibers are reinforced with polyester in the form of plates and the developed composites are subjected to end milling operations. Analysis of thrust force and torque showed that three factors, namely speed, feed rate and depth of cut, predominantly affect the responses [14]. Extensive studies have been done to analyze the behavior of natural fiber reinforced plastics and only few research works have evolved during the recent years to perform machining and machinability associated investigations.

In an earlier research, Vinayagamoorthy *et al.* [8] developed the nine new composites and made an extensive analysis on properties like tensile, flexural, compressive and impact strengths. It was concluded that, by a proper selection of reinforcement and resin proportions and by giving a suitable chemical treatment to natural fibers, natural fibers served as an alternative to synthetic fibers. As an extension of this work, three composites samples, showing best mechanical properties, were taken for the present machining studies. The samples are subjected to a 28 drilling operations according to mixed level D-optimal design methodology. The responses, namely thrust force and torque, are measured and the data are analyzed and optimized using response surface methodology. This resulted in the selection of the best levels for the factors. Confirmatory runs are conducted and the responses are compared with the model.

2. Material and Methods

Vetiveria zizanioides is a perennial grass whose roots can grow up to a maximum length of 12 meters. It is used as an aromatic agent in perfumes and as an agent for treatment of rheumatism in Indian traditional medicines. These roots have a tensile strength of 723 MPa and modulus of 49.8 GPa with strain at break of 2.4%. In the present study, the composite samples are prepared by using the hand layup method in the form of slabs, each of the size 300 mm x 300 mm x 12 mm. The hand layup method uses a table over which the resin is spread and a fiber layer is placed over it. Again, a layer of resin is applied over the fiber layer and this procedure is repeated until the proportions of fiber and resin are satisfied. Finally, a load is applied over it for about 24 hours for the uniform bonding of resin with fibers. The composition of vetiver fibers and E-glass fibers are varied in each sample to form 34 wt% in total and vinyl ester resin is maintained as 66 wt% in all samples. The composition of fiber and resin in the samples are presented in Table 1. The samples preparation method and the chemical treatment of the fibers were extensively discussed in the earlier study by the authors [8], and the mechanical properties of the developed samples are presented in Table 2.

Table 1. Composition of samples

Sample	Fiber Proportions (wt %)			Resin proportions (wt %)
	Vetiver	Jute	Glass	Vinyl ester
I	17	17	-	66
II	13	13	8	66
III	10	10	14	66

A Computer Numerical Controlled (CNC) vertical machining center, made by Bharat Fritz Werner, is used for drilling operations. This CNC system is controlled by Siemens 802D and has a maximum spindle speed of 6000 rpm and a tool traverse of 510 x 410 x 460 mm. High Speed Steel (HSS) drill tools of 10 mm diameter and M42 grade are used for drilling. As drill tools are available in the market, with only a standard angle of 90°, four drill tools were purchased and three of them were ground to 60°, 120° and 150° by using a tool and cutter grinder. The point angles are measured and ensured by using a tool maker microscope during this process. Work samples, of thickness 12 mm, are cut as a 100 mm square plate for drilling. A kistler make drill dynamometer of model 9257B is used to measure the thrust force and torque during drilling. This setup has a measuring range of -5 KN to 10 KN. The dynamometer is placed over the machine table and the work sample is fixed above it by using a machine vice. Four factors, namely speed, feed, tool angle and work sample, are selected as the input factors for the present study. Speed, feed and tool angle are assigned with four numeric levels and the work sample is assigned with three categorical levels. This type of design is known as a four-factor mixed level D-optimal design. The selection and assignment of the levels to all factors was done on the basis of a survey of the various research works [15-17], and the data are presented in Table 3.

Table 2. Mechanical properties of samples

Sample	Tensile strength (MPa)	Tensile modulus (MPa)	Tensile strain at break (%)	Flexural strength (MPa)	Flexural modulus (MPa)	Flexural strain at break (%)	Compressive strength (MPa)	Impact energy (J)
I	71.73	1736	9.5	133.11	2894	7	122.21	11
II	74.14	2105	7.5	131.9	3358	6.67	121.81	15.33
III	70.96	2318	7.5	137.6	2950	7	128.23	18.33

Table 3. Factors and levels

Factors	Type	Level	Level	Level	Level
Speed (n) rpm	Numeric	500	1000	1500	2000
Feed (f) mm/rev	Numeric	0.1	0.2	0.3	0.4
Tool angle (α) degree	Numeric	60	90	120	150
Work sample	Categorical	I	II	III	-

3. Statistical Design

Response surface method is one of the important statistical tools during designing an experiment. It helps in analyzing and optimizing the statistical data having responses that are affected by multiple factors. It provides three dimensional plots and contour plots for responses against the input factors through which the influence of various factors on the responses could be analyzed. D-optimal design is another important tool for analyzing responses under the influence of factors with different levels. In this design method, the variance of regression coefficients in the model equation is minimized. In general, factors are classified as numeric factors and categorical factors. Numeric factors are varied between any numerical value as per the system requirement or of the interest of researcher. Categorical factors cannot be varied between any ranges but they are of particular importance. D-optimal design is a technique for analyzing the influence of either or both the numeric and the categorical factors on the responses [18]. The significance and contribution of each factor on the response are analyzed using analysis of variance (ANOVA). The runs and responses are presented in Table 4.

Table 4. Experimental runs and responses

Run	Input Parameters				Output Parameters	
	Speed (n) rpm	Feed (f) mm/rev	Point angle of Tool (α) degree	Work sample (D)	Thrust force (F) N	Torque (T) Nm
1	500	0.1	60	II	90.3	5.21
2	500	0.1	120	I	87.2	4.01
3	500	0.1	120	I	88.7	4.02
4	500	0.1	150	III	108.3	5.5
5	500	0.1	150	III	107.6	5.48
6	500	0.2	60	III	102.1	6.27
7	500	0.3	150	II	99.3	4.11
8	500	0.4	60	I	90.9	5.1
9	500	0.4	60	I	91.5	4.18
10	500	0.4	60	II	102.5	5.89
11	500	0.4	150	III	120.4	6.49
12	1000	0.1	120	II	94.1	4.9
13	1000	0.4	90	III	114.5	6.7
14	1000	0.4	150	I	94.8	4.72
15	1500	0.1	60	I	82.7	4.32
16	1500	0.3	60	II	96.3	5.48
17	2000	0.1	60	II	91.6	5.19
18	2000	0.1	90	III	99.3	5.73
19	2000	0.1	150	I	89.5	4.81
20	2000	0.2	120	II	91.5	5.39
21	2000	0.2	150	III	109	6.02
22	2000	0.3	90	I	86.3	4.94
23	2000	0.3	150	I	90.4	4.56
24	2000	0.4	60	III	111.4	7.08
25	2000	0.4	60	III	110.3	7.1
26	2000	0.4	120	III	115.3	6.54
27	2000	0.4	150	II	105.5	5.6
28	2000	0.4	150	II	106.4	5.5

4. Discussion

4.1. Thrust Force (F)

Drilling operation involves the penetration of a tool through the work piece during its rotation; as a result, thrust force is impressed on the working zone. The magnitude of thrust force depends upon various machining parameters. ANOVA analysis for thrust force is presented in Table. 5. The model F-value of 115.68 and lack of fit F-value of 4.57 indicate that the model is significant and the lack of fit is non-significant relative to pure error. A P-value less than 0.05 indicates that the terms are significant. R^2 and adj R^2 values of 0.995 and 0.986, respectively, are closer to each other, which gives the indication of a maximum model adequacy. It was observed that work sample, feed and tool angle predominantly affect the thrust force with a contribution of 55.24% for work sample, 14.5% for feed and 4.64% for tool angle. Also, it was noticed that speed has no influence on the thrust force. A 55.24% contribution of work sample indicates that the selection of natural and synthetic fibers and their composition in the composite plays an important role in reducing the thrust force.

Interaction plots between the thrust force and input factors and the normal probability plot are presented from Figures 1a to 1d. It was observed that variation of speed from 500 rpm to 2000 rpm does not have much influence on the thrust force, whereas thrust force increases when feed and tool angle are increased. This is because the tool, at higher feed rates, penetrates the work piece more quickly than during the low feed rates. Faster penetration leads to an increase in the thrust force [12]. Also, as the tool angle increases the contact area between the cutting edge and the work surface increases leading to an increase in thrust force. These behaviors are commonly seen in all the samples but sample I shows a least thrust force followed by samples II and III. This indicates that the inclusion of glass fibers increases the thrust force and the increase in glass fiber composition also increases the thrust force [19]. This behavior is seen because hardness of glass fibers are greater than that of vetiver fibers. Hence, sample I is suitable for machining under reduced thrust force. The normal probability plot is a graphical representation for checking the adequacy of the model. If the distribution of points follows a straight line, then the model is adequate and can be effectively used for predicting the responses [20]. Figure 1d clearly follows a straight line which is a symbol of good model adequacy.

Table 5. ANOVA table for Thrust force

Source	Sum of Squares	Degrees of freedom	Mean square	F value	P value	% Contribution
Model	2803.5	17	164.91	115.68	<0.0001 **Significant**	-
Speed (*n*)	6.12	1	6.12	4.29	0.0651	0.22
Feed (*f*)	408.03	1	408.03	286.22	<0.0001	**14.5**
Tool angle (*α*)	130.82	1	130.82	91.77	<0.0001	**4.64**
Work sample (*D*)	1556.5	2	778.22	545.89	<0.0001	**55.24**
$n*f$	0.035	1	0.035	0.035	0.025	0.0012
$n*\alpha$	0.74	1	0.74	0.52	0.4876	0.026
$n*D$	2.95	2	1.48	1.04	0.3902	0.104
$f*\alpha$	1.79	1	1.79	1.26	0.2883	0.0635
$f*D$	39.6	2	19.8	13.89	0.0013	1.4
$\alpha*D$	14.26	2	7.13	5	0.0312	0.5
n^2	0.16	1	0.16	0.11	0.748	0.0056
f^2	26.77	1	26.77	18.78	0.0015	0.95
α^2	3.67	1	3.67	2.57	0.1398	0.13
Residual	14.26	10	1.43	-	-	-
Lack of fit	11.7	5	2.34	4.57	0.0605 **Not significant**	-
Pure error	2.56	5	0.51	-	-	-
Total	2817.7	27	-	-	-	-
R^2 = 0.995; Adj R^2 = 0.986						

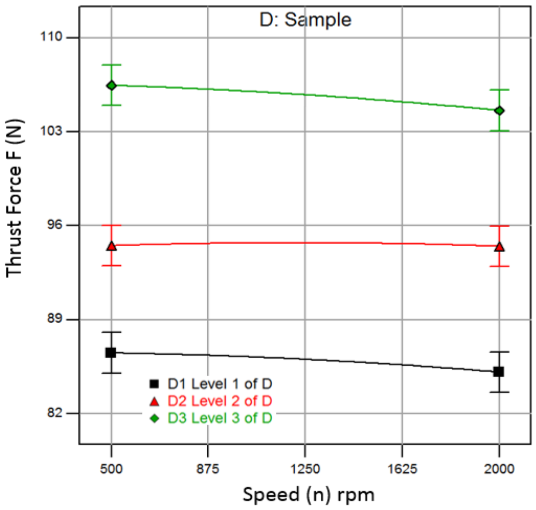

Figure 1a. Speed versus Thrust force

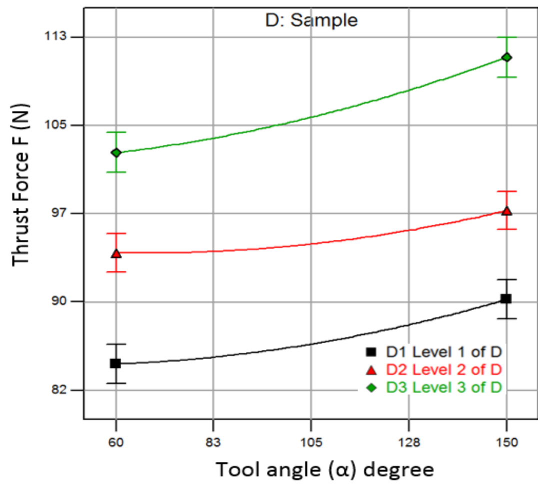

Figure 1c. Tool angle versus Thrust force

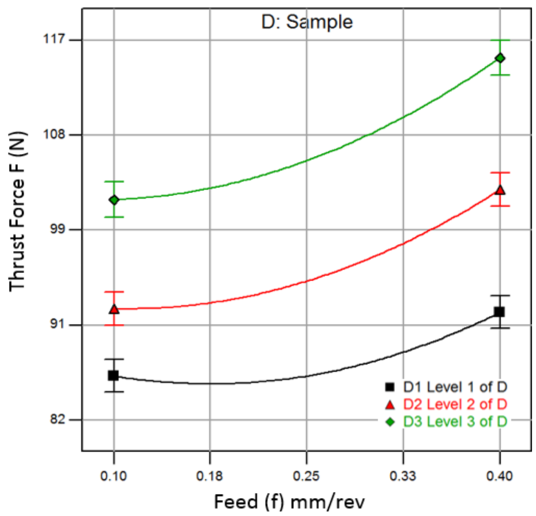

Figure 1b. Feed versus Thrust force

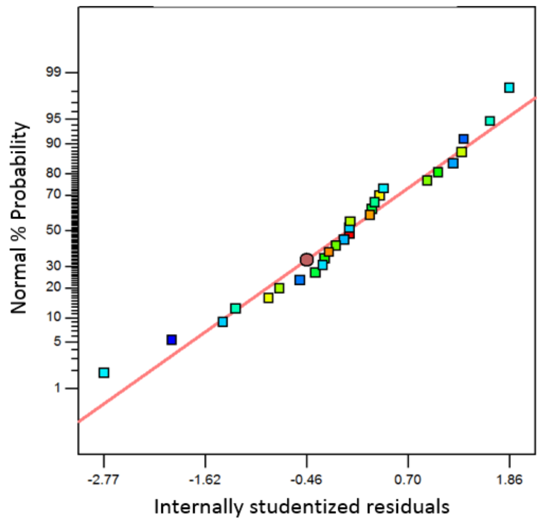

Figure 1d. Normal plot for thrust force

4.2. Torque (T)

During drilling, the drill tool is subjected to rotation at various speeds set by the operator. Hence, torque is developed and its magnitude depends on various machining parameters. The ANOVA table for torque is presented in Table 6. The model and lack of fit F-values of 13.16 and 1.17, respectively, indicates that the model is significant and the lack of fit is non-significant relative to pure error. R^2 and adj R^2 values of 0.95 and 0.88, respectively, are closer to each other, which gives the indication of a maximum model adequacy. It was observed that all the factors, namely speed, feed, tool angle and work sample, predominantly affect the torque with a contribution of 3.35% for speed, 9.29% for feed 3.77% for tool angle and 55.35% for work sample. A 55.35% contribution of work sample indicates that the selection of natural and synthetic fibers and their composition in the composite play an important role in reducing the thrust force. This contribution is almost equal to that of the contriburion of work sample with thrust force. Hence, work sample has a major influence on thrust force and torque.

The influence of each factor on the response is analyzed by using interaction plots. These plots present the behavior of the response under the influence for a combination of two input factors, namely speed-work sample, feed-work sample and tool angle-work sample. Interaction plots between the torque and input factors and the normal probability plot are presented in Figures 2a to 2d. It was observed that the increase in speed and feed increases the torque, whereas the increase in tool angle decreases the torque. The torque is found to be low for sample I between the ranges of speed, feed and tool angle. This is followed by sample II and sample III. This clearly indicates that the presence of glass fibers increases the torque and the increase in glass composition also increases the torque. Hence, sample I may be selected for machining under minimum torque conditions. This behavior is similar to the observations during thrust force and, hence, the overall performance of sample I was found to be satisfactory when compared to that of other samples. The normal probability plot as shown in Figure 2d which clearly follows a straight line, which is a symbol of a good model adequacy.

Table 6. ANOVA table for Torque

Source	Sum of Squares	Degrees of freedom	Mean square	F value	P value	% Contribution
Model	20.82	17	1.22	13.16	<0.0001 **Significant**	-
Speed (*n*)	0.73	1	0.73	7.88	0.0185	**3.35**
Feed (*f*)	2.02	1	2.02	21.7	0.0009	**9.29**
Tool angle (*α*)	0.82	1	0.82	8.84	0.014	**3.77**
Work sample (*D*)	12.04	2	6.02	64.64	<0.0001	**55.35**
$n*f$	0.011	1	0.011	0.12	0.7339	0.05
$n*\alpha$	0.25	1	0.25	2.7	0.1316	1.15
$n*D$	0.35	2	0.18	1.9	0.1998	1.6
$f*\alpha$	0.1	1	0.1	1.12	0.3143	0.46
$f*D$	0.22	2	0.11	1.18	0.3465	1.01
$\alpha*D$	0.28	2	0.14	1.49	0.2715	1.29
n^2	$3.43x10^{-6}$	1	$3.43x10^{-6}$	$3.68x10^{-5}$	0.9953	0.000015
f^2	0.17	1	0.17	1.82	0.2074	0.78
α^2	$3.7x10^{-4}$	1	$3.7x10^{-4}$	$3.97x10^{-3}$	0.951	0.0017
Residual	0.93	10	0.093	-	-	-
Lack of fit	0.5	5	0.1	1.17	0.433 **Not significant**	-
Pure error	0.43	5	0.086	-	-	-
Total	21.75	27	-	-	-	-

R^2 = 0.95; Adj R^2 = 0.88

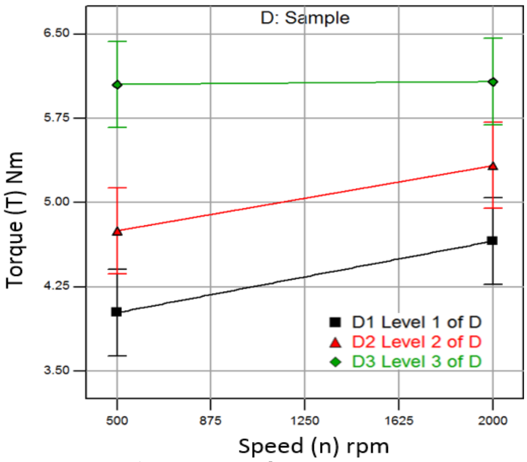

Figure 2a. Speed versus Torque

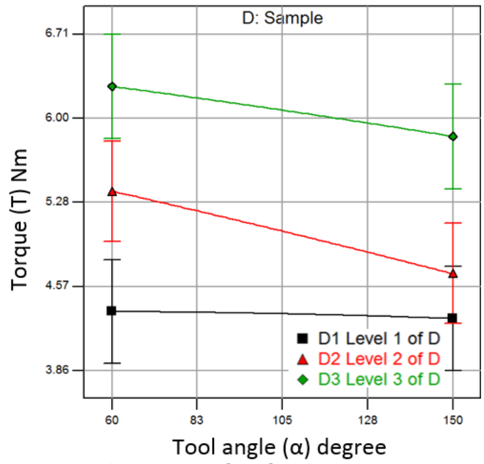

Figure 2c. Tool angle versus Torque

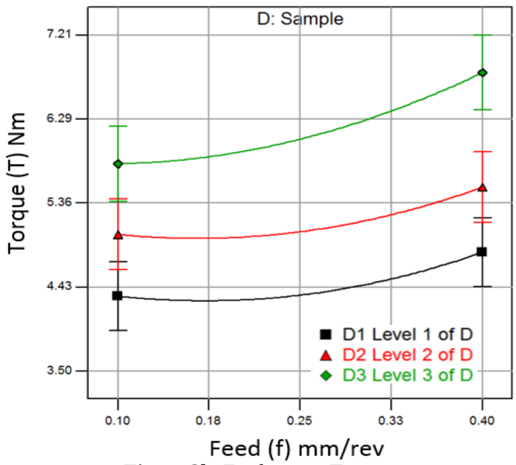

Figure 2b. Feed versus Torque

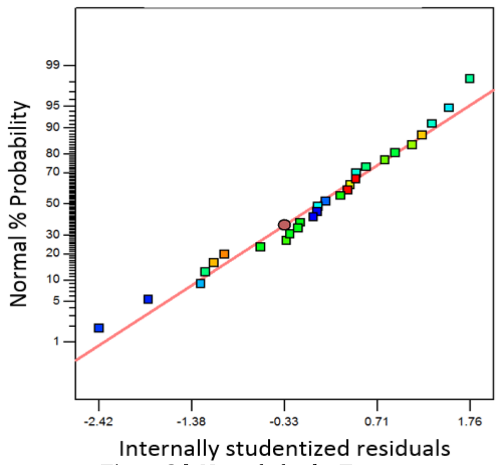

Figure 2d. Normal plot for Torque

4.3. Optimization

Design Expert 7 software is used in this study for statistical analysis and optimization. Multi-response optimization is carried out aiming to minimize the thrust force and torque. The optimized values of factors and responses are presented in Table 7. Seven runs are selected based on the desirability factor closer to unity. The first five runs show that a high level speed, a low level feed rate, sample I and a tool angle from 60° to 90° would be suitable for reducing the thrust force and torque with a desirability of 0.95. The sixth and the seventh runs show that a low level speed, a low level feed rate, sample I and a tool angle from 90° to 100° would be the optimum conditions with desirability of 0.85. Tools are ground to new tool angle values of 70°, 80° 90° and 100° and confirmatory runs are conducted. The average percentage of error between the model and confirmatory runs are 0.74% for thrust and 1.07% for torque. As the error percentages are minimal, the optimization is satisfactory and the model could be used to accurately predict the responses.

5. Conclusions

The present study focused on designing and optimizing thrust force and torque during the drilling of three new hybrid polymeric composites. The influence of various fibers in each composite on thrust and torque are investigated and optimization is carried out aiming to reduce the responses. The conclusions are as follows:

- The influence of work sample, feed and tool angle are predominant on thrust force and it was noticed that speed has no influence on the thrust force as presented in Table 5.
- All the factors, namely speed, feed, tool angle and work sample, affect the torque.
- A 55% contribution of work sample with both thrust force and torque indicates that the selection of natural and synthetic fibers and their composition in the composite plays an important role in reducing the thrust force.
- Presence of glass fibers and the increase in their content increase the thrust force and torque. Hence, a composite sample without the presence of glass fibers would be suitable for improving the machinability.
- Optimization of the model seems good with an overall desirabilty factor of 0.95, and the results of confirmatory runs are closer to the developed model with average errors of 0.74% for thrust force and 1.07% for torque.

Improving machinability is a primary objective of all manufacturers irrespective of the nature of the material. This exhaustive research helps end users to appropriately select the best machining conditions in order to improve the machinability.

Table 7. Optimization and confirmation

S. No	Speed n (rpm)	Feed f (mm/rev)	Tool angle α (degree)	Sample (D)	Desirability factor	D-Optimal Model		Confirmatory runs	
						Thrust F (N)	Torque T (Nm)	Thrust F (N)	Torque T (Nm)
1	2000	0.1	60	I	0.95	82.47	4.4	81.22	4.78
2	1975	0.1	60	I	0.95	82.74	4.41	83.17	4.5
3	2000	0.1	90	I	0.95	84.08	4.56	82.1	4.31
4	2000	0.1	70	I	0.95	83	4.46	82.16	3.9
5	2000	0.1	80	I	0.95	83.61	4.52	82.41	4.18
6	570	0.1	90	I	0.85	85.86	4.05	84.92	4.21
7	500	0.1	100	I	0.85	86.03	4.05	87.52	4.19

Error between model and confirmatory for Thrust force = 0.74%

Error between model and confirmatory for Torque = 1.07%

References

[1] V.N. Gaitonde, S.R. Karnik, J. Campos Rubio, A. EstevesCorreia, A.M. Abrao, J. Paulo Davim, "Analysis of parametric influence on delamination in high-speed drilling of carbon fiber reinforced plastic composites". Journal of Materials Processing Technology, Vol. 203 (2008), 431-438.

[2] T. Rajasekaran, K. Palanikumar, B.K. Vinayagam, "Application of fuzzy logic for modeling surface roughness in turning CFRP composites using CBN tool". Production Engineering Research and Development, Vol. 5 (2011), 191-199.

[3] K. Palanikumar, "Application of Taguchi and response surface methodologies for surface roughness in machining glass fiber reinforced plastics by PCD tooling". International Journal of Advanced Manufacturing Technology, Vol. 36 (2008), 19-27.

[4] I. Singh, N. Bhatnagar, "Drilling-induced damage in uni-directional glass fiber reinforced plastic (UD-GFRP) composite laminates". International Journal of Advanced Manufacturing Technology, Vol. 27 (2006), 877-882.

[5] Mohammed T. Hayajneh, Montasser S. Tahat, Joachim Bluhm, "A study of the effects of machining parameters on the surface roughness in the end-milling process". Jordan Journal of Mechanical and Industrial Engineering, Vol. 1 (2007) No.1, 1-5.

[6] K. Kadirgama, M.M. Noor, N.M. Zuki, M.M. Rahman, M.R.M. Rejab, R. Daud, K.A. Abou-El-Hossein, "Optimization of surface roughness in end milling on mould aluminium alloys (AA6061-T6) using response surface method and radian basis function network".

Jordan Journal of Mechanical and Industrial Engineering, Vol. 2 (2008) No.4, 209-214.

[7] R. Varatharajan, S.K. Malhotra, L.Vijayaraghavan, R. Krishnamurthy, "Mechanical and machining characteristics of GF/PP and GF/Polyester composites". Materials Science and Engineering B, Vol. 132 (2006), 134-137.

[8] R. Vinayagamoorthy, N. Rajeswari, "Mechanical performance studies on Vetiveria zizanioides/ Jute/glass fiber-reinforced hybrid polymeric composites". Journal of Reinforced Plastics and Composites, Vol. 33 (2014) No. 1, 81-92.

[9] Subhash Mandal, S. Alam, I.K. Varma, S.N. Maiti, "Studies on Bamboo/Glass Fiber Reinforced USP and VE Resin". Journal of Reinforced Plastics and Composites, Vol. 29 (2010) No. 1, 43-51.

[10] S.C. Amico, C.C. Angrizani, M.L. Drummond "Influence of the stacking sequence on the mechanical properties of glass/sisal hybrid composites". Journal of Reinforced Plastics and Composites Vol. 29 (2010) No. 1, 179-189.

[11] M.A. Leão, E.M.F. Aquino, S.R.L. Tinô, R.S. Fontes, "Licuri fibers: alternative reinforcement to polymeric composites", Journal of Reinforced Plastics and Composites, Vol. 30 (2011) No. 6, 516-523.

[12] S. Jayabal, U. Natarajan, U. Sekar, "Regression modeling and optimization of machinability behavior of glass-coir-polyester hybrid composite using factorial design methodology". International Journal of Advanced Manufacturing Technology, Vol. 55 (2011), 263-273.

[13] S. Prakash, K. Palanikumar, N. Manoharan, "Optimization of delamination factor in drilling medium-density fiberboards (MDF) using desirability-based approach". International Journal of Advanced Manufacturing Technology, Vol. 45 (2009), 370-381.

[14] R. Vinayagamoorthy, N. Rajeswari, "Analysis of cutting forces during milling of natural fibered composites using fuzzy logic". International Journal of Composites Materials and Manufacturing, Vol. 2 (2012) No. 3, 15-21.

[15] S. Jayabal, U. Natarajan, U. Sekar, "Regression modeling and optimization of machinability behavior of glass-coir-polyester hybrid composite using factorial design methodology". International Journal of Advanced Manufacturing Technology, Vol. 55 (2011), 263-273.

[16] S. Jayabal, U. Natarajan, "Optimization of thrust force, torque, and tool wear in drilling of coir fiber-reinforced composites using Nelder–Mead and genetic algorithm methods". International Journal of Advanced Manufacturing Technology, Vol. 51 (2010), 371–381.

[17] Birhan Işık, Ergün Ekici, "Experimental investigations of damage analysis in drilling of woven glass fiber-reinforced plastic composites". International Journal Advanced Manufacturing Technology, Vol. 49 (2010), 861–869.

[18] Montgomery DC. Design and analysis of experiments. 7th ed. New York: Wiley; 2009.

[19] K. Mohamed Kaleemulla, B. Siddeswarappa, "Effect of fibre content and laminate thickness on the drilling behavior of GSFRP composites under varied drill geometries". International Journal of Machining and Machinability of Materials, Vol. 10 (2011) No. 3, 222-234.

[20] T. Rajmohan, K. Palanikumar, "Modeling and analysis of performances in drilling hybrid metal matrix composites using D-optimal design". International Journal Advanced Manufacturing Technology, Vol. 64 (2013), 1249-1261.

JJMIE

Volume 8 Number 6, December 2014
ISSN 1995-6665
Pages 393 - 401

Jordan Journal of Mechanical and Industrial Engineering

Statistical Model for Surface Roughness in Hard Turning of AISI D3 Steel

Varaprasad Bhemuni[a *], Srinivasa Rao Chalamalasetti[b]

[a]*GVP School of Engineering (Technical Campus), Rushikonda, Visakhapatnam, India.*

[b]*Mechanical Engineering Department, Andhra University, College of Engineering (A), Visakhapatnam, India.*

Received 21 Jun 2014 *Accepted 7 Nov 2014*

Abstract

In the present experimental work, the effects of cutting speed, feed rate and depth of cut on surface roughness are investigated in hard turning of AISI D3 steel. AISI D3 steel is hardened to 62 HRC and is machined using a mixed ceramic tool. Mathematical models for surface roughness are developed using the Response Surface Methodology (RSM). Central Composite Design (CCD) is applied as an experimental design. Al_2O_3/TiC mixed ceramic tool with corner radius of 0.8 mm is employed to accomplish 20 tests with six centre points. The range of each parameter is set at three different levels, namely low, medium and high. The main effects of the factors and their interactions were considered in the present study using Analysis of variance (ANOVA). Various graphs and plots are drawn to evaluate the influence of the process parameters on surface roughness. Feed rate is the most influencing factor on surface roughness. Results revealed that the use of lower feed, lower depth of cut and higher cutting speed, while hard turning of AISI D3 hardened steel, ensures a better surface roughness.

Keywords: *Hard Turning, Surface Roughness, AISI D3, RSM, Main Effect Plots and ANOVA.*

1. Introduction

Hard turning is the process of single point cutting of hardened ferrous material with hardness more than 45HRC in order to obtain finished work pieces directly from hardened parts [1-5]. This process was developed as an alternative to grinding process in a bid to reduce the number of setup changes, process flexibility, compatible surface roughness, higher material removal rate, and less environment problems, which leads to a reduction in machining costs, an elimination of cutting fluids, an increase in the flexibility and efficiency, a reduction in part-handling costs and, finally, a decrease in the set-up times [1, 4]. Many industrial steel components, under the influence of critical loads from automotive and aerospace parts to bearing and forming tool, are made of hardened steel. These parts are produced by a series of sequential operations like turning, grinding and polishing, which are time consuming and costly. Therefore, hard turning is gaining importance to replace operations by single setup and single operation [6, 7]. The growth of hard turning process is indebted to the advent of new advanced cutting tools such as Cubic Boron Nitride (CBN), Poly Crystalline Boron Nitride (PCBN) and Ceramics since 1970 [4].

The surface quality is an index to evaluate the productivity of machine tools as well as the machined components. The surface roughness is used as a major quality indicator for the machined surfaces, which is the result of process parameters such as cutting conditions and tool geometry. In today's manufacturing industry, a special attention is being paid to the dimensional accuracy as well as surface finish and, hence, measuring and characterizing the surface finish can be considered as a machining performance index. Achieving a better surface quality, tool life and dimension accuracy are the crucial concerns in turning of hardened steels [4]. The cutting tool is one of the most critical elements in hard turning and the development of newer cutting tool materials has been characterized by an increase in wear resistance. Much work has been done on various hardened steels with CBN and PCBN cutting tools. According to the recent research, few studies have been reported on hard turning of AISI D3 with mixed ceramic (CC 6050).

Zou *et al.* [8] used Al_2O_3/TiN-coated tungsten carbide tools for finish turning of NiCr20TiAl nickel-based alloy under various cutting conditions and the cutting forces, surface integrity and tool wear are investigated and the inter diffusing and transferring of elements between Al_2O_3/TiN-coated tungsten carbide tool

* Corresponding author. e-mail: varaprasad.bhimuni11@gmail.com.

and $NiCr_20TiAl$ nickel-based alloy are studied. Fahad *et al.* [9] investigated the cutting performance of tungsten carbide tools with restricted contact length and multilayer chemical vapor deposition coatings, $TiCN/Al_2O_3/TiN$ and $TiCN/Al_2O_3$ TiN in dry turning of AISI 4140 and the results show that the coating layouts and cutting tool edge geometry can significantly affect heat distribution into the cutting tool. Hamdan *et al.* [10] presented an optimization method of the machining parameters in high-speed machining of stainless steel using coated carbide tool to achieve minimum cutting forces and better surface roughness using Taguchi's technique and pareto ANOVA and found that the feed rate is found to be more significant followed by the cutting speed and the depth of cut.

Suhail *et al.* [11] developed a method to identify surface roughness based on measurement of workpiece surface temperature and root mean square for feed vibration of the cutting tool during turning mild steel using grey relational analysis. Gopalsamy *et al.* [12] studied the machinability of hardened steel using grey relational approach and ANOVA to obtain optimum process parameters considering MRR, surface finish, tool wear and tool life for both rough and finish machining. Ahilan *et al.* [13] performed a multi-response optimization of turning parameters and nose radius over surface roughness and power consumed using Taguchi based grey relational approach and found that the main influencing parameter is cutting speed followed by feed rate and depth of cut. In turning operations, for a multi-response optimization Taguchi based grey relational approach is used [14, 15] to identify the optimum conditions that obtain better results. Prediction of flank wear and surface roughness during hard turning is performed using uncoated carbide inserts of various tool geometries [16].

Fnides *et al.* [17] investigated the productivity in terms of volume chip carved of six cutting tools for two different cutting conditions in straight hard turning of X38CrMoV5-1 (50 HRC). They found that, for the first set of cutting parameters (*Vc=120 m/min, Doc =0.15 mm*, and *f=0.08 mm/rev*), the productivity of the uncoated cermets CT5015, the coated cermets GC1525, the uncoated carbide H13A, the reinforced ceramic CC670, the coated car-bide GC3015, and the mixed ceramic CC650 are 2,160; 1,440; 6,480; 11,520; 23,040; and 70,560 mm^3, respectively. The productivity of these three selected tools, i.e., mixed ceramic CC650, reinforced ceramic CC670, and coated carbide GC3015, for the second set of cutting parameters (*f=0.08 mm/rev, Doc= 0.15 mm*, and *Vc = 90 m/min*) are 85,860; 12,960; and 30,780 mm^3, respectively. Their results prove that the mixed ceramic Al_2O_3+TiC (CC650) is more efficient than the other tools used in terms of productivity.

The main scope of the present work is the experimental investigation of the effect of machining parameters (i.e., cutting speed, feed rate, depth of cut) on surface roughness in hard turning process of AISI D3 which is widely used in manufacturing. ANOVA is used on the results obtained from experimentation to determine the main effect of parameters and their interactions. Moreover, RSM and regression analysis are used to establish the correlation between factors and responses.

2. Experimental Procedure

2.1. Material, Work piece and Tool

The work piece material used for experiments is AISI D3. The bar of diameter 68 mm x 360 mm long is prepared. Test sample is trued, centred and cleaned by removing a 2 mm depth of cut from the outside surface, prior to actual machining tests. A new insert was employed for each run of experiments in order to provide completely identical cutting edge conditions for each test. The chemical composition of the work piece material is given in Table.1. The workpiece is oil-quenched from 980^0C (1800^0F), hardened, followed by tempering at 200^0C to attain 62HRC. Figure 1 shows the image of cutting insert CC6050. Experimental set up is shown in Figure 2.

The lathe used for machining operations is Kirloskar; model Turn Master-35, spindle power 6.6KW. Surface roughness is measured using *Mitutoyo Surftest SJ 210* as shown in Figure 3 having measuring range of 17.5 mm and skid force less than 400 mN. Four readings with a sample length of 0.8 mm are recorded after each experiment and an average value is taken as the surface roughness. These values are obtained without disturbing the assembly of the work piece in order to reduce uncertainties.

Table 1 Chemical composition of AISI D3 (wt %)

C	Si	Mn	P	S	Cr	Ni	Mo	Al	Cu	Zn	Fe
2.06	0.55	0.449	0.036	0.056	11.09	0.277	0.207	0.0034	0.13	0.27	85

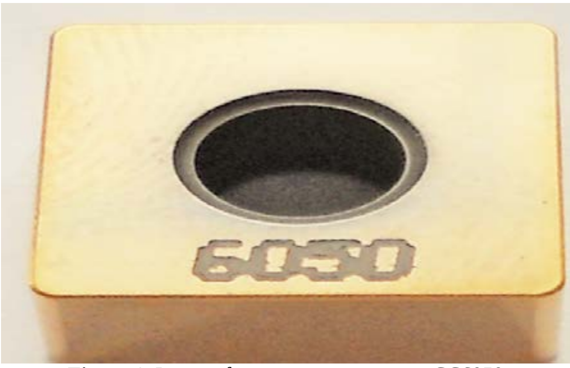

Figure 1. Image of ceramic cutting insert CC6050

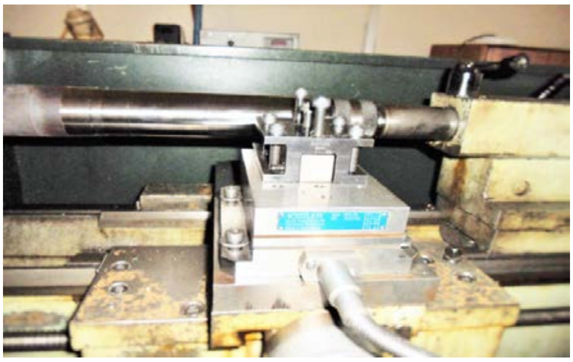

Figure 2. Experimental setup

Figure 3. Mitutoyo Surface Roughness tester SJ 210

The cutting insert used is a mixed ceramic removable, of square form with eight cutting edges and having designation SNGA 120408 T01020 *Sandvik* make CC6050 is a mixed ceramic grade based on alumina with an addition of titanium carbide. The high hot-hardness and the good level of toughness make the grade suitable as first choice for hardened steel (50 – 65HRC) in applications with good stability or with light interrupted cuts. The inserts are mounted on a commercial tool holder of designation PSBNR 2525 M 12 (ISO) with the geometry of active part characterized by the following angles: $\chi = 75°$; $\alpha = 6°$; $\gamma = -6°$; $\lambda = -6°$.

2.2. Experiments Design

RSM is a modelling approach for determining the relationship between the various factors and the responses with the desired criteria and searching the significance of these parameters on the responses. The RSM is useful for developing, improving and optimizing the processes, which provides an overall perspective of the system response within the design space [18]. In order to know surface quality values in advance, it is necessary to employ empirical models making it feasible to do predictions as a function of operational conditions. Using the design of experiments and applying the regression analysis, the modelling of the desired response to several independent process parameters can be obtained. The RSM is utilized to describe and identify the influence of the interactions of different process parameters on the performance characteristics when these are varied simultaneously. In the present investigation, the second-order RSM-based mathematical models for surface roughness (*Ra*) are developed with cutting speed (*Vc*), feed rate (*f*), and depth of cut (*Doc)* as the process parameters.

In the present study, the quantitative form of the relationship between the desired response and independent input process parameters can be represented by [18]:

$$Y = \phi(V_c, f, a_p) \quad (1)$$

Where *Y* is the desired response and ϕ is the response function. In the present investigation, the RSM-based mathematical models for surface roughness *Ra*, have been developed with cutting speed V_c, feed rate f and depth of cut (*Doc*) as the process parameters. The response surface equation for three factors is given by [18]:

$$Y = a_0 + a_1 V_c + a_2 f + a_3 a_p + a_{12} V_c f + a_{13} V_c a_p + a_{23} f a_p + a_{11} V_c^2 + a_{22} f^2 + a_{33} a_p^2 \quad (2)$$

Where *Y* is the desired response and a_0 is the free term of the regression equation, the coefficients a_1, a_2, a_3 and a_{11}, a_{22}, ...a_{33} are the linear and quadratic terms, respectively, while a_{12}, a_{13},..a_{23} are the interacting terms. The experimental plan is developed to assess the influence of cutting speed (V_c), feed rate (*f*), and depth of cut (*Doc*) on the surface roughness (*Ra*), regression coefficients to be determined for each response. The regression coefficients of linear, quadratic, and interaction terms of RSM-based mathematical models are determined by [18].

Three levels are defined for each cutting variable, as given in Table 2. The variable levels are chosen within the intervals recommended by the cutting tool manufacturer. Three cutting variables at three levels led to a total of 20 tests. The factors to be studied and the attribution of the respective levels are indicated in Table 3.

Table 2. Assignment of the levels to the variables

Parameters	**Range**		
	-1	0	+1
Speed (m/min)	145	155	165
Feed (mm/rev)	0.05	0.075	0.1
Depth of cut (mm)	0.3	0.6	0.9

3. Results and Discussion

Table 3 presents the experimental results of surface roughness (*Ra*) for various combinations of cutting conditions (cutting speed, feed rate and depth of cut) as per the design matrix.

The experimental data presented in Table 3, for which analysis has to be graphically done and represented. The following sections present the detailed discussion.

3.1. Statistical Analysis

The estimated regression coefficients for surface roughness *Ra* are shown in Table 4 and scatter plot is shown in Figure 4.

It can be observed from Figure 4 that, as the residuals are located on a straight line, the errors are distributed normally. Hence, the developed empirical models can represent the process significantly. Scatter plots identifies the relationship between two variables whether the relationship is positive, negative, or no relationship can be easily detected. Therefore, these models can be further used for the optimization of process parameters.

Table 3. Experimental results for surface roughness

S.No.	Coded Form			Un-Coded Form			Surface Roughness (Microns)	
	Speed	Feed	*Doc*	Speed (m/min)	Feed (mm/rev)	*Doc* (mm)	Actual	Predicted
1	-1	-1	-1	145	0.05	0.3	0.621	0.63319
2	1	-1	-1	165	0.05	0.3	0.561	0.57789
3	-1	1	-1	145	0.1	0.3	0.982	0.99469
4	1	1	-1	165	0.1	0.3	0.686	0.68439
5	-1	-1	1	145	0.05	0.9	0.79	0.81799
6	1	-1	1	165	0.05.	0.9	0.999	1.01269
7	-1	1	1	145	0.1	0.9	0.954	0.96349
8	1	1	1	165	0.1	0.9	0.889	0.90319
9	-1	0	0	145	0.075	0.6	0.876	0.81365
10	1	0	0	165	0.075	0.6	0.799	0.75585
11	0	-1	0	155	0.05	0.6	0.809	0.73825
12	0	1	0	155	0.1	0.6	0.899	0.86425
13	0	0	-1	155	0.075	0.3	0.759	0.71885
14	0	0	1	155	0.075	0.9	0.986	0.92065
15	0	0	0	155	0.075	0.6	0.787	0.79116
16	0	0	0	155	0.075	0.6	0.799	0.79116
17	0	0	0	155	0.075	0.6	0.786	0.79116
18	0	0	0	155	0.075	0.6	0.635	0.79116
19	0	0	0	155	0.075	0.6	0.931	0.79116
20	0	0	0	155	0.075	0.6	0.601	0.79116

Table 4. Estimated regression coefficients for surface roughness *Ra* (microns)

Term	**Coef**	**SE Coef**	**T**	**P**	**Remarks**
Constant	0.814091	0.02647	30.752	0.000	Significant
Speed(m/min)	-0.028900	0.02435	-1.187	0.263	Insignificant
Feed(mm/rev)	0.063000	0.02435	2.587	0.027	Significant
Doc (mm)	0.100900	0.02435	4.143	0.002	Significant
Speed(m/min)* Speed(m/min)	-0.015227	0.04644	-0.328	0.750	Insignificant
Feed(mm/rev)* Feed(mm/rev)	0.001273	0.04644	-0.027	0.979	Insignificant
Doc (mm)* *Doc* (mm)	0.019773	0.04644	0.426	0.679	Insignificant
Speed(m/min)*Feed(mm/rev)	-0.063750	0.02723	-2.342	0.041	Significant
Speed(m/min)* *Doc* (mm)	0.062500	0.02723	20296	0.045	Significant
Feed(mm/rev)* *Doc* (mm)	-0.054000	0.02723	-1.983	0.075	Insignificant
S = 0.0770070 R-Sq = 80.07% R-Sq(adj) = 62.14%					

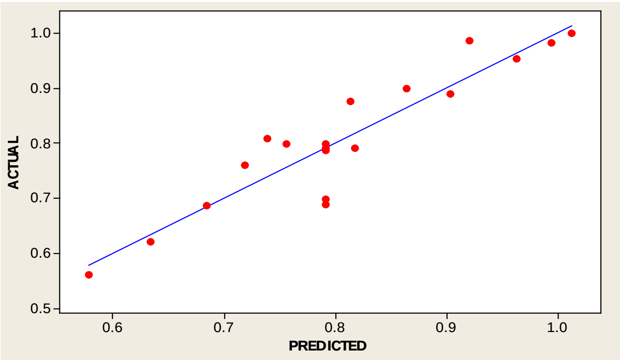

Figure 4. Scatter plot of Ra (actual Vs predicted)

3.2. Analysis of Variance

The ANOVA has been applied to check the adequacy of the developed models. The ANOVA table consists of a sum of squares and degrees of freedom. The sum of squares is performed into contributions from the polynomial model and the experimental value, and was calculated by the following equation:

$$ss_f = \frac{N}{N_{n_f}} \sum_{i=1}^{N_{n_f}} (\bar{y}_i - \bar{y})^2$$

The mean square is the ratio of the sum of squares to degrees of freedom; it was calculated by the following equation:

$$MS = \frac{MS_i}{DF_i}$$

F-value the ratio of mean square of regression model to the mean square of the experimental error, was calculated by the following equation:

$$F - value = \frac{MS_i}{MS_{error}}$$

This analysis was out for a 5% significance level, i.e., for a 95% confidence level. The percentage of each factor contribution (Cont. %) on the total variation, which indicates the degree of the influence on the result, was calculated by the following equation:

$$cont.\% = \frac{SS_i}{SS_{\text{mod}}} X100$$

A low P-value indicates a statistical significance for the source on the corresponding response. It is clear from the results of ANOVA that the depth of cut is the dominant factor affecting surface finish *Ra*. The second factor influencing *Ra* is cutting speed *feed rate. To understand the hard turning process in terms of surface roughness *Ra*, a mathematical model is developed using a multiple regression method. *Ra* model is given by equations 1 and 2. Its coefficient of correlation R^2 is 80.07%.

Table 5. Analysis of variance for surface roughness Ra (microns)

Source	DF	Seq SS	Adj SS	Adj MS	F	P
Regression	9	0.238291	0.238291	0.026477	4.46	0.014
Speed (m/min)	1	0.008352	0.008352	0.008352	1.41	0.263
Feed (mm/rev)	1	0.03969	0.03969	0.03969	6.69	0.027
Doc (mm)	1	0.101808	0.101808	0.101808	17.17	0.002
Speed (m/min)*Speed (m/min)	1	0.000034	0.000638	0.000638	0.11	0.75
Feed (mm/rev)*Feed (mm/rev)	1	0.000242	0.000004	0.000004	0	0.979
Doc (mm)**Doc* (mm)	1	0.001075	0.001075	0.001075	0.18	0.679
Speed (m/min)*Feed (mm/rev)	1	0.032512	0.032512	0.032512	5.48	0.041
Speed (m/min)**Doc* (mm)	1	0.03125	0.03125	0.03125	5.27	0.045
Feed (mm/rev)**Doc* (mm)	1	0.023328	0.023328	0.023328	3.93	0.075
Residual Error	10	0.059301	0.059301	0.00593		
Total	19	0.297592				

3.3. Main Effect Plots and Interaction Plots for Surface Roughness

The effect of process parameters on performance characteristic is easy to explain with the help of the main effects plot. In Figure 5, the main effects for average surface roughness (*Ra*) is plotted.

It is clearly observed that the feed strongly changes the surface roughness. The feed rate has an increasing effect. It is known that the theoretical geometrical surface roughness is primarily a function of the feed for a given nose radius and changes with the square of the feed rate value. The cutting speed has an important and a decreasing effect. Surface roughness is improved by increasing cutting speed, though the improvement is very limited at higher cutting speed (155-165 m/min). Producing a better surface finish at higher cutting speed is well known in metal cutting.

During experimentation, where hardened steel is machined, the cutting speeds are higher than those favouring BUE formation. The higher the velocity is, the less significant the plastic behaviour becomes. The lateral plastic flow of the workpiece material along the cutting edge direction may increase the peak-to-valley height of the surface irregularity. If the material presents less plasticity by increasing cutting speed and, hence, deformation velocity, the surface finish can be improved as a result of less significant lateral plastic flow and, thus, less additional increase in the peak-to-valley height of the machined surface.

For the depth of cut (*Doc*), the influence value is the second statistical significance on surface roughness. However, low depth of cut should be used in order to reduce the tendency to chatter. The depth of cut (*Doc*) has a little direct influence on the surface roughness; however, with the increases in *Doc*, above nose radius of tool values (0.8 mm), a chatter may result causing degradation of the workpiece surface. Therefore, if the tool work system is not very rigid, such as in cutting slender parts, very fine depth of cut should be employed to avoid chatter. In this way, very good surface finish can be obtained. For all machining tests, the *Ra* values observed are in the range of 0.561-0.999 microns, indicating that Ceramic tool is able to produce parts with surfaces equivalent to those resulting from grinding and other finishing processes.

3.4. Contour Plots for Surface Roughness Vs Speed, Feed and Depth of cut.

Contour plots play a very important role in the study of the response surface. By creating contour plots using software for response surface analysis, the optimum is located by characterising the shape of the surface. Circular shaped contour represents the independence of factor effects and elliptical contours may indicate factor interaction. The contours of the responses are shown in Figures 6a, 6b & 6c. The surface roughness clearly showed that the minimum roughness is at low value of feed, because feed is the most influencing factor for surface roughness. *Ra* is minimum at low depth of cut and low speed.

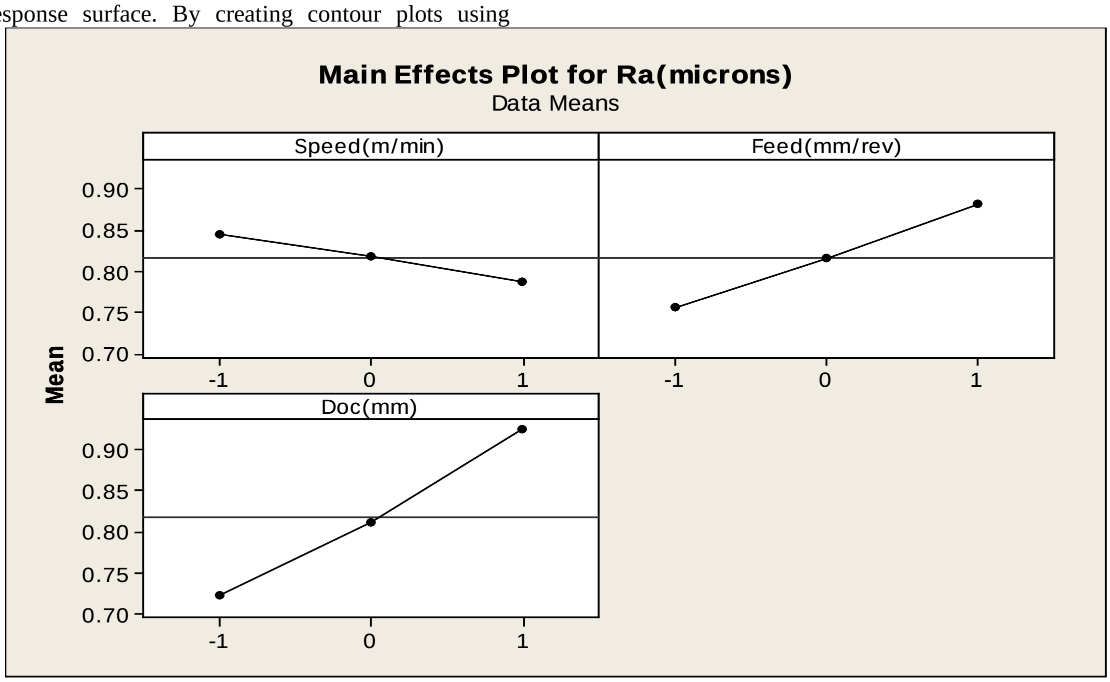

Figure 5. Main effect plots for mean Surface roughness against speed, feed and depth of cut.

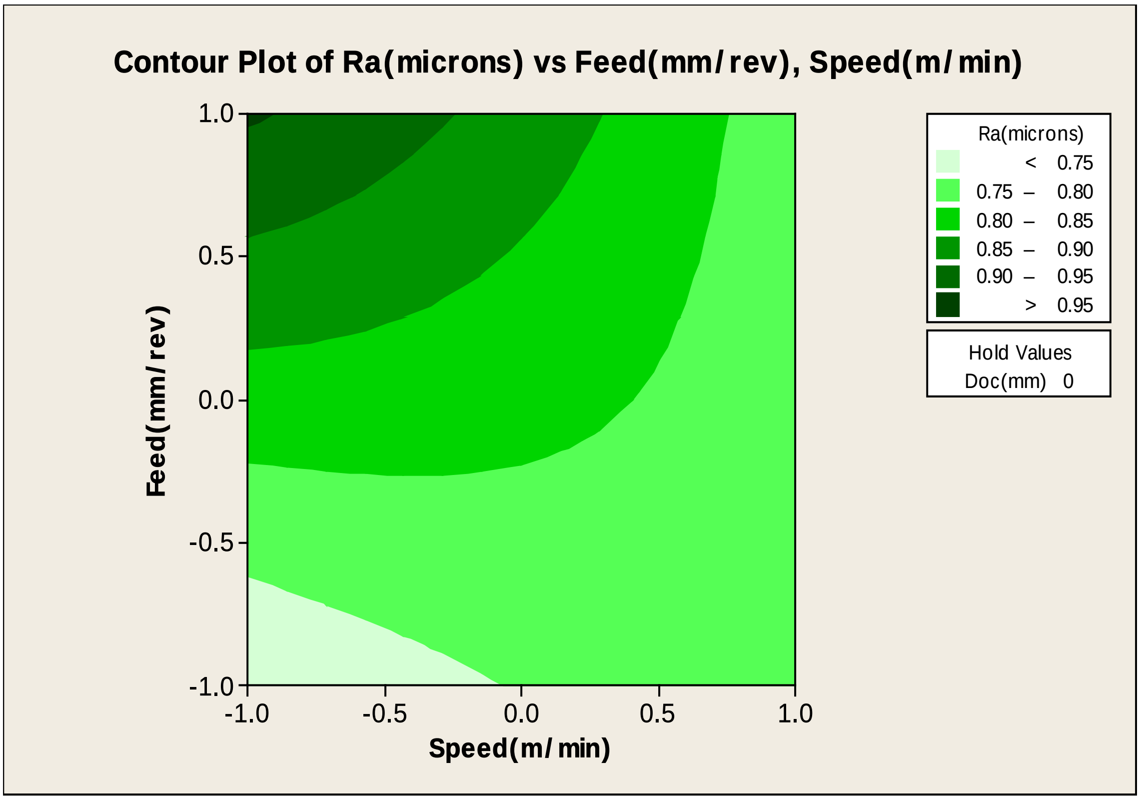

Figure 6a. contour plot of *Ra* vs Feed and Speed

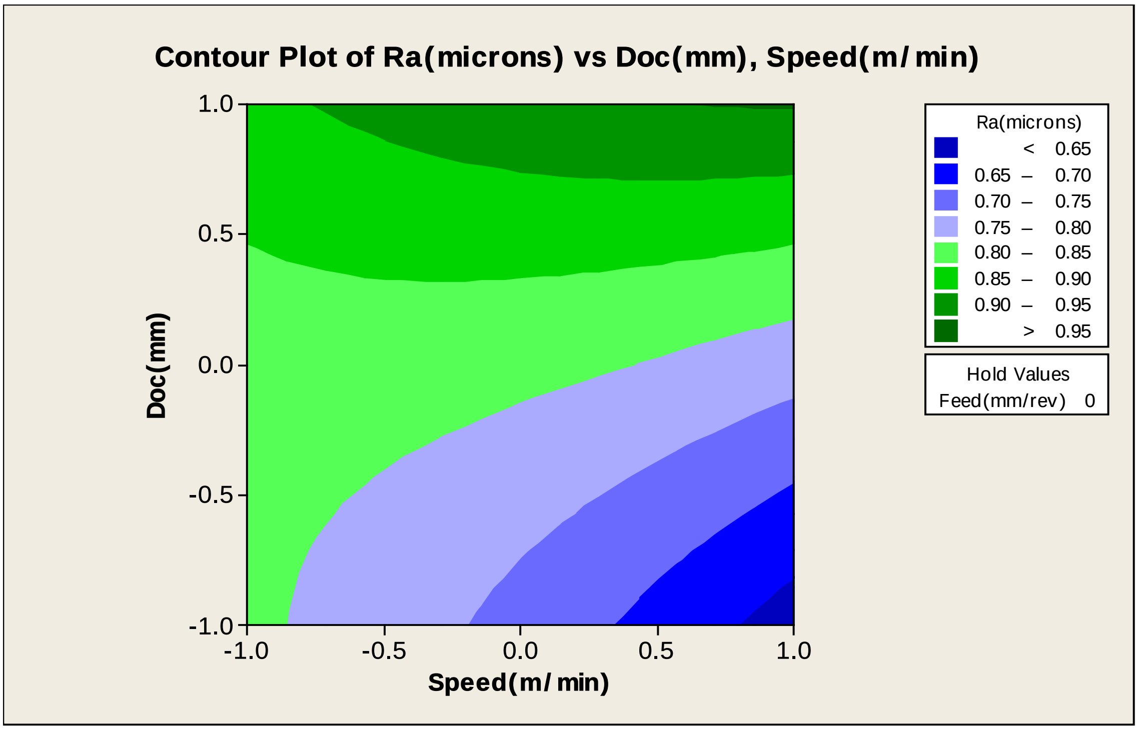

Figure 6b. contour plot of *Ra* vs a_p and Speed

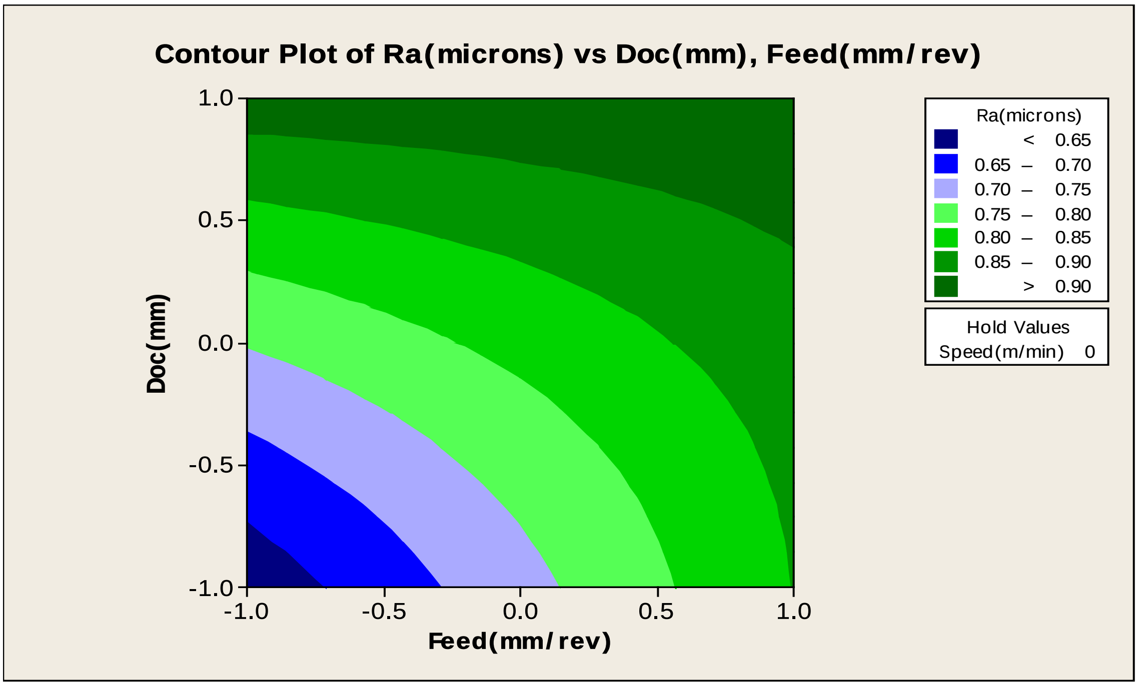

Figure 6c. contour plot of Surface roughness vs a_p and Feed

3.5. 3 D Surface Plots

3D Surface plots of *Ra* vs. different combinations of cutting parameters are shown in Figures 7a, 7b, 7c, and these figures obtained by RSM. Figure 7a presents the influences of cutting speed (*Vc*) and feed rate (*f*) on the surface roughness, while the depth of cut (*Doc*) is kept at the middle level. Figure 7b shows the estimated response surface in relation to the cutting speed (*Vc*) and depth of cut (*Doc*), while feed rate (*f*) is kept at the middle level. The effects of the feed rate (*f*) and depth of cut (*Doc*) on the cutting force components are shown in Figure 7c, while the cutting speed (*Vc*) is kept at the middle level. For each plot, the variables not represented are held at a constant value (the middle level). These 3D plots confirm the notes observed during the principal effects plots analysis.

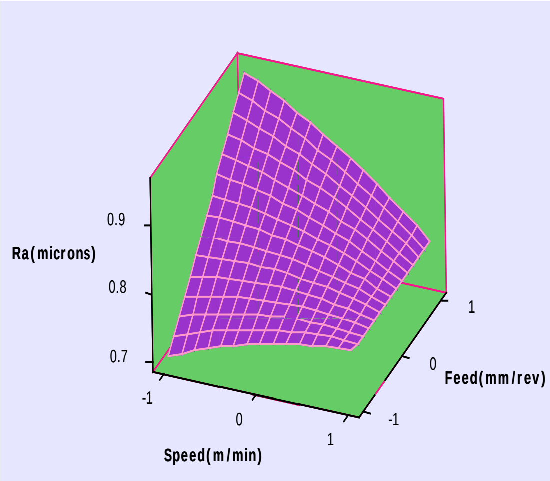

Figure 7a. Surface roughness vs Speed and Feed

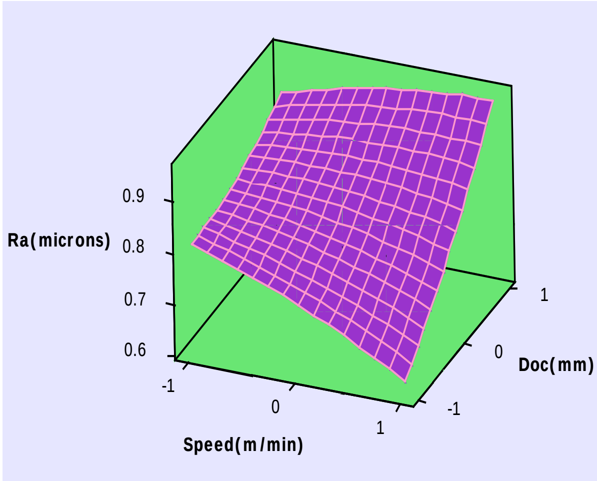

Figure 7b. Surface roughness vs Speed and *Depth of cut*

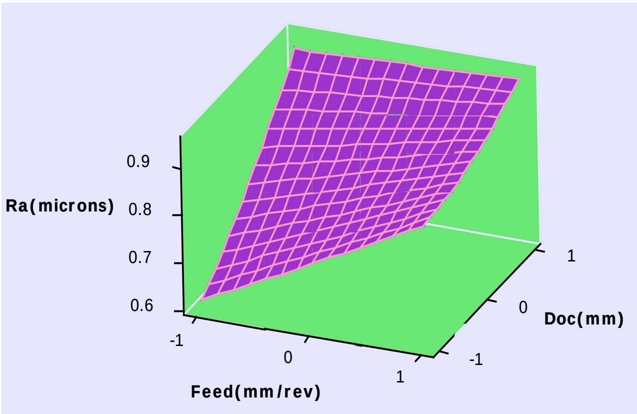

Figure 7c. Surface roughness vs Feed and Depth of cut

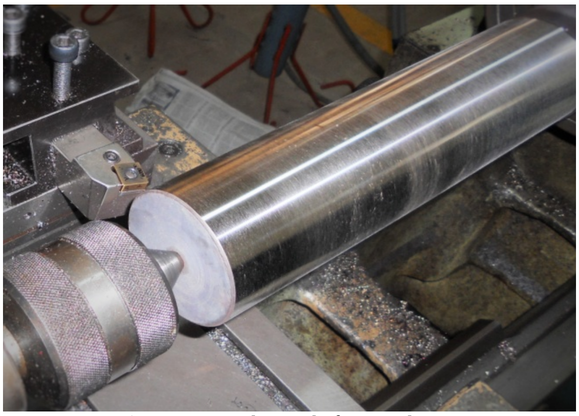

Figure 8a. Workpiece before machining

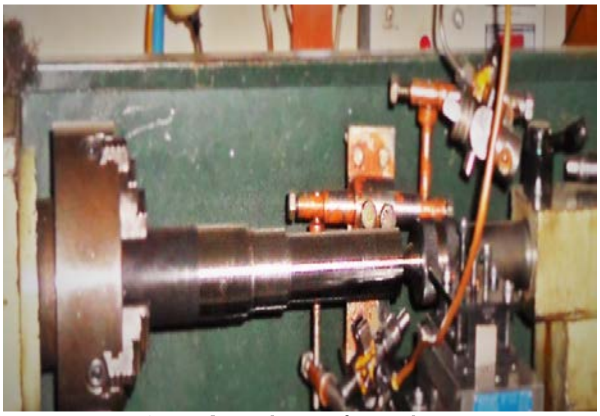

Figure 8b. Workpiece after machining

Figure 8. Workpiece before and after machining

4. Conclusions

The tests of hard turning, carried out on AISI D3 steel having 62 HRC which is machined with a mixed ceramic tool (insert CC6050), enabled us to develop statistical models of surface roughness criteria.

- These models are obtained using a multiple regression method in Minitab16 software. The results revealed that the feed rate seems to influence the surface roughness more significantly than the cutting speed.
- The depth of cut is found to be the second significant parameter after feed; thus, to get a good surface finish with a higher chip removal rate, the proposed process parameters are cutting speed at 165 m/min, feed rate at 0.05 mm/rev and depth of cut of 0.3 mm.
- The statistical models developed illustrate the degree of influence of each machining condition on surface roughness. These models can also be used for the optimization of hard cutting process.

This study confirms that dry hard turning of AISI D3 steel for the chosen cutting conditions shows the surface roughness to be close to that obtained in grinding.

References

[1] Özel, T., and Karpat, Y., "Predictive Modeling of Surface Roughness and Tool Wear in Hard Turning Using Regression and Neural Networks", International Journal of Machine Tools and Manufacture, Vol.45(2005), p.467-479.

[2] Zeren, E., and Özel, T, "Hard Turning Technology", Report No. MARL-01, Rutgers, The State University of New Jersey, 2002.

[3] Koenig, W., Berktold, A., and Koch, F., "Turning Versus Grinding-A Comparison of Surface Integrity Aspects and Attainable Accuracies", Annals of the CIRP, Vol. 42(1993) No.1, p. 39- 43.

[4] Mohammadi,A. and Zarepour,H., "Statistical Analysis Of Hard turning Of AISI 4340 Steel on surface finish and Cutting Region Temperature" , M0048010, Bahrain , Manama, AMPT 2008.

[5] Kountanya, R.K., "Optimizing PCBN cutting tool performance in hard turning",Proceeding of the Institution of Mechanical Engineers, part B:Journal of Engineerin manufacture, Vol. 222(2008), p. 969-980.

[6] Dogra,M., Sharma,V.S., Sachdeva,A., Mohan suri,N. and Dureja,J.S, "Tool wear, Chip Formation and Workpiece Surface Issues In CBN Hard Turning:A Review", Intetnational Journal of Pecision Engineering and Manufacturing,Vol.11(2010),p. 341-358.

[7] Horng,J-T., Liu,N-M., Chiang, K-T., "Investigating the machinability evaluation of hod- field steel in the hard turning with Al_2O_3/TiC mixed ceramic Tool based on the response surface methodology", Journal Of Materials Processing Technology, Vol. 208(2008), p. 532-541.

[8] Zou B., Chen M., and Li S., "Study on finish-turning of NiCr20TiAl nickel-based alloy using Al_2O_3/TiNcoated carbide tools". International Journal of Advanced Manufacturing Technology, Vol.53(2011), p.81–92

[9] Fahad M., Mativenga PT., and Sheikh MA., "A comparative study of multilayer and functionally graded coated tools in high-speed machining", International Journal of Advanced Manufacturing Technology, Vol. 62(2012), p. 43–57.

[10] Hamdan A., Sarhan AAD., and Hamdi M., "An optimization method of the machining parameters in high speed machining of stainless steel using coated carbide tool for best surface finish", International Journal of Advanced Manufacturing Technology,Vol. 58(2012), p.81–91.

[11] Suhail AH., Ismail N., Wong SV., and Jalil NAA., ,"Surface Roughness Identification Using the Grey Relational Analysis with Multiple Performance Characteristics in Turning operations", The Arabian Journal for Science and Engineering, Vol.37(2012) No.4, p. 1111-1117

[12] Gopalsamy BM., Mondal B., and Ghosh S., "Optimisation of machining parameters for hard machining: grey relational theory approach and ANOVA". International Journal of Advanced Manufacturing Technology, Vol.45(2009), p.1068-1086.

[13] Ahilan C., Kumanan S., and Sivakumaran N., "Application of Grey based Taguchi method in multi response optimization of turning process". Advances in Production Engineering & Management, Vol. 5(2010) No.3, p. 171-180.

[14] Tzeng CJ., Lin YH., Yang YK., and Jeng MC.,"Optimization of turning operations with multiple performance characteristics using the Taguchi method and Grey relational analysis", Journal of Materials Processing Technology, Vol.209(2009), p. 2753–2759.

[15] Kazancoglu Y., Esme U., Bayramoglu M., Guven O., and Ozgun S., "Multi-Objective Optimization of The Cutting Forces In Turning Operations Using The Grey-Based Taguchi Method", Materials and Technology, Vol. 45(2011) No.2, p. 105–110.

[16] Senthilkumar N., Tamizharasan T., and Anandakrishnan V., "An ANN approach for predicting the cutting inserts performances of different geometries in hard turning" Advances in Production Engineering & Management, Vol. 8(2013) No.4, p.231-241.

[17] Fnides B, Boutabba S, Fnides M, Aouici H, Yallese MA., "Cutting tools flank wear and productivity investigation in straight turning of X38CrMoV5-1 (50 HRC)". J App Eng Technol Vol 3(2013) No.1, p. 1–10.

[18] Montgomery, D.C. "Design and Analysis of Experiments"; John Wiley & Sons, Inc: New York, 1997; p. 395-476.

JJMIE

Volume 8 Number 6, December 2014
ISSN 1995-6665
Pages 403 - 408

Jordan Journal of Mechanical and Industrial Engineering

Melting Heat Transfer in Boundary Layer Stagnation Point Flow of MHD Micro - polar Fluid towards a Stretching / Shrinking Surface

Khilap Singh* , Manoj Kumar

Department of Mathematics, Statistics and Computer ScienceG.B. Pant University of Agriculture and Technology, Pantnagar, Uttarakhand, India

Received 20 Feb 2014 *Accepted 31 Oct 2014*

Abstract

The present study investigates the fluid flow and heat transfer characteristics occurring during the melting process due to a stretching / shrinking surface in micropolar fluid. A uniform magnetic field is applied normally to the surface. The governing equations representing fluid flow were transformed into nonlinear ordinary differential equations using similarity transformation. The equations thus obtained were solved numerically using the Runge–Kutta-Fehlberg fourth-fifth order method with shooting technique. The effects of the magnetic parameter on the fluid flow, couple stress coefficient and heat transfer characteristics, are illustrated graphically and discussed in detail. Significant changes were observed in the fluid flow, couple stress coefficient and heat transfer with respect to magnetic parameter.

Keywords: *Boundary Layer, Melting Heat, MHD, Micropolar Fluid, Stagnation-Point, Stretching Sheet*.

1. Introduction

The micropolar fluids are those which contain micro-constituents that can undergo rotation, the presence of which can affect the hydrodynamics of the flow. It has many practical applications, like, for example, analyzing the behaviour of exotic lubricants, colloidal suspensions, solidification of liquid crystals, extrusion of polymer fluids, cooling of metallic plate in a bath, animal blood, body fluids, among others. Eringen [1] introduced the theory of micropolar fluids that is capable to describe those fluids by taking into account the effect arising from local structure and micromotions of the fluid elements. Gamal and Rahman [2] studied the effect of MHD on thin films of a micropolar fluid and they observed that the rotation of the microelements at the boundary increase the velocity when compared with the case when there is no rotation at the boundary. Das [3] investigated the effect of the first order chemical reaction and thermal radiation on hydro-magnetic free convection heat and mass transfer flow of a microplar fluid through a porous medium. Satya Naraya *et al.* [4] investigated the effects of Hall current and radiation absorption on MHD free convection mass transfer flow of a micropolar fluid in a rotating frame of reference. Srinivasacharya [5] analyzed the heat and mass transfer characteristic of the forced convection on a vertical wall temperature and concentration in a doubly stratified micropolar fluid. Das [6] studied the effect of partial slip on steady boundary layer stagnation point flow of an electrically conducting micropolar fluid impinging normally through a shrinking sheet in the presence of a uniform transverse magnetic field. The unsteady MHD boundary layer flow of a micropolar fluid near the stagnation point of a two-dimensional plane surface through a porous medium was studied by Nadeem *et al.* [7]. Ishak *et al.* [8] investigated the heat transfer over a stretching surface with variable heat flux in micropolar fluid. Wang [9] investigated the shrinking flow where the velocity of boundary layer moves toward a fixed point and he found an exact solution of Navier-Stokes equations. A good list of references for micropolar fluids is available in Łukaszewicz [10]. Tien and Yen [11] investigated the effect of melting on forced convection heat transfer between a melting body and surrounding fluid. Epstein and Cho [12] analyzed the melting heat transfer of the steady laminar flows over a flat plate. The steady laminar boundary layer flow and heat transfer from a warm, laminar liquid flow to a melting surface moving parallel to a constant free stream has been studied by Ishak *et al.* [13]. Rosali *et al.* [14] studied micropolar fluid flow towards a permeable stretching /shrinking sheet in a porous medium numerically. Yacob *et al.* [15] investigated a model to study the heat transfer characteristics occurring during the melting process due to a stretching / shrinking sheet and they studied the effects of the material parameter, melting parameter and the stretching /shrinking parameter on the velocity, temperature, skin friction coefficient and the local Nusselt number. Cheng and Lin [16] analyzed the melting effect on transient mixed convective heat transfer from a vertical plate in a liquid saturated porous medium.

* Corresponding author. e-mail: singh.khilap8@gmail.com.

In the present work, we consider the boundary layer stagnation-point flow and melting heat transfer of a MHD micropolar fluid towards a stretching / shrinking surface. To the best of our knowledge, this problem has not been considered before, so that the results are new.

2. Mathematical formulation

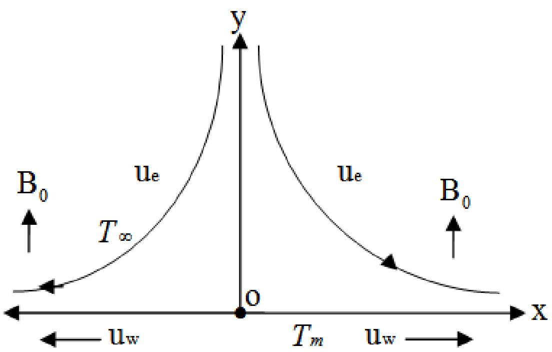

Figure 1: Flow configuration and Coordinate system

The graphical model of the problem is given along with flow configuration and coordinate system. The system deals with two dimensional stagnation point steady flow of micropolar fluids towards a stretching / shrinking surface and subject to a constant transverse magnetic field B_0. The velocity of the external flow is $u_e\,(x) = ax$ and the velocity of the stretching surface is $u_w\,(x) = cx$, where a is a positive constant and c is a positive (stretching surface) or a negative (shrinking surface) constant, x is the coordinate measured along the surface. It is also assumed that the temperature of the melting surface and free stream condition is T_m and T_∞, where $T_\infty > T_m$. The viscous dissipation and the heat generation or absorption has assumed to be negligible. Under these assumptions, the governing equations representing flow are as follows:

$$\frac{\partial u}{\partial x}+\frac{\partial v}{\partial y}=0 \tag{1}$$

$$u\frac{\partial u}{\partial x}+v\frac{\partial v}{\partial y}=u_e\frac{\partial u_e}{\partial x}+\frac{(\mu+k)}{\rho}\frac{\partial^2 u}{\partial y^2}+\frac{k}{\rho}\frac{\partial N}{\partial y}-\frac{\sigma B_0^2}{\rho}(u_e-u) \tag{2}$$

$$u\frac{\partial N}{\partial x}+v\frac{\partial N}{\partial y}=\frac{\gamma}{\rho j}\frac{\partial^2 N}{\partial y^2}-\frac{k}{\rho j}(2N+\frac{\partial u}{\partial y}) \tag{3}$$

$$u\frac{\partial T}{\partial x}+v\frac{\partial T}{\partial y}=\alpha\frac{\partial^2 T}{\partial y^2} \tag{4}$$

with the following boundary conditions:

$$u=u_w(x)=cx\,;\; N=-n\frac{\partial u}{\partial y}\,;\; T=T_m \quad at \quad y=0$$

$$u=u_e(x)=ax\,;\; N=0\,;\; T=T_\infty \quad as\; y\to\infty \tag{5}$$

and $$\kappa\left(\frac{\partial x}{\partial y}\right)_{y=0}=\rho\left[\lambda+c_s(T_m-T_0)\right]v(x,0)$$

here u and v are the velocity component along the x and y axis, respectively. Further, μ is dynamic viscosity, k is vortex viscosity, σ is electrical conductivity of the fluid, ρ is fluid density, T is fluid temperature, j is micro inertia density, N is microrotation, γ is spin gradient viscosity, α is thermal diffusivity, κ is the thermal conductivity, λ is the latent heat of the fluid and C_s is the heat capacity of the solid surface. We note that n is a constant such that $0 \le n \le 1$. The case when $n = 0$, is called strong concentration which indicates that no microtation near the wall. In case $n = 1/2$ it indicates that the vanishing of anti-symmetric part of the stress tensor and denote weak concentration and the case $n = 1$ is used for the modeling of turbulent boundary layer flows by Yacob *et al.* [15]. $\gamma=\left(\mu+\frac{k}{2}\right)l=\mu(1+\frac{K}{2})l$, where $K=\frac{\kappa}{\mu}$ is the micro polar or material parameter and $l=\frac{\upsilon}{a}$ as reference length. The total spin N reduces to the angular velocity.

3. Problem solution

Equations (2) - (4) can be transformed into a set of nonlinear ordinary differential equations by using the following similarity variables:

$$\gamma=\left(\mu+\frac{k}{2}\right)l=\mu\left(1+\frac{K}{2}\right)l,\; K=\frac{k}{2},\; l=\frac{\upsilon}{a},$$

$$\psi=\left(a\upsilon\right)^{1/2}xf(\eta),\; N=xa\left(\frac{a}{\upsilon}\right)^{1/2}g(\eta), \tag{6}$$

$$\theta(\eta)=\frac{T-T_m}{T_\infty-T_m}, \qquad \eta=\left(\frac{a}{\upsilon}\right)^{1/2}y$$

The transformed ordinary differential equations are:

$$\left(1+K\right)f'''+ff''+1-f'^2+Kg'+M\left(1-f'\right)=0 \tag{7}$$

$$\left(1+K/2\right)g''+fg'-f'g+\mathrm{K}\left(2g+f''\right)=0 \tag{8}$$

$$\theta''+\Pr f\theta'=0 \tag{9}$$

where primes denote differentiation with respect to η and $Pr = \upsilon/\alpha$ is Prandtl number. The boundary conditions (5) become:

$$f'(0)=\varepsilon,\; g\left(0\right)=-nf''\left(0\right),$$

$$\Pr f\left(0\right)+m\theta'\left(0\right)=0,\,\theta\left(0\right)=0 \tag{10}$$

$$f'\left(\infty\right)=1,\; g\left(\infty\right)=0,\; \theta\left(\infty\right)=1.$$

where $\varepsilon = c/a$ is the stretching ($\varepsilon > 0$) or shrinking ($\varepsilon < 0$) parameter, m is the dimensionless melting parameter and M is magnetic parameter which are defined as:

$$m = \frac{c_f \left(T_\infty - T_m\right)}{\lambda + c_s \left(T_m - T_0\right)},$$

$$M = \frac{\sigma B_0^2}{a\rho} \qquad (11)$$

The physical parameters of interest are the skin friction coefficient C_f, local Couple stress coefficient C_m and the local Nusselt number Nu_x, which are defined as:

$$C_f = \frac{\tau_w}{\rho u_e^2},$$

$$C_m = \frac{C_w}{x\rho u_e^2}, \qquad (12)$$

$$Nu_x = \frac{x q_w}{\kappa\left(T_\infty - T_m\right)}$$

where τ_w, c_w and q_w are the surface shear stress, the local couple stress and the surface heat flux respectively, which are given by:

$$\tau_w = \left(\mu + k\right)\left(\frac{\partial u}{\partial y}\right)_{y=0},$$

$$C_w = \gamma\left(\frac{\partial u}{\partial y}\right)_{y=0}, \qquad (13)$$

$$q_w = -\kappa\left(\frac{\partial u}{\partial y}\right)_{y=0}$$

hence using (6), we get:

$$\mathrm{Re}_x^{1/2} C_f = \left[1 + \left(1-n\right)K\right] f''(0),$$

$$\mathrm{Re}_x C_m = \left(1 + \frac{K}{2}\right) g'\left(0\right), \qquad (14)$$

$$\mathrm{Re}_x^{-1/2} Nu_x = -\theta'\left(0\right)$$

where $\mathrm{Re}_x = u_e\left(x\right)x/\upsilon$ is the local Reynolds number.

4. Results and discussion

The transformed equations (7) - (9), subject to boundary conditions (10), were solved numerically using the Runge-Kutta-Fehlberg fourth-fifth order method with shooting technique to obtain the missing values of $f''(0)$, $g'(0)$ and $\theta'(0)$ for some values of the magnetic parameter M, micropolar parameter K, melting parameter m and the stretching / shrinking parameter ε, while the Prandtl number Pr is fixed to unity and we take $n=0.5$ (weak concentration).

In order to validate the numerical results obtained, we compared our results with those reported by Ishak *et al.* [8], Wang [9], and Yacob *et al.* [15], as shown in Table 1; and they are found to be in a favorable agreement.

Figures 2, 3 and 4 show the variations of the skin friction coefficient $f''(0)$, the local couple stress coefficient $g'(0)$ and the local Nusselt number $-\theta'(0)$, respectively with ε for different value of M when $m=1$, $K=1$. It is also seen from these figures that for the shrinking case ($\varepsilon < 0$), the solution exists up to a critical value of ε (say ε_c) beyond which no solution exists. The values of $f''(0)$ are positive when $\varepsilon < 1$, and become negative when $\varepsilon > 1$. Physically, positive value of $f''(0)$ means the fluid exerts a drag force on the solid surface and negative value means the solid surface exerts a drag force on the fluid. The zero skin friction when $\varepsilon = 1$, since for this case the stretching velocity is equal to the free stream velocity. However, for this case, the heat transfer rate at the surface $-\theta'(0) \neq 0$ means there is a heat transfer between the fluid-solid interfaces (even when the friction is zero). The couple stress coefficient $g'(0)$ (Figure 3) shows similar behaviour as that of skin friction coefficient for the variation of the magnetic parameter M with the Stretching parameter ε. The negative value of $-\theta'(0)$, presented in Figure 4, shows that the heat is transferred from the warm fluid to cool solid surface. It is evident from Table 2 and Figure 2 that an increase in magnetic parameter M leads to a decrease in the value of $f''(0)$ absolute sense. It is clear form Table 2 and Figure 3 that the value of local couple stress coefficient $g'(0)$ decreases with the increase in the value of magnetic parameter M for $\varepsilon < 1$, whereas the value of local couple stress coefficient $g'(0)$ increases with increasing value of magnetic parameter M for $\varepsilon > 1$. This result in the decreasing manner of the heat transfer rate at the fluid-solid interface $\left|-\theta'(0)\right|$ for $\varepsilon < 1$, but opposite behaviours are observed for $\varepsilon > 1$.

It is observed from velocity profiles $f'(\eta)$ in Figure 5 that the value of $f'(\eta)$ decreases as M increases and from the angular velocity profiles $g(\eta)$ in Figure 6 show that the value of $g(\eta)$ initially increases as M increases and then changing the behaviour for large η the value of $g(\eta)$ decreases with M, thus due to the increase in magnetic parameter M the boundary layer thickness increases. For temperature (Figure 7), the change in magnetic parameter M there is a small change in the temperature $\theta(\eta)$. Consequently, thermal boundary layer undergoes negligible change with M. Finally, from all the figures (Figures 5–9) above, it can be easily seen that the far field boundary conditions are satisfied asymptotically and it signifies the correctness of the numerical scheme used.

Table 1. Comparison between *f ''(0)* and - *θ'(0)* calculated by the present method, Ishak *et al.* [8], Wang [9] and Yacob *et al.* [15] for various values of *m, ε, K* when *M=0*.

M	*ε*	*M*	*K*	Ishak et al. [8]	Wang [9]	Yacob et al. [15]		Present Result	
				f ''(0)	*f ''(0)*	*f ''(0)*	*-θ'(0)*	*f ''(0)*	*-θ'(0)*
	0	0	0	1.2326	1.232588	1.232588	-0.570465	1.232588	-0.570466
			1			1.006404	-0.544535	1.006404	-0.544535
		1	0			1.037003	-0.361961	1.037003	-0.361962
0			1			0.879324	-0.347892	0.879324	-0.347892
	0.5	0	0		0.7133	0.713295	-0.692064	0.713295	-0.692065
			1			0.582403	-0.680176	0.582403	-0.680176
		1	0			0.59909	-0.438971	0.59909	-0.438971
			1			0.506342	-0.432443	0.506342	-0.432443

Table 2 The values of Skin friction coefficient *f ''(0)*, local couple stress coefficient *g ' (0)* and local nusselt number – *θ ' =(0)* for various values of *M*, *ε* when *m*=1 and *K*=1.

M	***ε***	***f''(0)***	***g'(0)***	**- *θ'(0)***
0	0.75	0.26818	0.10379	-0.470624
0.5	0.75	0.23458	0.086155	-0.468501
1	0.75	0.19584	0.06638	-0.466002
0	1.5	-0.61692	-0.29904	-0.572001
0.5	1.5	-0.5596	-0.26514	-0.574801
1	1.5	-0.49625	-0.22813	-0.57793
0.5	- 0.25	0.76177	0.11516	-0.27859
0.5	-0.5	0.72995	0.03944	-0.27859
1	-0.25	0.3965	-0.01038	-0.23432
1	-0.5	0.136	-0.09535	-0.14615

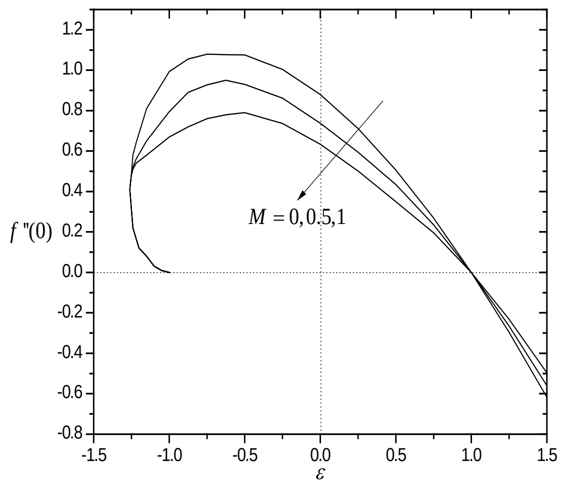

Figure2. Skin friction coefficient *f ''(0)* with *ε* for several value of *M* when *m=1, K=1*

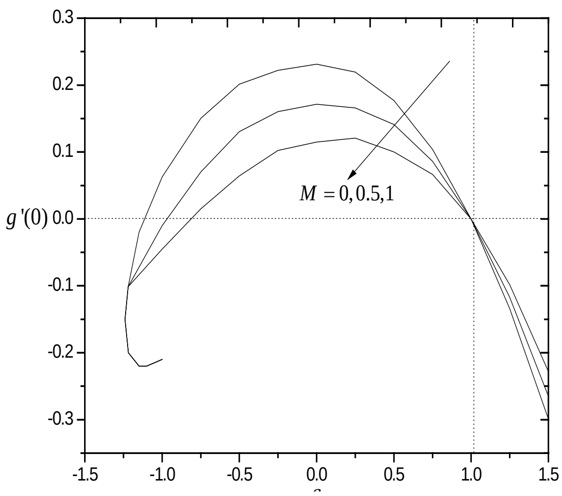

Figure3. Local Couple stress coefficient *g'(0)* with *ε* for several value of *M* when *m = 1, K = 1*

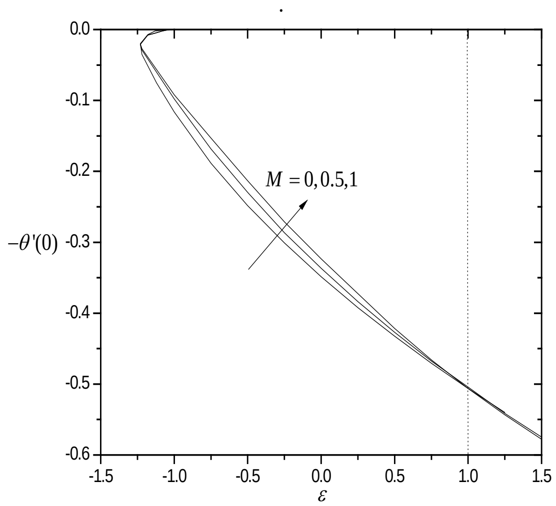

Figure 4. Heat transfer coefficient $-\theta'(0)$ with ε for several value of M when $m=1$, $K=1$.

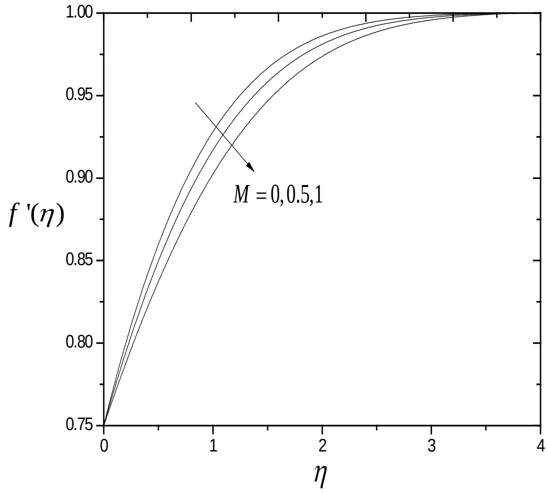

Figure 5. Velocity profiles $f'(\eta)$ for several value of M when $m=1$, $K=1$ and $\varepsilon = 0.75$

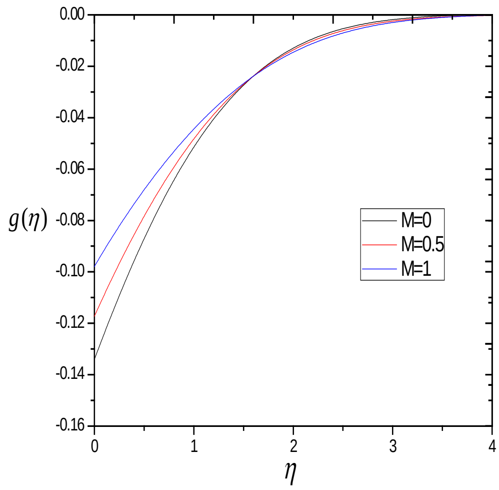

Figure 6. Angular velocity profiles $g(\eta)$ for several value of M when $m=1$, $K=1$ and $\varepsilon = 0.75$

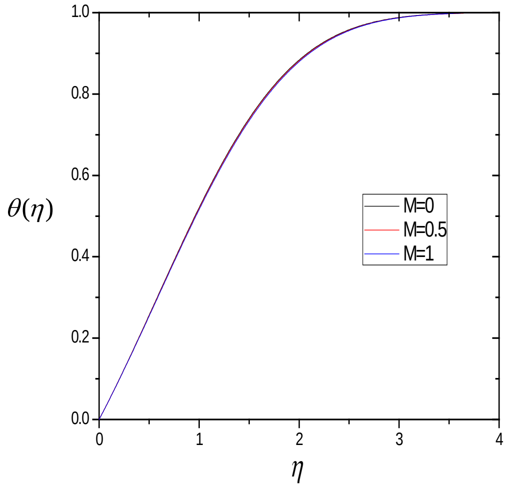

Figure 7. Temperature profiles $\theta(\eta)$ for several value of M when $m=1$, $K=1$ and $\varepsilon = 0.75$

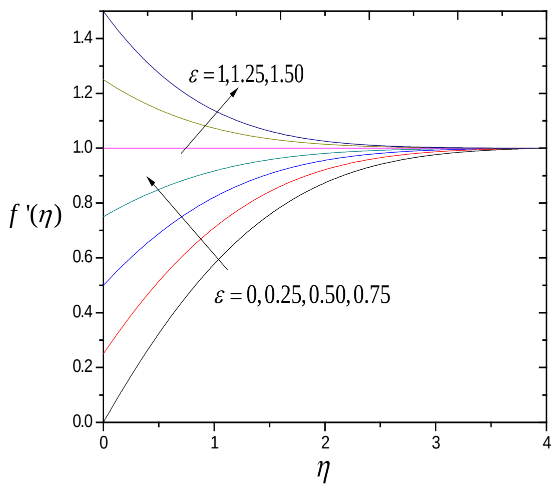

Figure 8. Velocity profile $f'(\eta)$ for different values of ε when $M=0.5$, $K=1$ and $m=1$.

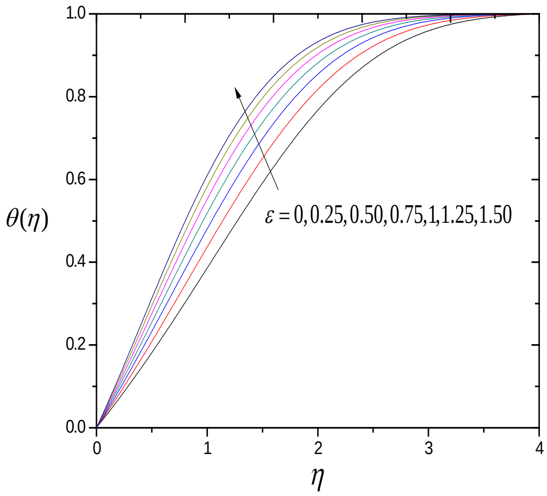

Figure 9. Temperature profile $\theta(\eta)$ for different value of ε when $M=0.5$, $K=1$ and $m=1$

5. Conclusions

We have studied the effects of the magnetic parameter on skin friction coefficient, couple stress coefficient and local Nusselt number (which represents the heat transfer rate at the surface) for the steady laminar boundary layer stagnation point flow and heat transfer from a warm micropolar fluid to a melting solid surface of the same material. It has been found that the skin friction coefficient, the couple stress coefficient and the heat transfer coefficient decreases with increase in magnetic parameter.

References

[1] Eringen A.C, Theory of micropolar fluid, Jour of mathematics and Mechanics, 16(1966),1-18.

[2] Gamal M, Rahman A, Studying effect of MHD on thin films of a micropolar fluid, Physica B, 404(2009) 3859-3866.

[3] Das K, Effect of chemical reaction and thermal radiation on heat and mass transfer flow of MHD micropolar fluid in a rotating frame of reference, Int Jour of Heat and Mass Transfer, 54(2001) 3505-3513.

[4] Satya Narayan P.V, Venkateswarlu B, Venkataramana S, Effects of Hall current and radiation absorption on MHD micropolar fluid in a rotating system, Ain Shams Engineering Jour 4 (2003), 843-854.

[5] Srinivasacharya D, Upendar M, Effect of double stratification on MHD free convection in a micropolar fluid, Jour of the Egyptian Mathematical Society, 21(2013) 370-378.

[6] Das K, Slip effects on MHD mixed convection stagnation point flow of a micropolar fluid towards a shrinking vertical sheet, Computers and Mathematics with Applications, 63 (2012) 255-267.

[7] Nadeem S, Hussain M, Naz M, MHD stagnation flow of a micropolar fluid through a porous medium, Meccanica, 45 (2010) 869–880.

[8] Ishak A, Nazar .R, Pop.I. Heat transfer over a stretching surface with variable heat flux in micropolar fluids. Phys Lett A 372 (2008) 559–561.

[9] Wang C.Y, Stagnation flow towards a shrinking sheet, Int Jour of Non-linear Mech 43(2008) 377-382.

[10] Łukaszewicz .G, Micropolar fluids: theory and application. Basel: Birkhäuser; 1999.

[11] Tien. C, Yen Y.C. The effect of melting on forced convection heat transfer. J Appl. Meteorol 4(1965), 523–527.

[12] Epstein M, Cho D.H, Melting heat transfer in steady laminar flow over a flat plate. J.of Heat Transfer, 98(1976), 531–533.

[13] Ishak .A, Nazar .R, Bachok N, Pop I. Melting heat transfer in steady laminar flow over a moving surface. Heat Mass Transfer, 46 (2010), 463–468.

[14] Rosali H, Ishak A, Pop I, Micropolar fluid flow towards a stretching / Shrinking sheet in a porous medium with suction 39(2012), 826–829.

[15] Yacob N.A , Ishak A , Pop I, Melting heat transfer in boundary layer stagnation – point flow towards a stretching /shrinking sheet in a micropolar fluid 47 (2011), 16–21

[16] Cheng W.T, Lin C.H, Transient mixed convective heat transfer with melting effect from the vertical plate in a liquid saturated porous medium. Int J Eng Sci 44(2006), 1023–36.

JJMIE

Volume 8 Number 6, December 2014
ISSN 1995-6665
Pages 409 - 415

Jordan Journal of Mechanical and Industrial Engineering

Fuzzy Rules Extraction Based on Deterministic Data (Case Study: Bank's Customers Rating)

Ramin Sadeghian*, Behnam Gholamaliei,

Leila Payandeh Peyman

Received 20 April 2014 *Accepted 20 Nov 2014*

Abstract

Financial institutions and banks are the type of organizations whose customer rating is very valuable. In the present paper, two algorithms are proposed and compared that can extract some fuzzy rules from deterministic data. Each fuzzy rule may be used as a class of customers. In the first algorithm, a method is proposed based on both experiment and fuzzy theory. In the second algorithm a heuristic approach is proposed. Additionally, for more explanations a case study in a real bank is presented.

Keywords: *Bank's Customers Rating, Fuzzy Rules Extraction, Deterministic Data Clustering, Linguistic Labels*.

1. Introduction

The knowledge acquisition from the existing data and information is essential for today's complicated world. The data mining and rules extraction from the raw data can be one method for knowledge acquisition [1]. In this paper, two algorithms are proposed to extract some fuzzy rules from the raw data. The extracted rules may be used in each field and situation. For instant, each rule may show a class of customers and consequently a service level of them.

The extracted rules can be applied for rating the customer of a specific bank. The customer rating can be very valuable for both customers and servicers. For example, top customers are considered as the customers of service level (1). These customers can receive the special services, while the service of other levels may be limited. However, the results of the present paper may also be used in any field, other than banking.

In many cases, banks use a set of raw and uncategorized information, which has been taken from the accounts of their customers. The information can be applied more effectively by processing.

By utilizing data mining methods, researchers and users will be able to extract some guidance from the given information. Of course, if there is a considerable ambiguity in the existing data, the deterministic data cannot be very helpful. Therefore, two proposed heuristic algorithms are able to extract fuzzy rules from the deterministic data. It is noteworthy that fuzzy rules and relations can describe uncertainty cases better than deterministic data [2-4].

Extracting the database of fuzzy rules from numerical data can be obtained by both tabling and clustering [5]. In the tabling approach, the input and output data are divided into several ranges, so a linguistic label is assigned to each range. Therefore, a table is shaped and the rules are determined [4]. Figure (1) shows a sample of tabulation of two-dimensional data.

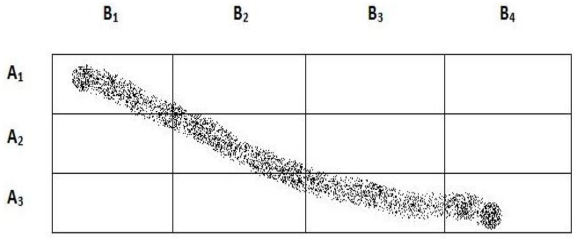

Figure 1. A sample of tabulation of two-dimensional data

The second approach utilizes clusters. The clustering approach places elements into a group based on some similarities and into different groups based on some dissimilarities [6].

In this approach, the data can be clustered by some specified clustering techniques, and each cluster may be considered as a rule. One of the advantages of this approach, of which the previous approach lacks, is that the fuzzy membership functions can be calculated easier [7-9]. Figure (2) shows a sample of two-dimensional deterministic data clustering.

* Corresponding author. e-mail: ramin_sadeghian@yahoo.com.

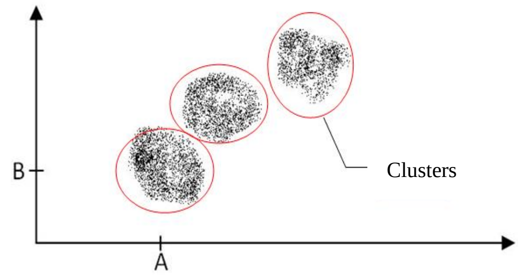

Figure 2. a sample of two-dimensional deterministic data clustering

Different approaches are used in describing the fuzzy sets such as "descriptive approach" and "approximate approach". The "descriptive approach" uses the terms as linguistic labels and its main objective is obtaining a qualitative form of the model [10, 11]. The "approximate approach" extracts fuzzy rules from data without any linguistic interpretation [12-14]. The fuzzy rules are the rules whose variables on left and right hand are fuzzy or linguistic.

Lan *et al.* provided a method to extract some nested fuzzy rules [15]. Ishibuchi *et al.* applied the genetic algorithm to select the best rule among many initial rules [16]. The genetic algorithm has also been applied in other studies [17, 18]. Some researchers used neural networks algorithm to extract rules [19, 20]. Novak *et al.* benefited from an algorithm, called GUHA, to find the appropriate linguistic labels [21]. The GUHA algorithm was among the first data mining methods and was presented in 1970's by Hajek [22].

Fuzzy rule extraction was presented in some applications. Kulluk *et al.* and Quteishat *et al.* presented some novel approaches for fuzzy rule extraction from neural networks [35, 36]. Wang *et al.* and Liu *et al.* proposed some methods for extracting fuzzy rules from fuzzy decision trees [37, 38]. Papageorgiou used fuzzy rule-extraction techniques in medical fields [39]. Also Chen *et al.* applied a rule extraction based approach in predicting derivative use for financial risk hedging by construction companies [40] and Chalaris introduced extraction of rules based on questionnaires [41].

2. Definitions

One of the assumptions of this paper is that each rule has multi-input sources (such as conditions) and only one output (as a consequence). The assumed rules are described as follows:

$$R_h : if \;\; x_1 \;\; is \;\; A_h^1 \;\; and \;\; \cdots \;\; and \;\; x_p \;\; is \;\; A_h^p \;\; then \;\; y \;\; is \;\; B_h \tag{1}$$

Where R_h $(1 \le h \le k)$ are the name of rules, x_j $(1 \le j \le p)$ are input variables, y is a output variable (consequence) and A_h^j, B_h are the linguistic labels of variables. Therefore the data can be displayed as following:

$$R_h \equiv (x_{1t}, x_{2t}, \ldots, x_{pt}, y_t) \;\; ; \;\; t = 1,2,\ldots,n \tag{2}$$

Note x_{1t}, x_{2t}, …, x_{pt}, y_t are the well-known values of variables.

The main idea of the present paper is that the placed similar data in a cluster may be described as a rule.

For this purpose, a suitable clustering algorithm (for example k-means) is used to cluster the existing data [1]. Next, the steps of the proposed algorithms (one of proposed algorithms) are done to find the extracted fuzzy rules. It is clear that the left hand side of the rules has n-1 variables and the right hand side of the rules has one variable only. So, according to Eq. (2), an n-dimensional space is obtained. Hence, when clustering is done, each cluster shows an n-dimensional sphere.

Since the obtained rules are formed from the set of linguistic labels, the rules can be defined as a Cartesian product similar to Eq. (3):

$$R: L_1 \times L_2 \times \ldots \times L_p \times T \tag{3}$$

Where *Li* is a set of labels used for the input variables and *T* is a set of labels used for the output variable.

Due to the nature of the data and clusters, the clustering techniques can be divided into four general categories:

- Deterministic data, deterministic clusters
- Deterministic data, fuzzy clusters
- Fuzzy data, deterministic clusters
- Fuzzy data, fuzzy clusters

In a clustering technique, if an element belongs to several clusters with different membership degrees, there is a fuzzy clustering. The fuzzy clustering methods can be performed by deterministic or fuzzy data. In this paper, two algorithms are presented to cluster the deterministic data as several fuzzy clusters.

3. Algorithms

3.1. Algorithm (I)

- Step 0: Begin
- Step 1: Determine the linguistic variables and labels for any data by experts - (in this case study by the bank's experts).
- Step 2: Use a suitable clustering technique to cluster the existing data.
- Step 3: Assign a fuzzy number to each member of clusters.
- Step 4: Compare the fuzzy numbers with their corresponding linguistic labels; and then select the label that is closest to the number.
- Step 5: According to the assigned labels in Step 4, extract and rewrite a fuzzy rule for each cluster.
- Step 6: End

The steps of the above algorithm are explained below.

Step 1: Define the linguistic variables

As mentioned in previous sections, fuzzy rules can be obtained using a set of linguistic labels. The definition of linguistic variables and labels may affect the efficiency of the algorithm. The arguments of linguistic variables are described by fuzzy numbers. Generally, a linguistic variable may be defined in four levels. In the first level, "variable name" (e.g., account balance), in the second level, "linguistic labels" (e.g., high, medium and low), in the third level, "membership function" of linguistic labels, and in the fourth level, "universal set."

Assume that the data are arranged using a table whose rows and columns represent the elements (e.g., bank customers) and the attributes of elements (e.g., customer account information), respectively. A linguistic variable is defined for each column. The first and second levels of linguistic variables may be defined by modeler, while their third and fourth levels should be defined by experts (e.g., expert in banking).

If you are not able to find an expert, you may use some another data or software similar to the report of Baturone et al. [5]. Table (1) shows a sample of the assignment of linguistic labels to fuzzy numbers.

Table 1. The assignment of linguistic labels into fuzzy number[23]

		Linguistic Variables	Fuzzy Numbers
	Sample1	Sample2	Sample3
Very Low			(0.0, 0.0, 0.1, 0.2)
Low		(0.0, 0.0, 0.2, 0.4)	(0.1, 0.25, 0.25, 0.4)
Medium	(0.4, 0.6, 0.6, 0.8)	(0.2, 0.5, 0.5, 0.8)	(0.3, 0. 5, 0. 5, 0.7)
High	(0.6, 0.8, 0.8, 1.0)	(0.6, 0.8, 1.0, 1.0)	(0.6, 0.75, 0.75, 0.9)
Very High			(0.8, 0.9, 1.0, 1.0)

Step 2: Data clustering

A cluster is a set of objects; its objects are similar to each other in some attributes, and are different from other objects in another attributes. For example, in the case of bank's customers, a cluster can include a set of customers whose account information have similarities, but are different from other customers. A good clustering technique may keep the mentioned feature. By utilizing this feature, the bank's managers may identify and forecast the behavior of customers to obtain better results [1]. A successful clustering is achieved through the execution of existing clustering algorithms. The use of different algorithms leads to different results, but there is not any approach for selecting the best algorithm [24]. In this paper, the K-means technique is used for clustering [1]. Despite that fact that the K-means technique was proposed for the first time over 50 years ago, it is still widely used for clustering. Simplicity, efficiency and empirical success are the main reasons for its popularity [25].

Definitely, any other clustering technique could also be used in this step. Clustering algorithms for high dimensional data were investigated in [26, 27]; time series data clustering were reviewed in [28]; the clustering problem in the data stream domain were studied in [29, 30]; and an overview of the approaches to clustering mixed data were given in [31].

Identifying the number of clusters in a data set (often labeled as *k*) is a fundamental issue in clustering analysis. To estimate the value of *k*, many studies have been presented and discussed in the literature [32].

Sun et al. [33] presented an algorithm based on the fuzzy k-means to determine the number of clusters automatically. It consists of a series of fuzzy k-means clustering procedures with the number of clusters varying from 2 to *k*. By investigating the clustering results for different values of *k*, the exact number of clusters is obtained in a given data set. The same approach for determining *k* is also used in the present paper.

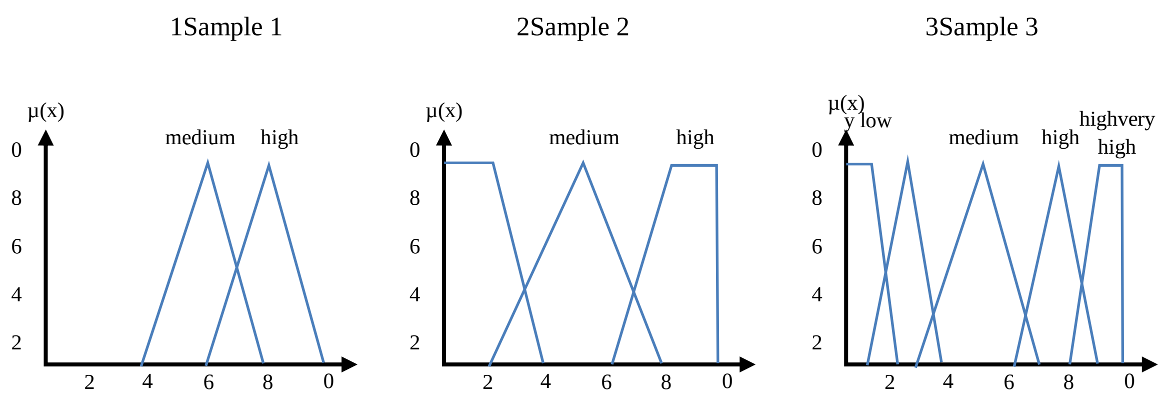

Figure 3. The assignment of linguistic labels into fuzzy numbers

Step 3: Determining the fuzzy numbers for the attributes of placed objects within clusters

Suppose the data is written in a table. The rows and columns of the table indicate the information of the bank's customers and the customer's accounts, respectively. Each attribute can be shown by a fuzzy number. In this paper, the triangular fuzzy numbers are used. In this step, for determining the fuzzy numbers the mean (μ) and standard deviation (σ) of data (data in each column) are applied. Hence, a triangular fuzzy number, such as (μ-σ, μ, $\mu + \sigma$), can be defined (see Figure (4)). Similarly, determine a triangular fuzzy number for each attribute (each column of table) and cluster.

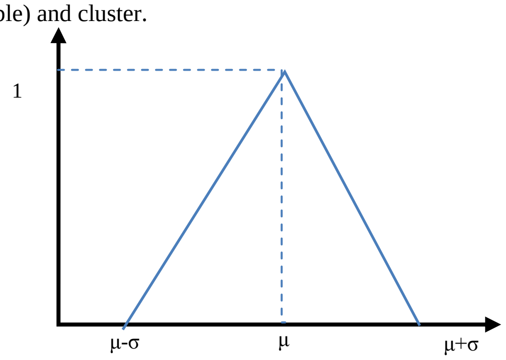

Figure 4. Determining triangular fuzzy number by μ, σ

Step 4: Select the appropriate label

In this step, you have to select the best label for any determined fuzzy number. A suitability criterion for a label means that its membership function is close to the desired fuzzy number. For measuring the closeness between two fuzzy numbers, there are several methods. In this paper two criteria as "Degree of Similarity" (*DOS*) and "Degree of Inclusion" (*DOI*) are applied [1]. The criteria can be defined as follows:

$$S(N,L) = \|N \cap L\| / \|N \cup L\| \tag{4}$$

$$I(N,L) = \|N \cap L\| / \|L\| \tag{5}$$

Where the symbol ||.|| shows the cardinality of a set, also N is an obtained fuzzy number in step (3) and L is the membership function of a linguistic label. $S(N,L)$ (degree of similarity between N and L) is used to determine the best L (as a linguistic label). L is selected if its *DOS* is the greatest. If the *DOS* of several linguistic labels are equal, *DOI* may be used to determine the best L. In this state, L is selected if its *DOI* is the greatest. Therefore, a linguistic label is assigned to each attribute.

Step 5: Rewriting the rules

In this step, the extracted rules can be rewritten like if–then rules. The number of rules may be equal to the number of clusters. For instance, a rule for cluster h can be written as follows:

$$R_h : if \;\; x_1 \;\; is \;\; A_h^1 \;\; and \;\; \cdots \;\; and \;\; x_p \;\; is \;\; A_h^p \;\; then \;\; y \;\; is \;\; B_h \tag{6}$$

Where x_1, x_2, ..., x_p, y are linguistic variables and Aih, Bh are the assigned labels in step (4). By rewriting the rules for all clusters, a rule base is obtained which can describe the behavior of the system in any conditions.

3.2. Algorithm (II)

- Step 0: Begin
- Step 1: Define a linguistic label and variable for each data by experts.
- Step 2: Cluster the deterministic data by an appropriate technique.
- Step 3: Calculate the "Degree of Dependency" to the cluster (*DoD*) for each attribute of objects within a cluster separately.
- Step 4: Find the equation of *DoD* changes in terms of "attribute values" for each attribute within a cluster separately.
- Step 5: Modify the obtained equations in step (4) according to the data concentrations.
- Step 6: Assign the suitable labels to the obtained equations in step (5).
- Step 7: Extract and rewrite the rules.
- Step 8: End.

Below, the above mentioned steps are explained.

Step 1: Defining linguistic variables

It is similar to step (1) in the first algorithm.

Step 2: Data clustering

It is similar to step (2) in the first algorithm.

Step 3: Calculating DoD

Each cluster includes a number of customers and their accounts have several attributes. A *DoD* can be calculated for each customer and attribute. If the number of customers is m and the number of attributes is n, the number of *DoDs* can be equal to $m \times n$. A *DoD* may be determined by equation (7):

$$DoD_{ijh} = 1 - \left| \frac{x_{ijh} - m_{jh}}{\max_i (x_{ijh} - m_{jh})} \right| \tag{7}$$

Where DoD_{ijh} is the degree of dependency to cluster h for each attribute j and customer account i. Also x_{ijh} is the value of attribute j and customer account i in cluster h and also *mjh* is the median of attribute j in cluster h. The symbol |.| shows an absolute function too.

Step 4: Finding the equation of *DoD* changes in terms of changes in the value of attributes

In discrete cases, the value of the attributes can be represented by fuzzy sets that include a number of ordered pairs, where the first element shows the value of an attribute and the second element shows *DoD*.

In the present paper, the values are continuous, so the horizontal axis shows the values of an attribute and the vertical axis shows *DoD*. A regression equation may be fitted for the existing data. This curve can be considered as a fuzzy number to assign the best linguistic label to the data (see Figure 5)

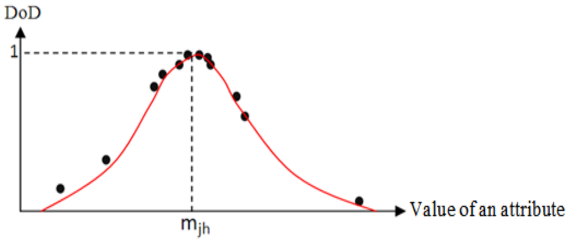

Figure 5. A sample of fitting a curve on data

Step 5: Improving the obtained equations according to the data concentrations

Generally, the values of attributes are concentrated in specified areas of domain (Figure 5). Also the existence of some useless data in first and end of domain can widen the domain and curve. The widened domain and curve can lead to some errors in the selection of appropriate linguistic labels and a reduction in the accuracy of the results. For this purpose, exclude a range of data from the beginning and end of domain. If the length of the old domain is d_1 and the length of the new domain is d_2, the multiplying proportion d_2/d_1 in the length of the graph horizontal axis may reduce the width of the chart and increase its focus on areas where the density of data is higher. This action will increase the accuracy of linguistic labels selection.

Step 6: Find the appropriate labels

Select a label that is closer to the obtained equation in step (5). The current step is similar to step (4) of the first algorithm, so you can implement it by equations (4) and (5).

Step 7: Rewriting the rules

This step is similar to step (5) of the first algorithm.

4. Case Study

The customer relationship management and customer requirements management in banks and financial institutions are very important. So rating customers based on the analyzed criteria can help organizations to present more favorable services. Data mining [14] and the presented algorithms in previous sections can be used as tools for evaluating, predicting customer behavior and customers rating in terms of some criteria. In this paper, it is shown how to implement the proposed algorithms. For this purpose, the information of 2500 accounts from a bank in Iran is studied [34]. The afore-mentioned information is clustered by the *k*-means method and is considered 5 clusters corresponding to 5 levels of customers rating.

In this case study, the following criteria of customers account information are considered:

1. **average:** The average of daily balance for each customer during one year.
2. **val-cheq:** The average amount of returned checks for each customer during one year.
3. **tran-bed:** Total debtor turnover of each customer during one year.
4. **tran-bes:** Total creditor turnover of each customer during one year.
5. **rem-bes:** The sum of the creditor balance of each customer during one year.
6. **remained:** The remaining creditor balance of each customer at the end of year.

The criterion "tran-bed" can be considered as a consequent of other criteria, so it is located in right hand side of the rules. The steps of the first algorithm can be performed as follows:

Step (1) Defining the linguistic variables (see Figures (6) to (11)).

Step (2) Clustering data by *k*-means method: since 5 clusters have less error, so 5 clusters are considered.

Steps (3-5) Selecting appropriate labels, their calculations, rules extraction and their rewriting.

Finally the five rules are obtained as follows:

- R1: If *(remained = VL)* and *(tran_bes = L)* and *(rem_bes = L)* and *(val_cheq = VS)* and *(average = VL)* $\Longrightarrow$ *(tran_bed = L)*
- R2: If *(remained = VL)* and *(tran_bes = S)* and *(rem_bes = L)* and *(val_cheq = VS)* and *(average = VL)* $\Longrightarrow$ *(tran_bed = S)*
- R3: If *(remained = VL)* and *(tran_bes = M)* and *(rem_bes = L)* and *(val_cheq = VS)* and *(average = VL)* $\Longrightarrow$ *(tran_bed = M)*
- R4: If *(remained = M)* and *(tran_bes = VS)* and *(rem_bes = S)* and *(val_cheq = S)* and *(average = M)* $\Longrightarrow$ *(tran_bed = VS)*
- R5: If *(remained = VL)* and *(tran_bes = M)* and *(rem_bes = L)* and *(val_cheq = VS)* and *(average = VL)* $\Longrightarrow$ *(tran_bed = M)*

Third and fifth rules are similar, so the fifth rule is removed, so only the first four rules can be considered.

Also by the second algorithm, five rules are obtained as following:

- R_1: If *(remained = VL)* and *(tran_bes = L)* and *(rem_bes = L)* and *(val_cheq = VS)* and *(average = VL)* $\Longrightarrow$ *(tran_bed = L)*
- R_2: If *(remained = L)* and *(tran_bes = S)* and *(rem_bes = L)* and *(val_cheq = VS)* and *(average = L)* $\Longrightarrow$ *(tran_bed = S)*
- R_3: If *(remained = VL)* and *(tran_bes = M)* and *(rem_bes = L)* and *(val_cheq = VS)* and *(average = L)* $\Longrightarrow$ *(tran_bed = M)*
- R_4: If *(remained = M)* and *(tran_bes = VS)* and *(rem_bes = S)* and *(val_cheq = VS)* and *(average = M)* $\Longrightarrow$ *(tran_bed = VS)*
- R_5: If *(remained = VL)* and *(tran_bes = M)* and *(rem_bes = L)* and *(val_cheq = VS)* and *(average = VL)* $\Longrightarrow$ *(tran_bed = L)*

Note that the extracted fuzzy rules from each of the two algorithms are different.

By extracting the fuzzy rules according to the needs of each bank, the customers can be rated into several levels. A bank can present services to its customers based on the determined levels. For example, the customers of the first cluster can be considered as high level customers (first level) because their account balance and turnover is large and their returned check rate is low; these customers can be useful for a bank. Therefore, a bank can prepare more services for this level of customers. The reward and punishment can also be applied similarly for other levels.

5. Conclusions

In this paper, two algorithms were presented to extract fuzzy rules from deterministic data. The proposed algorithms were performed in a case study on bank customers. One of the applications of fuzzy rules for banks may be rating their customers. Each customer in each level can receive some services depending on its level.

For investigating the validity of the algorithms, the information of 300 new customer accounts was extracted. The data were compared with the obtained rules from previous algorithms. The criteria values as input data and the value of "tran-bed" as output data were considered. The calculations show that the first algorithm 95.7% and the second algorithm 92.7% confirm the views of experts. Of course the confirmation of both algorithms is acceptable.

The advantage of the above methods over the other methods is that they can reduce the time and the required effort for extracting rules.

References

[1] Ghazanfari, M., Rezaei, M., *An introduction to fuzzy sets theory*, 1st ed. Tehran: Iran University Science and Technology; 2006.

[2] Araki, S., Nomura, H., Hayashi, I., and Wakami, N., "*A self-generating method of fuzzy inference rules*", Fuzzy Engineering toward Human Friendly Systems, (1991), 1047-1058.

[3] Ichihashi, H., "*Iterative fuzzy modeling and a hierarchical network*", IFSA, Bruselas, (1991), 49-51.

[4] Wang, L., and Mendel, J.M., "*Generating fuzzy rules by learning from exampl*es", IEEE Trans, Systems Man Cybernet, Vol. 22 (1992), 1414-1427.

[5] Baturone, I., Moreno-Velo, F.J., Gersnoviez, A., "*Identifying fuzzy systems from numerical data with Xfuzzy*", EUSFLAT – LFA, (2005).

[6] Walt Van, C.M., Barnard, E., "*Data characteristics that determine classifier performance*", In Proceedings of the Sixteenth Annual Symposium of the Pattern Recognition Association, South Africa, 2006, 160-165.

[7] Delgado, M., Gomez-Skarmeta, A.F., Martin, F., "*A methodology to model fuzzy systems using fuzzy clustering in a rapid-prototyping approach*", Fuzzy Sets and Systems, Vol. 97 (1998), 287-30.

[8] Setnes, M., "*Supervised Fuzzy Clustering for Rule Extraction*", IEEE TRANSACTIONS ON FUZZY SYSTEMS, Vol. 8 (2000) No. 4.

[9] Klawonn, F., Kruse, R., "*Constructing a Fuzzy Controller from Data*", Fuzzy Sets and Systems, Vol. 85 (1997), 177-193.

[10] Pedrycz, W., "*An identification algorithm in fuzzy relational systems*", Fuzzy Sets and Systems, Vol. 13 (1984), 153-167.

[11] Peng, X., and Wang, P., "*On generating linguistic rules for fuzzy models*", Uncertainty and Intelligent Systems, (1988), 185-192.

[12] Nie, J., and Linkens, D.A., "*Learning control using fuzzified self-organizing radial basis function network*", IEEE Trans, Fuzzy Systems, Vol. 1 (1993), 280-287.

[13] Nomura, H., Hayashi, I., and Wakami, N., "*A self-tuning method of fuzzy control by descent method*", IFSA, Bruxelles, (1991), 155-158.

[14] Simpson, P.K., and Jahns, G., "*Fuzzy Min-Max neural networks for function approximation*", Proc. IEEE lnternat. Conf. on Fuzzy Systems, (1993), 1967-1972.

[15] Abe, S., and Lan, M.S., "*A classifier using fuzzy rules extracted directly from numerical data*" Proc. 2nd IEEE Int'l Conf. on Fuzzy Systems (FUZZ-IEEE '93), San Francisco, CA, (1993), 1191-1198.

[16] Ishibuchi, H., Nakashima, T., Murata, T., "*Three-objective genetic-based machine learning for linguistic rule extraction*", Information Sciences, Vol. 136 (2001), 109-133.

[17] Cordon, O., del Jesus, M.J., Herrera, F., "*Genetic learning of fuzzy rule-based classification systems cooperating with fuzzy reasoning methods*", International Journal of Inteligent Systems, Vol. 13 (1998), 1025-1053.

[18] Ishibuchi, H., Nakashima, T., "*Improving the performance of fuzzy classifier systems for pattern classification problems with continuous attributes*", IEEE Transactions on Industrial Electronics, Vol. 46 (1999), 1057-1068.

[19] Abe, S., Lan, M.S., Thawonmas, R., "*Tuning of fuzzy classifier derived from data*" , International Journal of Approximate Reasoning, Vol. 14 (1996), 1-24.

[20] Mitra, S., De, R.K., Pal, S.K., "*Knowledge-based fuzzy MLP for classification and rule generation*", IEEE Transactions on Neural Networks, Vol. 8 (1997), 1338-1350.

[21] Novak, V., Perfilieva, I., Dvorak, A., Chen, G., Wei, Q., Yan, P., "*Mining pure linguistic associations from numerical data*" International Journal of Approximate Reasoning, Vol. 48 (2008), 4–22.

[22] Hajek, P., "*The question of a general concept of the guha method*", Kybernetika, Vol. 4 (1968), 505–515.

[23] Boroushaki,S., Malczewski,J., "*Using the fuzzy majority approach for GIS-based multicriteria group decision-making*" , Computers & Geosciences, Vol. 36 (2010), 302–312.

[24] Grekousis, G., Hatzichristos, T., "*Comparison of two fuzzy algorithms in geodemographic segmentation analysis: The Fuzzy C-Means and GustafsoneKessel methods*", Applied Geography, Vol. 34 (2012).

[25] Anil K. Jain, "*Data clustering: 50 years beyond K-means*", Pattern Recognition Letters, Vol. 31 (2010).

[26] Kriegel, H.P., Kroger, P., Zimek, A., "*Clustering high-dimensional data: a survey on subspace clustering, pattern-based clustering and correlation clustering*", ACM Transactions on Knowledge Discovery from Data, Vol. 3 (2009), No. 1.

[27] Bai, L., Liang , J.Y., Dang, C.Y., Cao, F.Y., "*A novel attribute weighting algorithm for clustering high-dimensional categorical data*", Pattern Recognition, Vol. 44 (2011) No. 12.

[28] Liao, T.W., "*Clustering of time series data survey*", Pattern Recognition, Vol. 38 (2005) No. 11.

[29] Aggarwal, C.C., Han, J.W., Wang , J.Y., Yu, P.S., "*A framework for clustering evolving data streams*", in: Proceedings of the 29th VLDB Conference, Berlin, Germany, 2003.

[30] Cao, F.Y., Liang, J.Y., Bai, L., Zhao, X.W., Dang, C.Y., "*A framework for clustering categorical time-evolving data*", IEEE Transactions on Fuzzy Systems, Vol. 18 (2010) No. 5.

[31] Hunt, L., Jorgensen, M., "*Clustering mixed data*", WIREs Data Mining and Knowledge Discovery, Vol. 1 (2011) No. 4.

[32] Mirkin, B., "*Choosing the number of clusters*", WIREs Data Mining and Knowledge Discovery, Vol. 1 (2011) No. 3.

[33] Sun, H.J., Wang, S.R., Jiang, Q.S., "*FCM-based model selection algorithms for determining the number of clusters*", Pattern Recognition, Vol. 37 (2004) No. 10.

[34] Tarokh, Mohammad J. and Sharifian, Kobra, "*Clustering the bank customers and its analysis by the customer value pyramid*", 6th IIEC conference, 2009.

[35] Sinem Kulluk, Lale Özbakır, Adil Baykasoğlu, "Fuzzy DIFACONN-miner: A novel approach for fuzzy rule extraction from neural networks", Expert Systems with Applications, Vol. 40 (2013) No. 3, 938-946.

[36] Anas Quteishat, Chee Peng Lim, "A modified fuzzy min–max neural network with rule extraction and its application to fault detection and classification", Applied Soft Computing, Vol. 8 (2008) No. 2, 985-995.

[37] Xianchang Wang, Xiaodong Liu, Witold Pedrycz, Lishi Zhang, "Fuzzy rule based decision trees", Pattern Recognition, Vol. 48 (2015) No. 1, 50-59.

[38] Xiaodong Liu, Xinghua Feng, Witold Pedrycz, "Extraction of fuzzy rules from fuzzy decision trees: An axiomatic fuzzy sets (AFS) approach", Data & Knowledge Engineering, Vol. 84 (2013), 1-25.

[39] Elpiniki I. Papageorgiou, "A new methodology for Decisions in Medical Informatics using fuzzy cognitive maps based on fuzzy rule-extraction techniques", Applied Soft Computing, Vol. 11 (2011) No. 1, 500-513.

[40] Jieh-Haur Chen, Li-Ren Yang, Mu-Chun Su, Jia-Zheng Lin, "A rule extraction based approach in predicting derivative use for financial risk hedging by construction companies", Expert Systems with Applications, Vol. 37 (2010) No. 9, 6510-6514.

[41] Manolis Chalaris, Ioannis Chalaris, Christos Skourlas, Anastasios Tsolakidis, "Extraction of Rules based on Students' Questionnaires", Procedia - Social and Behavioral Sciences, Vol. 73 (2013), 510-517.

المملكة الأردنية الهاشمية

الجامعة الهاشمية

المجلة الأردنية
للهندسة الميكانيكية والصناعية

JJMIE

مجلة علمية عالمية محكمة

تصدر بدعم من صندوق البحث العلمي

http://jjmie.hu.edu.jo/

ISSN 1995-6665

المجلة الأردنية للهندسة الميكانيكية والصناعية

مجلة علمية عالمية محكمة

المجلة الأردنية للهندسة الميكانيكية والصناعية: مجلة علمية عالمية محكمة تصدر عن الجامعة الهاشمية بالتعاون مع صندوق دعم البحث العلمي في الأردن

ترسل البحوث إلى العنوان التالي

رئيس تحرير المجلة الأردنية للهندسة الميكانيكية و الصناعية

الجامعة الهاشمية

كلية الهندسة

قسم الهندسة الميكانيكية

الزرقاء - الأردن

هاتف : 3903333 5 00962 فرعي 4537

Email: jjmie@hu.edu.jo

Website: www.jjmie.hu.edu.jo